NITRIC OXIDE-RELEASING NANOMATERIALS AND HYDROGELS AS VERSATILE AND ROBUST ANTIBACTERIAL AGENTS

by

HAMED MASSOUMI

(Under the Direction of Elizabeth J. Brisbois)

ABSTRACT

Therapeutic agents like nitric oxide (NO), can be linked to nanoparticles to fortify their selectivity and targeted delivery while impeding systemic toxicity and efficacy loss. Titanium dioxide nanoparticles (TiNPs) owe their rise in biomedical sciences to their versatile applicability. Structural modifications to immobilize NO-releasing moieties can improve TiNP's antibacterial impact. For the first time, *S*-nitroso-*N*-acetyl-penicillamine (SNAP), an NO donor molecule, was covalently immobilized on TiNPs to form the NO-releasing TiNP-SNAP nanoparticles. In addition, another NO donor small molecule, *S*-Nitroso-*N*-acetyl-l-cysteine Ethyl Ester (SNACET) was incorporated into a thermo-responsive Pluronic gel F-127 to fabricate a hydrogel that is capable of releasing NO in physiological conditions. It was shown that the hydrogels exhibit bactericidal efficacy relative to their SNACET content. Both the NO-releasing TiNPs and Pluronic hydrogels exhibit tunable NO release properties that can have a wide range of biomedical applications such as in wound healing dressings, antibacterial coatings, and polymer fillers.

INDEX WORDS: Nitric Oxide, Titania Nanoparticles, Antibacterial, Biocompatibility, Pluronic Gel, Wound Healing

NITRIC OXIDE-RELEASING STRUCTURES AS VERSATILE AND ROBUST ANTIBACTERIAL AND WOUND HEALING AGENTS

by

HAMED MASSOUMI

BS, Iran University of Science and Technology, Iran, 2014

MS, University of Tehran, Iran, 2017

A Thesis Submitted to the Graduate Faculty of The University of Georgia in Partial Fulfillment of the Requirements for the Degree

MASTER OF SCIENCE

ATHENS, GEORGIA

2021

NITRIC OXIDE-RELEASING STRUCTURES AS VERSATILE AND ROBUST ANTIBACTERIAL AND WOUND HEALING AGENTS

by

HAMED MASSOUMI

Major Professor:	Elizabeth J. Brisbois
Committee:	Ross A. Marklein
	Hitesh Handa

Electronic Version Approved:

Ron Walcott
Vice Provost for Graduate Education and Dean of the Graduate School
The University of Georgia
December 2021

DEDICATION

To my wife who never lost faith in me and stood beside me at all times and gave me the strength to carry on, especially in those moments that I lost faith in myself.

TABLE OF CONTENTS

Page

LIST OF TABLES vii

LIST OF FIGURES viii

CHAPTER

1 Introduction and Literature Review 1

1.1 Nitric Oxide Regulatory Functions 1

1.2 Nitric Oxide Donors 5

1.3 Nitric Oxide Applications in Biomedical Research 8

1.4 Nitric Oxide Delivery Systems 19

1.5 Hypothesis and Objective 24

2 Nitric Oxide Release and Antibacterial Efficacy Analyses of *S*-nitroso-*N*-acetyl-penicillamine Conjugated Titanium Dioxide Nanoparticles 28

2.1 Introduction 28

2.2 Materials and Methods 29

2.3 Results and Discussion 39

2.4 Conclusion 55

3 *S*-Nitroso-*N*-acetyl-L-cysteine Ethyl Ester (SNACET) Incorporated Pluronic F-127 Hydrogel for Topical Applications 57

3.1 Introduction 57

3.2 Materials and Methods 59

3.3 Results and Discussion 64
3.4 Conclusion 71
4 Summary and Recommendations 74
REFERENCES 78

LIST OF TABLES

Page

Table 1: Content of free amine and thiol groups on the surface of TiNP-APTES and TiNP-NAP respectively 41

Table 2: Viability reduction of bacteria cells (%) after exposure to TiNP-SNAP.....52

LIST OF FIGURES

Page

Figure 1: Nitric oxide regulatory functions in different organs 2

Figure 2: Some NO donor molecules reported in literature.....6

Figure 3: The reaction of liberating 2 moles of NO for every 2 moles of RSNO donor 7

Figure 4: Titanium dioxide nanoparticle applications 21

Figure 5: Poloxamer ABA three-block structures 23

Figure 6: Synthesis route of TiNP-APTES, TiNP-NAP and TiNP-SNAP 39

Figure 7: Representative FTIR spectra of modified TiNPs 43

Figure 8: Representative ^{13}C CP/MAS NMR spectra of modified TiNPs.....44

Figure 9: Zeta potential and DLS measurements for modified TiNPs 45

Figure 10: Representative SEM images of TiNPs 47

Figure 11: Representative SEM image with overlay EDS elemental maps.....48

Figure 12: *In vitro*, NO release kinetics of the TiNP-SNAP 50

Figure 13: Bactericidal efficacy analysis of TiNP-SNAP 52

Figure 14: Cytocompatibility of TiNP and TiNP-SNAP leachates 54

Figure 15: Sample preparation steps for for SNACET-Pluronic hydrogels 62

Figure 16: Chemical structure of *S*-Nitroso-*N*-Acetyl-L-Cysteine Ethyl Ester (SNACET) and decomposition reaction of RSNOs.....64

Figure 17: Storage stability of 1, 2, and 5 wt% SNACET Pluronic Gel.....66

Figure 18: The NO release kinetics of Pluronic gels containing 68

Figure 19: Antibacterial activity of SNACET Pluronic gel.....71

CHAPTER 1

INTRODUCTION AND LITERATURE REVIEW

1.1 Nitric Oxide Regulatory Functions

In 1977, Ferid Murad studied the effect of nitroglycerin and discovered the production of nitric oxide (NO) from the vasodilating compounds. Therefore, he speculated that NO could be the driving force for endogenous smooth muscle cell (SMC) relaxation and theorized NO production by endogenous factors such as hormones. Nonetheless, his speculations were not supported by enough experimental evidence by that time [1]. By the year 1980, the discoveries of Robert F. Furchgott about acetylcholine's vasodilating action marshaled the world of research about endothelium-derived relaxing factor (EDRF). Inadvertently it was demonstrated by him that the acetylcholine-induced vasodilation is strictly endothelium-dependent. Furthermore, he proposed that endothelial cells' unknown signaling molecule must directly affect SMC relaxation [2]. The quest for finding the EDRF was completed by the results Louis J. Ignarro obtained from a series of carefully designed analyses to figure out that EDRF produced and released from artery and vein is in fact, NO [3]. Finally, in 1986, when Furchgott and Ignarro presented their successful individual discoveries in a conference, although separately, for the first time, a gaseous compound was introduced to exhibit signaling property in the biological system [4]. These discoveries led these three researchers being awarded the 1998 Nobel prize in physiology or medicine [5].

After the Nobel prize-winning discoveries of NO's physiological role in the human body as a key gaseous signaling molecule, a colossal cascade of research shed light on further NO biological potentials [1, 2, 4-6]. Nitric oxide possesses versatile biological functions such as platelet activation and adhesion inhibition, antithrombosis, bactericidal actions, biofilm dispersion and prevention, endothelialization induction, signaling action in the immune responses, and angiogenesis promotion (**Figure 1**) [7]. This bioregulatory molecule is synthesized in the human body (endogenously) by a family of enzymes known as NO synthase (NOS), which catalyze NO production from L-arginine. There are at least three distinct NOS enzymes that are named on the basis of the origin of the NO molecule. Endothelial NOS (eNOS) from endothelial cells, neuronal NOS (nNOS) from neurons, and inducible NOS (iNOS) from immunological cells like macrophages [8].

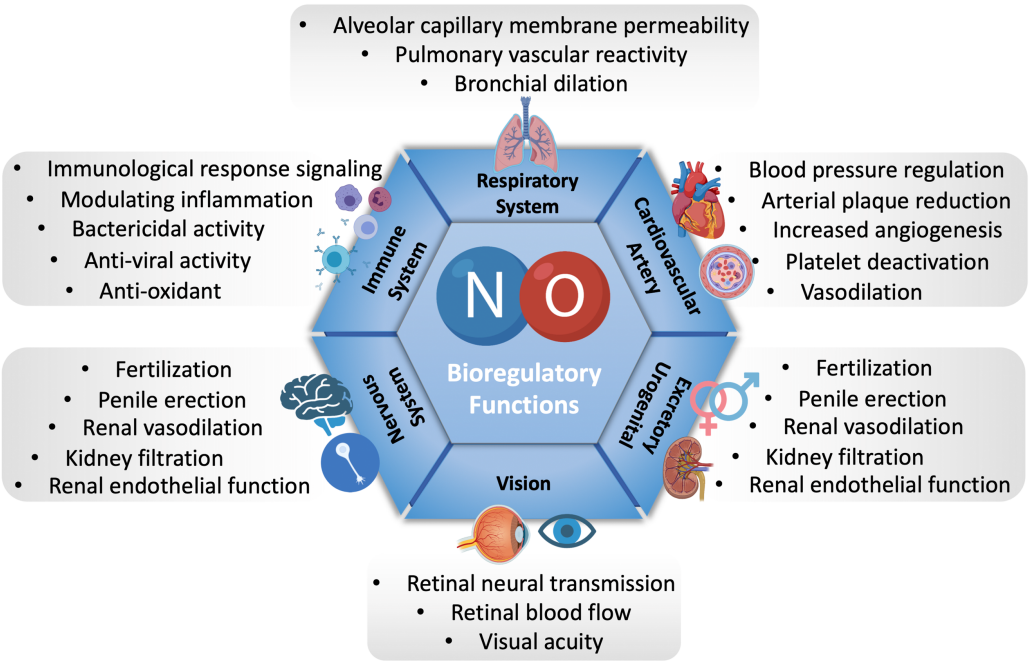

Figure 1. Nitric oxide regulatory functions in different organs in the body. Created with BioRender.com.

Primarily, the inhibition of platelet adhesion, activation, and aggregation on the endothelial lining of blood vessels is due to the activity of endothelial NO synthase (eNOS) enzyme, which rewards the thrombogenicity properties through soluble guanylate cyclase (sGC) signaling pathway [9]. Nitric oxide in its conventional pathway of physiological activities is known to bind to the heme iron moiety of sGC to create iron complexes promoting the formation of cyclic guanosine monophosphate (cGMP) as a second messenger originated from guanosine triphosphate (GTP). The upregulation of cGMP leads to a reduction in intracellular Ca^{+2} levels by activating protein kinase G (PKG) [9, 10]. In response to this cascade of cGMP synthesis and intracellular calcium concentration reduction, the phosphoinositide 3-kinase (PI3) enzyme is inhibited which consequently reduces the affinity of platelets to GPIIb/IIIa binding sites [7, 9, 11].

There are numerous articles about the usage of NO in cancer therapy and its effect on cancer cells with a mechanism slightly similar to the antiplatelet inhibition mechanism. In cancer cells, NO at low concentrations will target cGMP, phosphorylate Akt, and hypoxia-inducible factor 1 α. All of the NO interactions at low concentrations in cancerous cells will promote antiapoptotic responses and provides pro-growth of cancer cells which can lead to tumor progression and metastasis [12, 13]. However, the upregulation of cGMP leads to vasodilation which leads to enhanced chemotherapy efficacy by enhanced permeability and retention (EPR) effect in cancer cells [14, 15]. Moreover, NO can play a pivotal role as an inhibitory for efflux system in the multidrug-resistant (MDR) tumor cells and therefore, reduces the drug resistance of cancer MDR cells which is a great complication in cancer treatment [16]. Hence, delivering NO to cancer cells can, directly and indirectly, impact cancer treatment in patients [13, 14, 16].

Other than vasodilation and antithrombotic effects of NO, which are extensively studied [17-19], the antibacterial activity of this highly reactive molecule promotes promising results against a broad spectrum of bacteria, especially antibiotic-resistant strains, by producing two possible lethal compounds. First, the production of peroxynitrite ($OONO^-$) by reacting with superoxide (O_2^-) which can induce lethal oxidative stress to the bacteria cells [20]. In addition, the peroxynitrite compounds can nitrosate amino acids which means that they can alter and disturb the membrane proteins and damage the DNA strands within the pathogen's cell structure [21]. Second, the production of *S*-nitrosothiols (RSNOs). In the second mechanism, NO initially is oxidized to N_2O_3 (nitrous anhydride) which then reacts with sulfhydryl groups on cysteine residues of membrane proteins to produce RSNO moieties which will be lethal to bacterial cells by altering the protein functionality [20, 21]. Furthermore, it is demonstrated that NO can induce biofilm dispersal in many bacterial strains and mediate the cell-to-cell communication mechanism known as quorum sensing within the biofilm which disrupts the biofilm development [22].

The depletion of NO in the human body that can be due to the aging process, post-surgery injuries, or health conditions, is known to be the driving force of many health issues such as high blood pressure, restenosis, intimal hyperplasia, excessive vascular SMC migration, and proliferation, neointima layer formation, prolonged inflammation, and inefficient wound healing, impeded immune system, or increased risk of viral and bacterial infections [23-26].

1.2 Nitric Oxide Donors

All of the remarkable advantages of the NO molecule denote promising results if an exogenous delivery system could be exploited to provide therapeutic amounts of NO to desired locations. Nevertheless, there are challenges in NO delivery systems. Nitric oxide is a highly unstable and reactive radical that possesses a high affinity in reacting with oxygen molecules, thiol compounds, or oxyhemoglobin in the surrounding environment, and its half-life is only a few seconds in physiological conditions [7]. Hence, delivering NO to the desired sites, such as *in vivo* or from blood-contacting medical devices, within a prolonged time and a therapeutic capacity has been a challenging source of research. To this end, several types of NO donor molecules have been introduced that are capable of storing NO in their molecular structure and dissociating it spontaneously under physiological conditions. *S*-nitrosothiols (RSNOs), *N*-diazeniumdiolates (NONOates), metal NO complexes, and organic nitrites are a few of the NO donor molecules widely used in biomedical research (**Figure 2**) [27-36]. In the recent two decades, NONOates (1-amino-substituted diazen-1-ium- 1,2-diolate), as a family of NO donors have been studied extensively due to their relatively high stability and their spontaneously NO release ability in biological conditions. The synthesis of this class of NO donors requires a high-pressure reaction of NO gas with primary or secondary amine groups of the donor molecule in a basic environment and low temperature [37]. Upon hydrolysis reaction, thermal, photochemical, and enzymatical stimuli, every mole of the NONOate donor is capable of delivering (releasing) 2 mole equivalents of NO molecule [25, 37, 38]. One of the well-known examples of this class of NO donors is diethylenetriamine/NONOate (DETA/NONOate) which has an extended half-life of 20 h, making it a suitable candidate

for biological stimuli in applications such as wound healing in which a sustainable NO reservoir can be beneficial over a long period. However, the harmful byproducts of the diazeniumdiolates reduction reaction (e.g. carcinogenic nitrosamine compounds) are a hindrance to their clinical applications [39]. Indeed, the toxicity of NONOates has not yet been completely approved and there is a need for more in-depth research to establish the long-term effect of usage of NONOate compounds for targeted delivery and controlled release of NO [40].

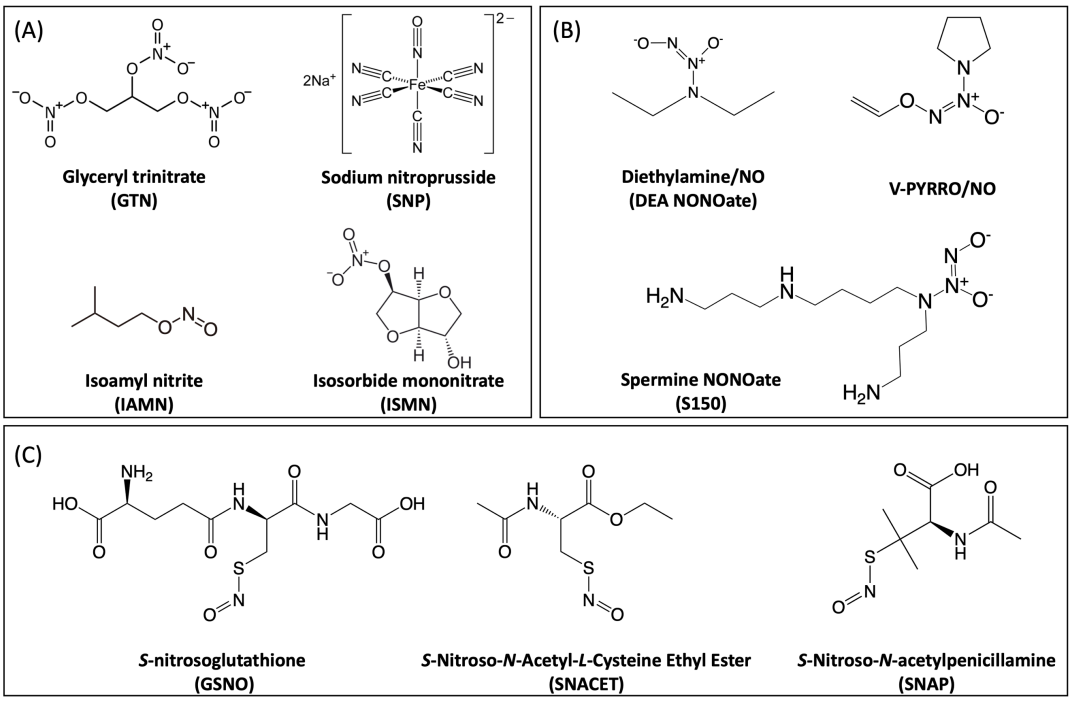

Figure 2. Some examples of NO donor molecules reported in literature. (A) Organic nitrates and nitrites like glyceryl trinitrate (GTN) [27], sodium nitroprusside (SNP) [28], Isoamyl nitrite (IAMN) [29], and Isosorbide mononitrate (ISMN) [30] used as NO donor drugs for coronary artery disease. Releasing NO in reaction to specific enzymes. (B) Examples of diazeniumdiolates (NONOates) NO donors such as diethylamine/NO (DEA NONOate) [31], V-PYRO/NO [32], and spermine NONOate (S150) [33] as one of the most studied NO donor groups in research which release NO upon exposure to elevated temperatures and acidic or low pH environments. (C) RSNO molecules such as *S*-nitrosoglutathione (GSNO) [34], *S*-Nitroso-*N*-Acetyl-L-Cysteine Ethyl Ester (SNACET) [35], and *S*-Nitroso-*N*-acetylpenicillamine (SNAP) [36] are adducts of R-SH and NO, and are considered as excellent source of NO. The NO release rate from RSNOs is influenced by the presence of metal ions, reducing agents and enzymes, heat, light and pH.

Within a wide range of NO donor molecules, owing to their biocompatibility, antibacterial, and antithrombotic properties, and most importantly their relative stability a tremendous amount of attention has been given to RSNOs which are the adducts of R-SH and NO compounds. The thiol moiety (–SH) in the precursor of the RSNO molecular structures provides reaction sites for nitrosation [41]. Some of the most common examples of RSNO structures are *S*-nitrosoglutathione (GSNO), *S*-nitroso-*N*-acetyl-L-cysteine Ethyl Ester (SNACET), and *S*-nitroso-*N*-acetylpenicillamine (SNAP) [41, 42]. Comparing to the NONOate class of NO donors, RSNOs owing to the natural endogenous occurrence within the normal blood in the human body are considered more bioinspired [43]. Various factors can influence the NO release from RSNO donors via the S–NO bond cleavage upon exposures to heat, light, metal ions, reducing agents, enzymes, and pH [40]. It has been generally accepted that thermal decomposition in RSNOs occurs by an unimolecular and homolytic decomposition mechanism while an NO radical will separate from the -SNO moiety leaving an open thiyl radical to react with another thiyl radical to form a disulfide (RSSR) byproduct with two NO molecules [44, 45] (**Figure 3**).

Figure 3. One of the well-known NO donors from RSNO family (SNAP) and the reaction of liberating 2 moles of NO for every 2 moles of RSNO donor

The long-lasting NO release profile, reduced cytotoxicity, and relevantly easier synthesis procedure have promoted RSNO class of NO donors to a very promising and

robust source of NO delivery. Many research studies and pre-clinical trials on RSNO donors have demonstrated their effectiveness as NO-based therapeutic agent [7, 40].

1.3 Nitric Oxide Applications in Biomedical Research

As mentioned before, NO plays pivotal physiological and pathophysiological roles in a healthy body including but not limited to neurotransmission, neuronal communication, vasodilation, platelet adhesion/activation and thrombosis inhibition, inflammation, and wound healing [40]. However, severe health conditions derived by risk factors such as malnutrition and poor diet [46], tobacco and drug consumption [47], high age, family history, sedentary or stressful lifestyle, diabetes [48], invasive surgeries, the introduction of foreign objects to tissues [49], etc. can lead to a reduction in the bioavailability of vital NO, especially at relevant biointerfaces such as wounds or medical device surfaces. In such conditions, an external source of NO can be utilized to properly make up for the shortcoming of NO signaling [26]. What follows is some of the applications in biomedical medical engineering that seek to introduce NO to overcome the scarcity of NO in needed locations.

1.3.1 Blood-Contacting Medical Devices

Endothelial cells that line up on the inner wall of blood vessels are capable of continuous production of NO with a surface flux of $0.5–4 \times 10^{-10}$ mol cm^{-2} min^{-1} known as biological flux range. Evidently, if the integrity of the healthy vasculature in a body gets disturbed (due to injuries and procedures such as placing intravenous catheters, stents, or grafts) the NO flux levels deviate from the biological range leading to an imbalance between thrombosis and hemorrhage, and may even alter the proliferation and migration

of SMCs [50]. Hence, one of the most elegant applications of NO is to develop blood-contacting medical devices which are capable of releasing NO spontaneously or on-demand, when they come in contact with tissues, especially blood [25, 51].

One of the medical devices that has been in use for several years and possesses dominant application in obstructive artery diseases is stents [52]. However, the usage of stents carries risks of post-surgery complications such as thrombosis and incomplete endothelialization for which drug eluting stents have emerged to address these issues [25]. Multiple studies are reported to attempt NO-releasing stents production in order to reduce the risk of post-surgery restenosis, control inflammation and boost the healing process [25]. Using liposome carriers to release eNOS from a top-coated stent [53], as well as biodegradable polymeric matrixes containing RSNO compounds to topcoat vascular stents to release NO upon poly(lactic-co-glycolic-co-hydroxymethyl propionic acid) (PLGH) degradation [54], and layer-by-layer coating on a stent to encapsulate DETA-NONOate donor to release NO over the course of 5 days within a physiological range [51] are only a very few examples of NO application in improving vascular stents.

Other than stents, many indwelling medical devices come in contact with bodily fluids and blood. Catheters for instance have been in use in medical practices for so long and there is a significant burden on healthcare system due to catheter-related infections [55]. The infection problem due to catheterization is even more concerning in susceptible and most severely ill group of patients like children and elderly people and the reported number of infections are higher in long-term catheter implementations [56, 57]. The NO-releasing polymers that can be used potentially in fabricating catheters or modifying catheter polymeric walls to release NO are research topics to mainly address the risk of

thrombosis and bacterial infection upon catheter placement [7, 58-62]. Several ways are introduced to develop polymeric surfaces which are capable of storing or releasing NO in physiological conditions. Some of the diverse protocols to generate such surfaces are the simple blending techniques to encapsulate a known amount of an NO donor molecule within the polymeric matrix. Although this technique offers the easiest production method it comes with some downsides such as high leaching and loss of NO donor molecules, as well as initial burst release due to the presence of NO reservoir near to the surface of the polymeric matrix [63]. Brisbois et al. incorporated SNAP in Elast-eon E2As to fabricate catheters using a dip coating technique [64]. A trilayer configuration of E2As-(SNAP/E2As)-E2As for the catheters was reported to significantly decrease thrombose formation from 5.06 ± 1.44 in a E2As control samples to 1.56 ± 0.76 cm^2 in treatment groups on a 7 d *in vivo* study in a sheep model. The antibacterial studies also revealed 90% (1-log) reduction in infection rate on treatment SNAP incorporated catheters.

Another simple method to produce NO releasing polymeric surfaces is using solvent swelling techniques to impregnate the NO donor molecules into the polymeric matrix [7, 17, 58-62, 65, 66]. Devine et al. recently reported a modified silicone rubber polymeric matrix using heparin surface immobilization and SNAP swelling techniques to reduce platelet activation, thrombus formation, and bacterial infection by synergetic effects of heparin and NO [67]. It was demonstrated that platelet adhesion to the SNAP-heparin bearing surface reduced more than 84% comparing to control medical grade silicone rubber tubing and while there were clearly visible. Moreover, in a 4 h *in vivo* extracorporeal circuit (ECC) model on a rabbit model, Devine et al. reported less than 20% platelet

consumption by NO releasing silicone rubber circuits, while the control tubes were completely occluded within the 2 h of the study with a visible blood clot.

Chemical immobilization of an NO donor molecule to the polymeric backbone can reduce the risk of leaching problems and depletion of NO reservoir, hence, enhance the NO delivery kinetics. Hopkins et al. covalently attached SNAP molecule to PMDS matrix to create a highly stable NO releasing polymeric platform capable of releasing NO with a flux higher than 0.5×10^{-10} mol cm^{-2} min^{-1} for over a month and a release period of 125 d [59]. The antibacterial efficacy of the SNAP-PDMS films was evaluated using a CDC bioreactor model analysis by which they showed 4-, 3-, and 2-log reduction in viable bacteria adhered to the surface of treatment films compared to control PDMS over 3, 14, and 28 days respectively.

1.3.2 Blood Compatible Sensors

It is invaluable to measure the blood gas and electrolyte levels in a real-time manner with high accuracy. However, due to prevalent blood compatibility issues, these sensors tend to exhibit erratic analysis performance and therefore, most of the measurements are being done *in vitro* instead of *in vivo,* leaving an extra burden on clinical practices and finally being less efficient than a real-time sensor could have been [68]. Noteworthy, the main obstacle in utilizing real-time indwelling sensors remains to be platelet adhesion and blood clot formation on the sensor occluding on the surface of the detectors, leading to the misreading of the values due to enforced changes to the normal environment of the sensor (altered pH, O_2, and CO_2 levels due to adsorbed cells, etc.), or becoming quiescent completely [69]. Frost et al. prepared an amperometry oxygen-sensing catheter using a NONOate-Si rubber composite ((*Z*)-1-[*N*-methyl-*N*-[6-(*N*-methylammoniohexyl)amino]]-

diazen-1-ium-1,2-diolate, abbreviated as DMHD-6/NONOate was used as the NO donor) [70]. This composite was used as the topcoat to the O_2 detector. It was demonstrated that with the continuous release of NO from the topcoat of the sensor, with a flux of over 10^{-10} mol cm^{-2} min^{-1} for more than 20 h, the partial pressure of oxygen (PO_2) values measured by the implanted sensor were significantly similar to the *in vitro* measurements while the values obtained from a non-coated implanted sensor deviated significantly from the *in vitro* results to be lower than the accurate numbers. More recently, Zhang et al. designed an NO-releasing intravascular (IV) potentiometric sensor for measuring partial pressure of carbon dioxide (PCO_2) [71]. The fabrication of the sensor took place by top coating a dual lumen catheter type silicone tube in which the sensor was placed. The coating portion of the fabricated device contained SNAP that enabled the sensor to release NO with a flux between ~19 – 0.5 × 10^{-10} mol cm^{-2} min^{-1} over the course of 8 d with the highest release measured on day 0 and the least on day 8. The results from a 20 h *in vivo* porcine model illustrated significant clot forming reduction ~80 mm to ~5 mm on the control group comparing to NO-emitting sensors. Moreover, the accuracy of PCO_2 measurements on the control group significantly decreased after only 2 h of sensor implantation in the femoral artery of the same animal with an overestimated values due to metabolic activity of cells trapped inside the clot region around the sensor. Fabrication of these types of sensors is a promising application devoted to the usage of NO technology and can be a beneficial asset in clinical practices where long-term accurate measurements of the blood gas and electrolyte levels in a real-time is required.

1.3.3 Antibacterial Applications

Many studies have used multiple agents to combat bacterial infections. For instance, usage of methicillin, vancomycin, cefazolin, and β-lactams in orthopedic and cardiac surgery [72-75]. With the rather increasing problem of multidrug-resistant bacteria, the urge to find more effective and suitable solutions to impede bacterial infections as well as attachment and biofilm formation on medical devices necessitates more thorough studies [76]. For many years researchers and pharmaceutical industries were focused on developing robust, individual antibiotics has led to the challenge of antibiotic resistance almost nowhere since not only the new chemicals are merely the same, but bacteria tend to establish a resistance to the newly introduced agents within only 2 years [77]. Furthermore, bacteria possess a survival strategy which makes it even less susceptible to conventional antibiotics, and that is to form multicellular communities which are protected from their surrounding environment by a polymeric matrix, known as biofilms [78]. Biofilms are 1000 times harder to be disrupted and eradicated comparing to freely floating or in another word, planktonic bacteria [22]. Conversely, after the discovery of NO biocidal properties, many promising results have been obtained, showing the efficacy of NO against a growing list of organisms such as bacteria, fungi, viruses, and also against biofilms [79-81]. In addition, Privett et al. studied the inability of bacteria in fostering resistance mechanisms against NO [82]. The evaluation of potential development of NO resistance was done by using spontaneous and serial passage mutagenesis assays on multiple bacteria organisms including *Staphylococcus aureus* (*S. aureus*), Methicillin-resistant *S. aureus* (MRSA), *Staphylococcus epidermidis* (*S. epidermidis*), *Escherichia coli* (*E. coli*), and Pseudomonas aeruginosa (*P. aeruginosa*). After 20 d of passaging the

bacteria strains that were exposed to NO with concentrations below MIC values, in both spontaneous and serial passage metagenesis assays, none of the strains developed resistance to NO which was demonstrated by evaluating the MIC values to find out that the values remained the same for initial passages before exposure to NO and after 20 d persistent of exposure. These antibacterial properties of NO have made it a promising agent in combating bacterial infection in hospital settings. While the required dose of NO for killing bacteria is 200 ppm, it has been reported that NO in lower doses is capable of preventing planktonic bacteria from adhering and colonizing on the surface of medical devices [17, 83].

One of the major problem in long-term hospitalized patients as well as critical-care patients who need central venous catheter (CVC) is the infection problem related to catheter implantations and according to Centers for Disease Control and Prevention (CDC) reports a significant number of people (approximately 30,000 to 200,000 patients) are suffering from catheter-related bloodstream infections (CRBSIs) every year only in the United States [84]. The infection problem in CVC application can be addressed by the usage of antibacterial lock solutions [85]. Kumar et al. created a novel catheter lock solution using *S*-Nitroso-*N*-acetyl-l-cysteine Ethyl Ester (SNACET) to utilize the antibacterial properties of NO in a lock solution. It is shown in their studies that a SNACET lock solution with 75 mM concentration is capable of having a flux of NO over 3×10^{-10} mols cm^{-2} min^{-1} after 18 h of being in physiological conditions and it can reduce bacterial adhesion to the surface of a medical-grade silicone rubber tubing more than 99% against both Gram-negative *E. coli* and Gram-positive *S. aureus*. Of note, in an attempt in evaluating the lock solution's ability in combating established bacterial infection, Kumar

et al. observed that the SNACET lock solution was effective in dispersing >90% of adhered bacteria to the outer wall of the tubing even without coming in direct contact with the bacterial bacteria within 2 h of injection in the lumen of the silicone tube [35].

Finally, it has been reported that bacteria under the right conditions and time produce a robust extra polymeric substance (EPS) and colonize within the EPS, forming biofilms difficult to disperse [86, 87]. So far, one of the most promising treatments to these harsh infection conditions is NO-releasing substrates that not only can prevent biofilm formation but can also disperse the biofilm it comes in contact with [88-90].

1.3.4 Wound Healing Applications

Wounds can be generally defined as the loss of physical integrity in a tissue due to external and internal damaging stimuli such as malignant physical, chemical, electrical reciprocations, aging, or cell death [91]. After the onset of tissue damage, almost immediately, processes begin in a sequential as well as simultaneous order of events that are mostly related and constituents of a process well defined as wound healing [92, 93]. Although wound healing is a highly complex procedure that contains many physiological actions and is still not completely understood, numerous studies focus on developing new methods of manipulation to facilitate the process of healing. In fact, this is one of the most ancient biological investigations that mankind has been practicing from the dawn of history by using herbals like aloe vera, achillea, Curcuma longa, Ginko Biloba green leaves, or natural substances like honey, ghee, or even mud and clay, boosting the wound healing process [94-96]. When an injury happens, the wound healing process consisting of four significantly distinctive steps starts immediately. In the four-phase definition of wound healing, the process starts with hemostasis. Afterward, inflammation occurs, followed by

the proliferation phase, and the remodeling phase which is the final stage of wound healing [97, 98]. However, there is a common three-phase definition of wound healing in which hemostasis and inflammation are considered as one step [99]. Independent of the number of phases speculated in the process of wound healing, there is a substantial number of events emerging from every phase, not necessarily ending before the initiation of the following step. Briefly, in the first stage, hemostasis (i.e., both intrinsic and extrinsic coagulation cascades) initiates majorly to inhibit and suppress blood loss [100]. While it is generally accepted that hemostasis and inflammation are two peculiar steps, they can interfere and overlap [101]. For instance, while blood clotting is in progress, vasoconstriction promotes more platelet activation and thrombocyte aggregation. Vasodilation consequently nourishes the injury site with more leukocytes, which are the critical components for the second phase –inflammation. White blood cells (WBC) are vital to the inflammation phase. While neutrophils, eosinophils, and basophils are engulfing the wound site, phagocytosis, reactive oxygen species (ROS), and protease secretion, as well as angiogenesis signaling, initiate by WBCs and can last up to 7 days. As the inflammation phase winds up, proliferation/granulation begins with the formation of fibrous tissue (fibroplasia), new blood vessels (angiogenesis), new epithelial cells (re-epithelialization), as well as new extracellular matrix (ECM) deposition. Finally, the remodeling/maturation phase orchestrated by newly formed fibroblast cells occurs after wound closure, with degradation and reorganization of collagen compound in the wound site, which can last from weeks to years [91, 97]. These highly complex processes can easily deviate from their preferred path, leading to non-healing, chronic wounds, fragmented, impaired tissue, or scar remnants [98, 99, 102]. Especially wound healing

can go awry in the presence of challenging risk factors, such as diseases [103], high age [104], bacterial infection [105], mechanical constraint [106], enzymatic stress [107], hypoxia, and ischemia [108, 109].

One of the signaling molecules which plays a pivotal role in wound healing procedure, is NO [7]. Many recent studies have shown that NO can accelerate and facilitate wound healing by participating in many stages of the wound healing process [110]. Enhanced ECM secretion from fibroblast cells [111], increased fibroblast and keratinocyte cells proliferation, differentiation, and migration [112], modulated inflammation by attracting cytokines including interleukin (IL)-8, TGF-β1, monocytes, and neutrophils, and escaladed angiogenesis [113] are proven to be the effects of NO on wound healing in numerous studies. Given all the processes and challenges that wound healing is facing and the benefits of NO in physiological conditions in a proper concentration, it is obvious that the usage of NO in wound healing technologies is a promising research subject [114]. Taleb et al. illustrated the role of NO in metformin pretreatment to increase skin flap survival [115]. They showed that the survival rate of skin flap by 150, 200 and 300 mg/kg metformin administration is directly related to the amount of NO production in a rat model. It was shown that by applying an NO synthase inhibitor N-nitro-L-arginine methyl ester hydrochloride (L-NAME) the effect of metformin is abolished and on the contrary, by administrating L-arginin, which leads to more NO production, even subtherapeutic amounts of metformin exhibited higher protection [115].

As it was mentioned earlier the inducible nitric oxide synthase (iNOS) is produced only in response to acute inflammatory stimuli, and it is realized that the concentration of iNOS significantly exceeds that of the other two constitutive NO producing enzymes (i.e.

eNOS and nNOS) in the event of wounding [116]. The excess amount of NO being produced by iNOS in the wound site will increase the NO concentration to the nM–μM region which corresponds to antibacterial behavior of NO as well as proinflammatory activity of NO [117]. Therefore, in initial wound healing phases NO in high concentration plays a pivotal role in regulating the inflammation response and reducing pathogenic infections. After the initial stages of wound healing and the depletion of iNOS the lower concentration of NO in the range of pM–nM produced by the other two enzymes with take part in regulating angiogenesis, proliferation, and tissue maturation [118, 119]. With a downstream effects on the recruitment of keratinocytes, NO regulates the cytokines (e.g. monocytes, neutrophils, and interleukins) that initiate inflammation [118].

Indeed, in the very initial stages of injury the healthy healing process starts with platelet activation/aggregation and clot formation that leads to blood loss inhibition. Even in the initial stage, NO plays a critical role, although in this case, reduction in NO concentration in response to ROS production from injured vasculature provides the opportunity for platelets to get activated and adhere to the site of injury [120].

In order to deliver NO into the wound site in a sustainable, and controlled manner, hydrogels seem to be reliable matrices due to their structural advantages such as ease of fabrication and workability, maintaining a moist and O_2 permeable environment, elasticity, and strength [121]. Amadeu et al. fabricated a GSNO blended Pluronic F-127 hydrogel to test the wound healing efficacy of their composition on a rat model excisional wound model [122]. By applying the GSNO containing gel on a dorsal level of the wound on a daily basis for 4 days, they observed improved wound contraction, reduced inflammatory cells, and increased collagen deposition, fibroblast proliferation, and the number of mast

cells. Overall, the study showed improved wound healing and 77% more wound reepithelization. In a more recent study, Póvoa et al. fabricated an NO releasing collagen spung (CS) containing GSNO that was capable of releasing total amount of ~1.7 nmol mg^{-1} of NO in 150 min upon exposure to humid environment [123]. It was indicated that the topical delivery of NO to the wound site increases the collagen deposition, neovascularization, and migration and infiltration of leucocytes, macrophages, and keratinocytes into the wound site which are all related to the facilitated and accelerated wound healing process.

1.4 Nitric Oxide Delivery Systems

While the role of NO in biological functions is well established, the ongoing challenge and the research topic in the spotlight remained to be targeted delivery of NO in a sustainable and controlled manner. Although numerous NO donor molecules are developed to deliver NO in different fashions, the main problem is the instability of most of the well-known NO donor molecules [124]. To improve the stability and achieve targeted delivery of NO to specific tissues or biointerfaces, many substrates such as synthetic and natural biopolymers [125-127], polydimethylsiloxane (PDMS) [128-130], polyurethanes (PU) [131-133], liposomes, micelles, and nanoparticles, have been developed to carry NO donor molecules.

Incorporating NO donor molecules into medical devices, and biomedical substrates has been shown to increase their hemocompatibility, antibacterial efficacy, and thromboresistance [7]. There are several reports about RSNO-biomaterial incorporation techniques such as simple physical blending, solvent swelling, and covalently conjugating

[17, 60, 129, 134-138]. While blending and impregnating polymers with NO donors can increase the stability of NO donors and increase the NO-releasing time, the covalent conjugation of NO donors is considered one of the most promising techniques since it regulates the undesired leaching and loss of NO donors, eventually increasing the biomaterial applicability [139]. Another approach to achieve sustained NO release is by conjugating NO donors to nanoparticles. Frost et al. introduced covalent attachment of the RSNO moiety to fumed silica nanoparticles that can be used as a filler within a polymeric matrix to prevent leaching and loss of NO donors [140]. Grommersch et al. also utilized nanoporous diatomaceous silica earth nanoparticles to deliver NO molecules through chemical surface modifications [141]. Malone-Povolny et al. modified porous and nonporous silica nanoparticles to covalently bound an RSNO structure to the particles [132]. Ghalei et al. recently reported the conjugation of SNAP molecule to halloysite nanotubes [142]. However, initial burst release, low payload, a short period of NO release, and imposed cytotoxicity left the quest to explore nano substrate that can provide longer NO release, higher yield, and conversion rate with low cytotoxicity, and finally, better biocompatibility ongoing.

The propitious usage of nanoparticles in medicine has been on a rise for the past decades as it can be rewarding under many circumstances. Not only do they possess beneficial applications solely due to their unique properties, linking a therapeutic agent to nanoparticles can enhance their selectivity and targeted delivery, induce multifunctionality, moderate side effects, amplify therapeutic efficacy and impede systemic cytotoxicity [143, 144]. Among all of the nanoparticles, titanium dioxide (TiO_2) nanoparticles (TiNPs) have been given prominent attention for the past decades, owing to their unique properties such

as chemical stability, hydroxyl-rich surface, biocompatibility, non-toxicity to mammalian cells, hypoallergenicity, photodynamic properties, high refractive index, and relevantly low cost [145]. Titanium dioxide nanoparticles have been used extensively in great number of applications (**Figure 4**) anti-cancer therapy [146, 147], photoactivated antibacterial surface coatings [148-150], biosensors [151], cosmetics [152], food and drug colorant [147], water treatment technologies [153, 154], anti-corrosion applications [155], and white paint production [156, 157]. Furthermore, the antibacterial capacity of TiNPs under UV irradiation technics has been extensively studied and exploited for years, although there are concerns for utilization of UV irradiation as it can induce adverse effects such as cell death and host tissue cell necrosis [147, 152]. Therefore, extensive research is being done to improve TiNP antibacterial efficacy by embedding other elements to the TiNP structure to obtain higher bactericidal efficacy, facilitate, or even obviate light activation of the particles [145, 147, 158].

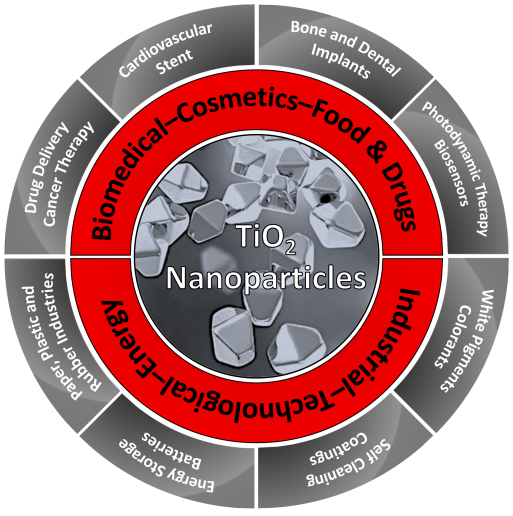

Figure 4. Titanium dioxide nanoparticle applications in industries and biomedical engineering.

Other than the mentioned methods to deliver NO to the targeted area (e.g. medical devices, cancer tumor, etc.) the topical delivery of NO in wound healing, as mentioned before, is proven to be immensely beneficial. Therefore, fabricating materials that can stabilize NO donor molecules, and release them upon topical application can be very promising approach in the application of NO in wound healing [123].

Among all the NO delivery vehicles, gels and hydrogels have attracted so much attention in wound healing applications due to some of the unique properties they possess. Workability, good swelling capacity, maintaining physical integrity and flexibility, impeding initial burst release of NO, and highly porous structure are the properties that make hydrogels appealing candidates for wound healing and topical drug delivery applications [159, 160]. Hydrogels can be fabricated from natural and synthesis biocompatible polymers. Chitosan, alginate, and gelatin as some of the well-known natural biopolymers used in fabricating wound healing hydrogels [161-163]. Polyethylene glycol (PEG), polylactic acid (PLA), polyvinyl alcohol (PVA), and polyglycolic acid (PGA), and so many other synthetic polymers also have been utilized solely and in combination with other compounds to produce wound healing hydrogels [164-166].

One of the hydrogel materials that possess a reverse thermal gelation characteristic is Pluronic F-127 (PF-127, Poloxamer 407) which is one of the copolymers from poloxamer ABA three-block structures comprised of poly(ethylene oxide)-poly(propylene oxide)-poly(ethylene oxide) (PEO-PPO-PEO) units (**Figure 5**) [167, 168].

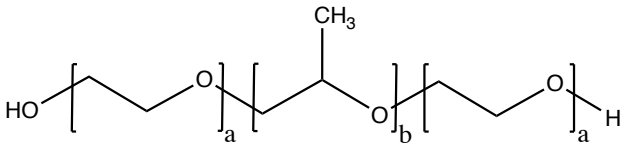

Figure 5. Pluronic F-127 is one of the copolymers from poloxamer ABA three-block structures where a and b in the general chemical structure will be 100 and 65 respectively.

The three-block structure of PF-127 with hydrophilic PEO and hydrophobic PPO units enables the polymeric matrix to self-assemble micelles in an aqueous environment [169]. Due to the reverse thermal gelation behavior of F-127, the hydrogel forms a gel in elevated temperatures (ambient and body temperatures) as opposed to lower refrigerated temperatures (0-4 °C) in which it acquires a liquid form [170].

It has been reported by Kant et al. that PF-127 is capable of enhancing wound healing if applied to a cutaneous wound [159]. It is reported that a gel comprised of 25% PF-127 in a normal saline solution applied topically on open excision wounds for 14 days (once a day), can increase wound contraction compared to a normal saline-treated control group on days 7 and 14. The effect of topical application of PF-127 expands from increased expression of vascular endothelial growth factor (VEGF) and transforming growth factor-beta1 (TGF-β_1), to increased proliferation of fibroblast cells, microvessels density, and finally, ECM production (collagen deposition), all of which lead to a faster and more effective wound healing [171-173]. One of the special characteristics of PF-127 is its reversible gelation process, which facilitates the incorporation of NO donors into its matrix at low temperatures where the NO donor molecule is more stable and the liquid PF-127 is easier to work with [168]. It is noteworthy that PF-127 has been approved by the US Food and Drug Administration (FDA) to be used in healthcare systems and it has been used in many clinical practices such as cancer treatment, wound healing, drug delivery, etc. that

has been reviewed thoroughly by Akash et al. [169]. Additionally, PF-127 can directly alter some cellular activities by translocating into the cells and mediating mitochondrial respiration, transducing apoptosis signaling, and especially mitigating drug efflux transporters such as breast cancer resistance protein (BCRP), multidrug resistance proteins (MRPs), and P-glycoprotein (P-gp) that will lead to more efficacy of the cancer therapy drugs [174]. Moreover, some of the research outcomes offer the efficacy of PF-127 in passing through the blood brain barrier (BBB) and facilitating targeted delivery of bioactive drugs [175].

As briefly mentioned before, NO can accelerate wound healing by participating in many stages of the wound healing process [110]. Enhanced ECM secretion from fibroblast cells [111], increased fibroblast and keratinocyte cells proliferation, differentiation, and migration [112], modulated inflammation by attracting cytokines including interleukin (IL)-8, TGF-β1, monocytes, and neutrophils, and escaladed angiogenesis [113] are proven to be the effects of NO on wound healing in numerous studies. Of course, the problem of NO delivery in the wound site can still be a major obstacle to translational applications. There are research attempts trying to encapsulate NO donors into PF-127 to increase its stability and controlled release [176, 177]. Studies have illustrated the prolonged release of NO and reduced burst release while GSNO donors are incorporated in the PF-217 matrix [168, 178-180].

1.5 Hypothesis and Objective

The application of NO in biological settings are copious and according to numerous explicit and authentic research outcomes, NO is proven to be a very strong asset to facilitate

the healing processes in many health conditions, while it possesses a strong and broad range of antimicrobial activity. Therefore, investigating novel ways to increase the NO applicability, controlled and stable delivery in biomedical settings with less leaching and cytotoxicity issues can expand its implementation capacity to address more healthcare issues. To this end, development of new NO releasing agents and substrates like nanoparticles and hydrogels will expand the opportunity in utilizing NO application in biomedical engineering and health care systems. Here we describe two new NO delivery systems by 1) chemically modifying TiO_2 nanoparticles and 2) physical blending of SNACET molecule to Pluronic F-127 gel.

Therapeutic agents can be linked to nanoparticles to fortify their selectivity and targeted delivery while impeding systemic toxicity and efficacy loss. Titanium dioxide nanoparticles (TiNPs) owe their rise in biomedical sciences to their versatile applicability. In this study, TiNP is used as a novel NO delivery substrate for the first time with a chemical immobilization of an NO donor molecule to the nanoparticles. The hydroxyl-rich surface of TiNP provided the opportunity for silane functionalization of the nanoparticles using an amino silane agent, (3-Aminopropyl)triethoxysilane (APTES), and further, free amine functional groups enabled covalent conjugation of N-acetyl-d-penicillamine (NAP) thiolactone as the precursor of the NO donor molecule SNAP. Finally, nanoparticles equipped with thiol functionality underwent nitrosation reaction using *tert*-butyl nitrite to generate SNAP conjugated TiNPs (TiNP-SNAP). Fourier transform infrared spectroscopy (FTIR), nuclear magnetic resonance (NMR), and electron dispersive X-ray spectroscopy (EDS) analyses are used to evaluate the quality of surface modifications and scanning electron microscope (SEM) imaging is utilized to evaluate their

morphological retention throughout the course of modifications. Ninhydrin and Ellman's assays are employed to measure the quantity of amine and thiol functional groups embedded on the nanoparticles, and chemiluminescence is used to determine the NO payload and release behavior. Furthermore, *in vitro* evaluations are conducted to evaluate the cytocompatibility of the TiNP-SNAP nanoparticles and their antimicrobial efficacy against Gram-positive *Staphylococcus* aureus and Gram-negative *Escherichia coli* bacteria strains.

It is established that NO can be a potential wound therapeutic agent owing to its ability to regulate inflammation and eradicate bacterial infections. To utilize NO for wound healing, two general strategies have been practiced; exploiting endogenous reservoirs to liberated NO through catalytic reactions or injection of agents to increase NO production, or supplementing NO using an exogenous source. Moreover, the usage of NO as a single wound healing agent which is capable of delivering multiple signaling functionalities increases its merit and versatility and offers a very promising solution to the wound healing challenges and complications that aroused by it. In this study, for the first time, the exogenous delivery of NO using SNACET as a small NO donor molecule was evaluated by utilizing a thermo-responsive Pluronic F-127 hydrogel. It was hypothesized that incorporation of SNACET molecule into the hydrogel structure will facilitate NO's topical application and will improve Pluronic hydrogels' application in wound healing by implying antibacterial activity with a concentration dependent behavior. To this end, different weight percentages (i.e. 1, 2, and 5 wt%) of SNACET molecule was incorporated to Pluronic using an aqueous solutions of 30% (w/v) F127 prepared in PBS (10 mM, pH 7.4) containing 100 μM EDTA. Furthermore, the NO release behavior of the structure was

evaluated using a real time NO analyzer (NOA). The storage stability and antibacterial activity of the SNACET-Pluronic gel also was evaluated to illustrate its potential future applications in wound healing.

CHAPTER 2

NITRIC OXIDE RELEASE AND ANTIBACTERIAL EFFICACY ANALYSES OF *S*-NITROSO-*N*-ACETYL-PENICILLAMINE CONJUGATED TITANIUM DIOXIDE NANOPARTICLES

2.1 Introduction

As mentioned earlier, titanium dioxide nanoparticles have been used extensively in anti-cancer therapy, photoactivated antibacterial surface coatings, biosensors [146-151], and many more applications in technological and industrial fields. Furthermore, antibacterial capacity of TiNPs under UV irradiation techniques has been extensively studied and utilized for years, although there are concerns for utilization of UV irradiation as it can induce adverse effects such as cell death and host tissue cell necrosis [147, 181]. Therefore, research is being done to improve TiNP antibacterial efficacy by embedding other elements to the TiNP structure to obtain higher bactericidal efficacy, facilitate, or even obviate light activation of the particles [145, 147, 158].

In this study, TiNP is used as a novel NO delivery material for the first time with a chemical immobilization of an NO donor molecule to the nanoparticles. The hydroxyl-rich surface of TiNP provided the opportunity for silane functionalization of the nanoparticles using an amino silane agent, (3-Aminopropyl)triethoxysilane (APTES), and further, free amine functional groups enabled covalent conjugation of *N*-acetyl-D-penicillamine (NAP) thiolactone as the precursor of the NO donor molecule SNAP.

Finally, nanoparticles equipped with thiol functionality underwent nitrosation reaction using *tert*-butyl nitrite to generate SNAP conjugated TiNPs (TiNP-SNAP). Fourier transform infrared spectroscopy (FTIR), nuclear magnetic resonance (NMR), and electron dispersive X-ray spectroscopy (EDS) analyses were used to evaluate the quality of surface modifications and scanning electron microscope (SEM) imaging revealed their morphological retention throughout the course of modifications. Ninhydrin and Ellman's assays were utilized to measure the quantity of amine and thiol functional groups embedded on the nanoparticles, and chemiluminescence was used to determine the NO payload and release behavior. Furthermore, *in vitro* evaluations were conducted to evaluate cytocompatibility of the TiNP-SNAP nanoparticles and their antimicrobial efficacy against Gram-positive *Staphylococcus aureus* and Gram-negative *Escherichia coli* bacteria strains.

2.2 Materials and Methods

2.2.1 Materials

TiNP (Nanopowder 99.5%, 10-30 nm anatase and rutile mixture) was purchased from SkySpring Nanomaterials Inc. (Houston, USA). *N*-acetyl-D-penicillamine (NAP), (3-aminopropyl)triethoxysilane (APTES), cyclam, potassium bromide (KBr), anhydrous toluene, L-cysteine hydrochloride monohydrate (≥ 98.0% purity), ninhydrin reagent (2% solution), Ellman's reagent (5,50-dithiobis(2-nitrobenzoic acid), DTNB) (≥ 98.0% purity), glycine hydrochloride (≥ 99.0% purity), Luria-Bertani (LB) broth, and LB broth with agar media powders, ethylenediaminetetraacetic acid (EDTA), sterile phosphate buffer saline (PBS) powder 0.01 M, pH 7.4, containing 138 mM NaCl, and 2.7 mM KCl, were purchased from Sigma-Aldrich (St. Louis, MO). Absolute ethanol (≥ 99.8% purity), anhydrous

pyridine, acetic anhydride, chloroform, Acros Organics copper (II) chloride dihydrate (≥ 99% purity, hexane, hydrochloric acid (technical grade), isopropanol, acetone, and *tert*-butyl nitrite were purchased from Fisher Scientific (Hampton, NH). Sodium acetate (NaAc) was obtained from VWR International (West Chester, PA). The bacteria strains *S. aureus* (ATCC 6538) and *E. coli* (ATCC 25922), and the 3T3 mouse fibroblast cells (ATCC 1658) for cell compatibility experiments were purchased from American Type Culture Collection (ATCC). Dulbecco's modified Eagle's medium (DMEM) and trypsin-EDTA were purchased from Corning (Manassas, VA). The antibiotic mixture of Penicillin-Streptomycin and fetal bovine serum (FBS) were obtained from Gibco-Life Technologies (Grand Island, NY). Colorimetric assay Cell Counting Kit-8 (CCK-8) with WST-8 monosodium salt was obtained from Sigma Aldrich (St. Louis, MO). Deionized water (DI water) was used to prepare all aqueous solutions. PBS 0.01 M containing 100 μM EDTA was used in the material characterizations and NO analysis experiments unless noted otherwise.

2.2.2 TiNPs Surface Silanization

The surface silanization of nanoparticles was carried out following the previously reported protocol with slight modifications [155]. Briefly, TiNP (3 g) was dispersed in an aqueous hydrochloric acid solution (pH 2) using an ultrasonic water bath for 1 h at room temperature (RT). Further, the nanoparticles were washed with DI water followed by centrifugation (Allegra X-30 Series Benchtop Centrifuge, Beckman Coulter, Brea, CA) at 12,000 rpm for 10 min (three times) and two times with isopropanol and one time with acetone to remove impurities, such as chloride ions, and absorbed moisture. Finally, the particles were centrifuged and dried overnight in an oven at 120 °C. The purified TiNPs

were then dispersed in dry toluene (100 mL) using a sonication bath for 30 min in a nitrogen atmosphere. For surface silanization, 3 mL (3-aminopropyl)triethoxysilane (APTES) was added to the TiNPs dispersion and refluxed at 120 °C for 12 h under a nitrogen atmosphere with constant stirring to obtain TiNP-APTES. The particles were centrifuged at 12,000 rpm for 10 min, washed with dry toluene several times to remove any unreacted APTES, and dried overnight in the oven at 100 °C.

2.2.3 SNAP Functionalization of TiNP-APTES

2.2.3.1 N-acetyl-D-penicillamine (NAP) Thiolactone Synthesis

The NAP-thiolactone was synthesized by following the reported procedure [182]. Briefly, 5 g of NAP was dissolved in 20 mL of pyridine in a round bottom flask and chilled in an ice bath for 30 minutes. Ice-cold acetic anhydride (10 mL) was slowly added to the reaction mixture and stirred for 30 minutes. Afterward, the reaction mixture was removed from the ice bath and stirred at RT for 20 h. Following the completion of the reaction, pyridine was removed from the reaction mixture using a rotary evaporator (IKA RV 10 auto pro V-C) to obtain an orange crude residue. The crude residue was dissolved in 20 mL of chloroform, washed, and rinsed three times with 20 mL of 1 M HCl. The organic layer was dried over anhydrous sodium sulfate and filtered. The chloroform was removed using the rotary evaporator to obtain crystalline solid, which was further washed with hexane to remove the colored impurity and dried to obtain a light yellow colored pure NAP-thiolactone.

2.2.3.2 NAP Attachment to TiNP-APTES

NAP attachment to dried TiNP-APTES was done with slight modifications of a protocol published by Frost et al [183]. The silanized TiNP-APTES (1 g) was

homogeneously dispersed in dry toluene (15 mL) using a sonication bath for 30 min followed by the addition of NAP-thiolactone (500 mg). A tethering reaction took place within 24 h under vigorous stirring in the dark at RT. The TiNP-NAP was obtained by centrifuging the mixture at 12,000 rpm for 10 min, and the obtained powder was washed with dry toluene three times prior to the drying step. Obtained TiNP-NAP after washing steps was left in a desiccator for 24 h and at RT to dry.

2.2.4 Nitrosation and SNAP Functionalization

Synthesized TiNP-SNAP, as the final product, was obtained using an established SNAP conjugation reaction protocol (nitrosation), with minor changes [183]. Briefly, tert-butyl nitrite first was chelated of any copper contamination by mixing an equal volume of it with 20 mM cyclam solution with vigorous shaking three times. Each time, the *t*-butyl nitrite layer was isolated from the contaminated portion of the mixture. Finally, the chelated and pure *t*-butyl nitrite was refrigerated at 4 °C in an amber vial to be protected against the light for further usage. Previously modified TiNP-NAP (500 mg) was homogeneously dispersed in 7.5 mL dry toluene using 30 min of sonication. Cleaned *t*-butyl nitrite (500 µL) was added to the mixture, and the reaction mixture was stirred at RT for 1 h to obtain TiNP-SNAP. The product was washed with dry toluene several times and isolated from the mixture using centrifugation at 12,000 rpm for 10 min and kept in a desiccator for 30 h at RT to dry and kept at –20 °C for further usage.

2.2.5 Primary Amine Quantification

To measure the surface silanization efficiency and quantify the amount of amine groups introduced to the surface of TiNP, a ninhydrin assay was implemented. Briefly, TiNP-APTES were dispersed in 0.05% glacial acetic acid (0.2 mg/mL) and were mixed

with ninhydrin reagent (1 mL) in an amber vial. The mixture was kept in a boiling water bath for 10 min. Thereafter, the mixture was left to cool down to RT and 95% ethanol (5 mL) was added to the mixture to make the final volume of 8 mL. The mixtures were centrifuged at 12,000 rpm for 10 min to separate the nanoparticles from the reaction solution. The absorbance value of the reaction solutions at 570 nm was determined using a UV-vis spectrophotometer (Cary 60, Agilent Technologies, Santa Clara, CA). To quantify the amine content using the UV-vis absorbance values, a calibration curve of known amine content was made using glycine hydrochloride with the molar absorptivity of 7.36×10^3 M^{-1} cm^{-1}.

2.2.6 Thiol Content Quantification

The quantity of thiol groups on the surface of TiNP-NAP was measured using Ellman's assay [141]. Briefly, DTNB (5,50-dithio-bis-[2-nitrobenzoic acid]) solution containing 2 mM DTNB and 50 mM sodium acetate (NaAc) was prepared and (50 µL) mixed with PBS (100 µL), DI water (800 µL), and the sample (50 µL). The absorption values at a wavelength of 412 nm were recorded using UV-vis spectroscopy. l-cysteine with a molar absorptivity of 14.16×103 M^{-1} cm^{-1} was used to generate a calibration curve of known thiol concentration and was used to determine the thiol content of unknown samples.

2.2.7 Fourier-Transform Infrared Spectroscopy (FTIR) and Nuclear Magnetic Resonance (NMR) Analysis

The surface modification and further successful functionalization of TiNPs were analyzed by Fourier transform infrared spectroscopy (FT-IR) using PerkinElmer Spectrum 3 FT-IR spectrometer. The TiNP powders before and after modification were mixed with

potassium bromide (KBr) with a ratio of 1:100 and formed into a disk for FT-IR analysis. Each spectrum was collected over a wavenumber range of 500 and 4000 cm^{-1} with a scan rate of 16 and a resolution of 8 cm^{-1}. Bruker NEO 600 MHz spectrometer was used for Solid-state cross-polarization magic angle spinning carbon-13 nuclear magnetic resonance (CP/MAS 13C NMR) analysis. Due to low carbon count, the CP/MAS 13C NMR spectra for TiNP-APTES particles were obtained from the summation of 8 spectra at 256 scans at a spinning speed of 10 kHz. However, for TiNP-NAP, a well-resolved 13C NMR spectrum was observed from the single spectra at 256 scans at a spinning speed of 10 kHz.

2.2.8 Morphological and Surface Analysis

2.2.8.1 Dynamic Light Scattering (DLS) and Zeta Potential Measurements

The Zeta potential of the particles was estimated using a Zetasizer nano-ZS ZEN3600 (Malvern instruments Ltd. US) at different surface modification stages to evaluate their colloidal stability. Moreover, the dynamic light scattering (DLS) analysis was also employed to evaluate the average particle size at different modification stages. Following the previously established protocol [156], with slight modifications, TiNPs, TiNP-APTES, TiNP-NAP, and TiNP-SNAP were dispersed in DI water (0.05 mg mL^{-1}) using a sonication bath for 30 min. Before running the instrument, each suspension was vortexed for 2 min and left to settle for 1 min.

2.2.8.2 Scanning Electron Microscopy Analysis

Field emission scanning electron microscope (FESEM - FEI Teneo, FEI, Inc., Hillsboro, OR, USA) equipped with an Energy dispersive X-ray spectroscopy (EDS) detector was employed to observe the morphological changes in the nanoparticles at different stages of modification. Nanoparticles were dispersed in DI water (0.1 mg mL^{-1})

for adhesion on a double-sided adhesive carbon tape on the aluminum specimen mount, dried overnight under ambient conditions, and sputter coated with gold-palladium using Leica EM ACE600 Coater. Samples were imaged using the scanning electron microscope at a working distance of 10 mm at 10 kV. Furthermore, the qualitative investigation of successful surface modification and SNAP functionalization of TiNPs was done using EDS to identify the sulfur element (S) dispersion as well as oxygen (O), carbon (C), and titanium (Ti) elements.

2.2.9 Nitric Oxide Loading Capacity and Release Kinetics of TiNP-SNAP Nanoparticles

Sievers chemiluminescence Nitric Oxide Analyzer (NOA) 280i (Zysense, Weddington, NC, USA) was utilized to analyze the real-time NO release behavior in terms of NO loading capacity and release kinetics under physiological conditions. Samples were prepared on the day of the experiment according to prior reported protocol with slight changes [141, 142]. The synthesized TiNP-SNAP (1 mg) was homogeneously dispersed in 1 mL 0.01 M PBS solution (pH 7.4) by 30 min of sonication (n = 3). The suspension further was transferred into a dialysis tubing with a molecular weight cut-off (MWCO) of 3.5–5 kDa secured at both ends to ease the operation process and facilitate the transfer of the nanoparticles to the sample cell of the instrument. Once the dialysis bags were submerged in PBS within the sample cell of the NOA, 0.25 M copper (II) chloride (1 mL) and 0.5 M ascorbic acid (1 mL) were injected into the NOA cell, which led to catalytic decomposition of the S–NO bond on the particles and release of the NO content loaded on the TiNP-SNAP. To obtain the total amount of loaded NO, the trapezoidal rule was used to calculate the area under the release curve [142].

The synthesized TiNP-SNAP (1 mg) was homogeneously dispersed in 1 mL 0.01 M PBS solution (pH 7.4) with 100 μM EDTA by 30 min of sonication (n = 3), followed by transfer to the dialysis bags as described above. To evaluate the NO release kinetics under physiological conditions, the dialysis bags were submerged in 3 mL 0.01 M PBS solution (pH 7.4) with 100 μM EDTA inside an amber NOA sample cell. The sample cell was incubated in a 37 °C water bath to maintain a physiological temperature and was supplied with pure nitrogen gas (N_2) at a constant flow of 200 mL min^{-1}. The cell pressure of the NOA cell was set to be 9.8 Torr with an oxygen supply pressure of 6.6 psi. The NO gas emitted from the TiNP-SNAP was purged by the N_2 and continuously swept by vacuum to the chemiluminescence reaction chamber where the concentration of NO molecule was measured within 1 s time intervals. To evaluate the release kinetics over 20 h, data were collected for each sample at several time points (0, 2, 4, 6, 12, 14, 16, and 20 h) until the release profile plateaued at a constant value. Samples were incubated in an incubator at 37 °C in 3 mL 0.01 M PBS (pH 7.4) incorporated with 100 μM EDTA inside an amber vial between measurements.

2.2.10 *In Vitro* Antibacterial Efficacy of TiNP-SNAP Over 24 h

To assess the antibacterial efficacy of the modified TiNP-SNAP, *S. aureus*, and *E. coli* were used as the representative Gram-positive and Gram-negative bacteria, respectively. An established 24 h direct contact assay was used to identify antibacterial behavior of TiNP-SNAP in comparison to control TiNPs dispersed in PBS (pH 7.4) with different concentrations (0.01, 0.1, and 5 mg mL^{-1}) [142]. An isolated colony of *S. aureus* and *E. coli* was inoculated in LB broth in a shaker incubator at 150 rpm at 37 °C. After 16 h, inoculums containing bacteria in their log-phase of growth were centrifuged at 3,500

rpm for 7 min, and the supernatants were decanted. The bacteria pellets were vortexed in sterilized PBS (pH 7.4). Obtained bacteria suspensions were centrifuged at 3500 rpm for 7 min again, and the pellets were resuspended in sterilized PBS using a vortex mixer. Sterile PBS was used to dilute the bacteria suspensions to obtain an approximate concentration of 10^7 colony forming units (CFU) in 1 mL PBS. Bacterial solution (100 µL) was mixed with 100 µL of different concentrations of TiNP-SNAP suspended in PBS (n = 4) in a 96-well plate. Bacteria containing wells without nanoparticles were used as negative controls. The plates were incubated at 37 °C in a shaker incubator at 150 rpm for 24 h while protected from exposure to ambient light. After incubation, 50 µL of solution in each well was plated on an LB agar plate using a spiral plater (EDDY JET 2W, IUL Instruments, Cincinnati, OH, USA) and then incubated at 37 °C for 24 h prior to counting the CFUs. An automated colony counter unit (SphereFlash IUL Instruments, Cincinnati, OH, USA) was used to determine the concentration of CFUs (CFU mL^{-1}) on each plate and consequently calculate the viable bacteria reduction of different test groups. The % reduction in bacterial viability was calculated according to Equation 1 below (where C = CFU mL^{-1}):

$$\text{Bacteria viability reduction}(\%) = \frac{C_{Control} - C_{Sample}}{C_{Control}} \times 100 \quad (\boldsymbol{Eq.\,1})$$

2.2.11 *In Vitro* Cell Viability Studies

Leachates from the particles (concentration of 0.01 – 5 mg mL^{-1}) were prepared following a previously reported protocol [141]. Briefly, 1 mL of each particle suspension in DI water was transferred into a 5 cm dialysis bag (molecular weight cut off = 3.5–5 kDa), secured at both the ends, and soaked in 10 mL of DMEM media supplemented with 10% fetal bovine serum and 1% penicillin−streptomycin for 24 h at 37 °C. After 24 h, the

dialysis bags were removed, and leachates were used for further assessment. The cytotoxicity evaluation of SNAP-TiNPs and control TiNPs was conducted as per the ISO 10993-5 in vitro cytotoxicity test. For this, NIH-3T3 mouse fibroblast cells at 5000 cells mL^{-1} were seeded into a cell culture treated 96-well plate and incubated in a humidified incubator at 37 °C, 5% CO_2 for 24 h. Leachates obtained from SNAP-TiNPs and controls were exposed to cells in a well plate (10 μL) and incubated for another 24 h in an incubator at 37 °C. The cell viability test was performed using cell counting kit–8 (CCK-8) in accordance with the manufacturer's protocol (Sigma, OH). CCK-8 dye (10 μL) was added to each well and incubated for 1 h, after which the absorbance of the cells was measured at 450 nm wavelength using a microplate reader (Cytation 5 imaging multi-mode reader, BioTek). Data obtained from the study are presented as relative cell viability of TiNP-SNAP samples compared to the control cells in DMEM media that received no treatment calculated using Equation 2 below, where A = Absorbance at 450 nm.

$$Relative\ cell\ viability\ = \frac{A_{TiNP} - A_{TiNP-SNAP}}{A_{cells\ in\ DMEM}}\ (\boldsymbol{Eq.2})$$

2.2.12 Statistical Analysis

All the data obtained in this study are reported as mean ± standard deviation (SD) with a sample size of 3 (n = 3) unless stated otherwise. To evaluate the statistically significant differences between values a standard two-tailed *t*-test was used and is presented in the form of *p*-values.

2.3 Results and Discussion

2.3.1 Chemical Surface Modifications

The NO-releasing SNAP-functionality was immobilized on the surface of the TiO_2 nanoparticles using thiolactone chemistry (**Figure 6**).

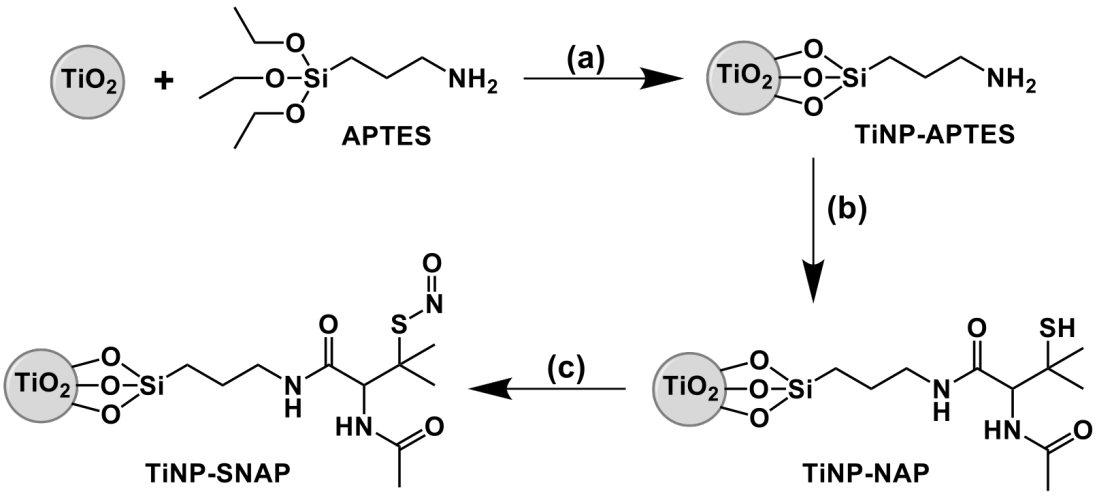

Figure 6. Synthesis route of TiNP-APTES, TiNP-NAP and TiNP-SNAP. Acid treated TiNPs were reacted with APTES using a reflux system under nitrogen gas atmosphere at 120 °C for 12 h (a), followed by NAP thiolactone reaction at RT with vigorous stirring for 24 h (b). Finally, nitrosation reaction with *t*-butyl nitrite at RT for 1 h led to the production of SNAP immobilized TiNPs (c). Toluene was used as the solvent for all the reactions.

First, APTES was chosen as the silanization agent due to its suitable reactivity and conformational properties that provide higher yields in surface modification reactions [141]. The inherent reactivity of APTES is due to its three ethoxy groups readily available to be anchored with the hydroxyl groups of the TiNPs via condensation reaction liberating ethanol as a byproduct. Thorough toluene washing steps removed the unreacted amino silanes and provided nanoparticles for further modification steps. The available amine-rich surface was further reacted with NAP-thiolactone, which is a self-protected derivative of penicillamine. The ring-opening reaction of NAP-thiolactone provided free thiol groups

on the surface of the nanoparticles that were converted to the *S*-nitrosothiol SNAP functionality in the presence of the *tert*-butyl nitrite nitrosating agent.

2.3.2 Primary Amine Quantification

The silanization process was verified by quantifying the primary amine content on the TiNPs by performing the ninhydrin assay. Both qualitative and quantitative measurements of primary amine groups have been reported using a ninhydrin reagent [142, 184]. In a mildly acidic environment and elevated temperatures (100 °C), within 10 min, the hydroxyl group in the ninhydrin reagent structure undergoes a nucleophilic displacement by the amine content on the surface of the nanoparticles leading to the generation of a purple-colored (Ruhemann's purple) complex, which exhibits absorbance at 570 nm [185]. Generation of the free dye complex is advantageous since it can be separated from the particle mixture that might interfere with the UV-vis spectroscopy results. Results from the ninhydrin assay revealed that 0.24 ± 0.01 μmol mg^{-1} (n = 3) of primary amine groups are conjugated to TiNPs after APTES reflux reaction at an elevated temperature of 120 °C and several washing steps to remove excess unreacted APTES from the mixture.

2.3.3 Thiol Content Quantification

Free sulfhydryl groups (thiol groups) can be quantified through a well-reported spectrophotometric Ellman's assay [87]. Ellman's assay relies on free dye formation as the product of a chemical reaction between 5,5'-dithio-bis-(2-nitrobenzoic acid), known as DTNB or Ellman's reagent, and thiol groups. The disulfide and dianion mixture of 2-nitro-5-thiobenzoic acid (TNB^{2-}) in water is a yellow-colored dye that exhibits an absorbance at 412 nm in UV-vis spectroscopy. The absorbance values are proportional to the amount of

the thiol group presented in the reaction [186]. Meanwhile, NAP-thiolactone as the precursor of the NO donor moiety has a protected sulfur bond, and the –SH is exposed only through a ring-opening conjugation reaction [187, 188]. Therefore, after the NAP attachment to TiNP-APTES, Ellman's assay can adequately estimate the reaction yield. The results revealed the quantity of thiol groups on the surface of the TiNP-NAP to be 0.20 ± 0.01 μmol mg^{-1}, which results in a conversion rate of 83.33% of amines to thiol functionalities (**Table 1**). A wide range of conversion rates (~2-80%) is reported previously in the literature for covalent attachment of NAP-thiolactone to silanized surfaces [141, 142, 183, 189-191]. The higher conversion rate achieved in this study can be explained by the increased hydrodynamic stability of the nanoparticles during the NAP attachment reaction. During reaction with NAP-thiolactone, surface charges of the silanized nanoparticles were altered with hydrodynamic charges provided with free sulfhydryl groups which in turn increased the hydrodynamic stability of NAP-attached TiNPs [192]. This hypothesis correlates with the zeta potential analyses described below. These results agree with previously reported NO-releasing modified nanoparticles [141, 142].

Table 1. Ninhydrin and Ellman's assays demonstrated the content of free amine and thiol groups, respectively, on the surface of the modified nanoparticles.

Amine content (μmol/mg)	Thiol content (μmol/mg)	Conversion rate (%)
0.24 ± 0.01	0.20 ± 0.01	83.33

2.3.4 FT-IR and NMR Analysis of Functionalized TiO_2 Nanoparticles

FT-IR analysis was performed to evaluate the surface functionalization and chemical modifications of the TiNPs at each modification stage for the unmodified and

surface-modified TiNPs (**Figure 7**). A broad peak in the range 3450-3200 cm^{-1} along with a peak around 1630 cm^{-1} was observed for TiNP, which are attributed to the stretching vibration of hydroxyl groups chemically bound to the surface of the TiNP and deformation vibration of adsorbed water present on the TiNP surface respectively. The broad peak for the Ti–O–Ti bond stretch was also observed between 850 and 600 cm^{-1}. Several new vibrational modes related to the organic moieties were observed after the surface functionalization of TiNP with APTES. The characteristic $–CH_2$ stretch and bending peak for the methylene group ($–CH_2$) of the APTES backbone was observed at 2929 cm^{-1} and 1319 cm^{-1}, respectively. The relatively broad peaks at 3413 cm^{-1} and a sharp peak at 1623 cm^{-1} were appeared due to $–NH_2$ stretch and bending, respectively. The other two characteristic absorption peaks for Si–O–Si (asymmetric) and Si–O–Si (symmetric) observed at 1118 cm^{-1} and 1026 cm^{-1}, respectively, further confirmed the successful surface modification of TiNP with APTES leading to amine rich titania surface [155]. The NAP-thiolactone reaction with TiNP-APTES was also evident with the two characteristic peak appearances in the FT-IR spectra at 1756 and 1657 cm^{-1} corresponding to –C=O stretch for the two different amide bonds. The broad $–NH_2$ stretch band observed at 3413 cm^{-1} for TiNP-APTES was also shifted to 3246 cm^{-1} after reacting with NAP-thiolactone. The peak at 1554 and 1292 cm^{-1} can be assigned for the –N–H bending and –C–O stretch (ester), respectively. Further, the appearance of a new peak at 650 cm^{-1} corresponding to the –SNO bending confirmed the successful transformation of TiNP-NAP to TiNP-SNAP via nitrosation reaction [141, 142].

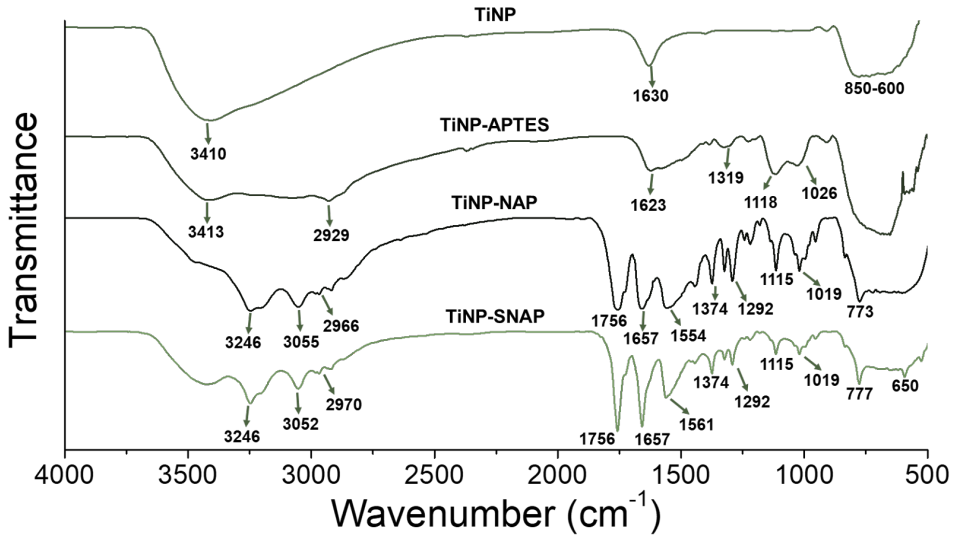

Figure 7. Representative FTIR spectra of TiNP, TiNP-APTES, TiNP-NAP, and TiNP-SNAP.

The surface modification of the TiNPs was further characterized by CP/MAS ^{13}C NMR to confirm the modification of TiNPs by APTES followed by the subsequent attachment of NAP (**Figure 8**). In **Figure 8a** three characteristic NMR signals were observed at 10.26, 22.84, and 42.99 ppm for the three propyl carbon atoms of the APTES moiety (marked as 1, 2, and 3). However, no NMR signal for the ethoxy carbon atoms of the APTES moiety was observed, which confirmed the attachment of APTES to the TiNP with the liberation of the ethoxy unit as ethanol [142]. The ring-opening reaction between the amine moiety of APTES and the NAP-thiolactone increased the carbon content attached to TiNPs, as evident by the NMR signals intensity for the TiNP-NAP (**Figure 8b**). All characteristic carbon peaks were observed for the attached NAP moiety, which further corroborated the covalent linkage of NAP-thiolactone to the TiNP-APTES.

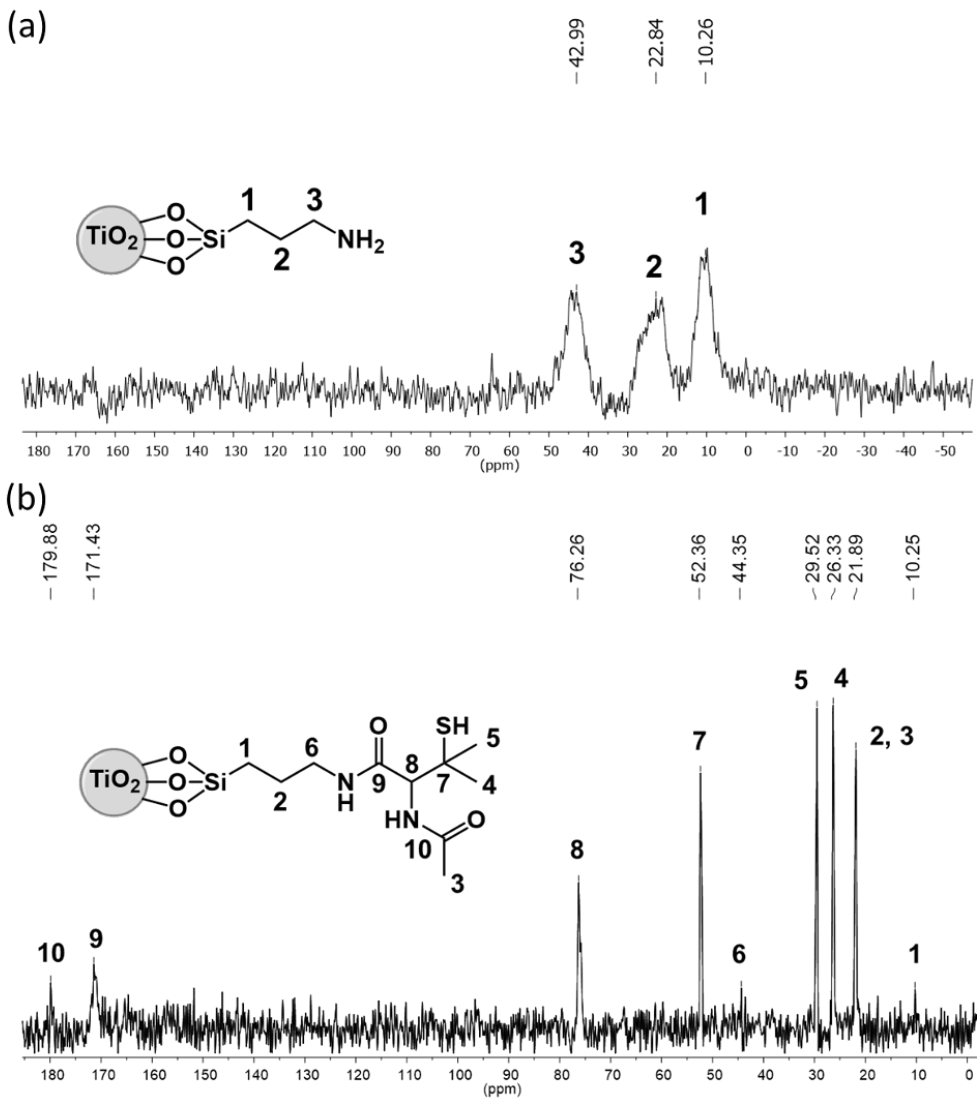

Figure 8. Representative ^{13}C CP/MAS NMR spectra of (a) TiNP-APTES, and (b) TiNP-NAP. (a) Three characteristic NMR signals were observed at 10.26, 22.84, and 42.99 ppm for the three propyl carbon atoms of the APTES moiety (marked as 1, 2, and 3). (b) Two characteristic carbonyl carbon atom peaks for NAP thiolactone unit were observed at 171 and 179 ppm along with other characteristic carbon peaks.

2.3.5 Morphological Analysis

2.3.5.1 DLS and Zeta Potential Analysis

Nanoparticle modifications are usually accompanied by alterations in surface electrical charges and consequently impose changes to the particles' colloidal stability. The

TiNPs are known to possess a hydroxyl-rich surface that leads to a negative surface charge (zeta potential = –41.5 ± 1.75 mV). Immediately after silanization, the modified TiNP-APTES surface became amine rich (NH_2) and subsequently an increase in the zeta potential (–5.1 ± 0.99 mV) was observed. Further, the ring-opening reaction between amine and NAP-thiolactone made the TiNP-NAP surface thiol rich (–SH) due to which an attenuation in zeta potential (–32.3 ± 2.8 mV) was observed. Furthermore, after the conversion of free thiols to nitrosothiols, the reduction of thiol content also mitigated the surface charge and therefore an increase in zeta potential value (–10.7 ± 2.95 mV) was observed (**Figure 9**).

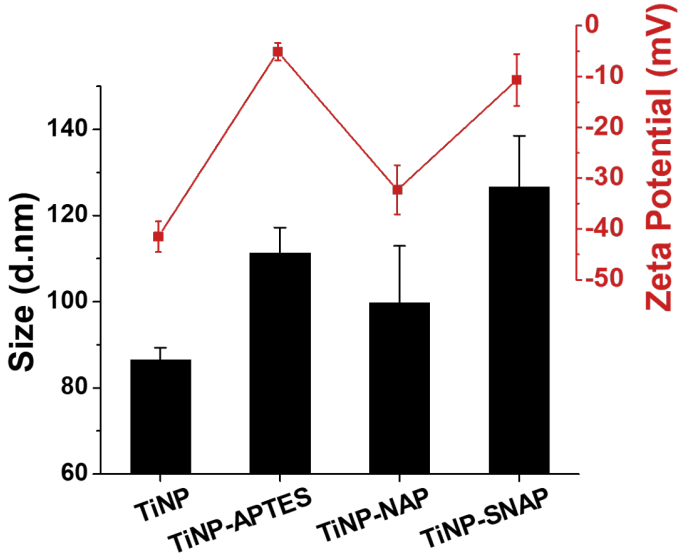

Figure 9. DLS (black bars) and zeta potential (red line) measurements of TiNPs at different stages of surface modification (n = 3).

These results are in agreement with previously reported zeta potentials for nanoparticle surface modifications [155, 192]. The change in zeta potential value after each surface modification also plays a significant role in the dispersion behavior and the stability of the modified NPs. The increase in the zeta potential value of NPs increases the probability of aggregation and therefore, an increase in hydrodynamic diameter of NPs is obvious. The DLS analysis for TiNPs, TiNP-APTES, TiNP-NAP, and TiNP-SNAP

revealed the average particle sizes to be 86.5 ± 2.8, 111.3 ± 5.9, 99.6 ± 13.3, and 126.6 ± 11.9 nm, respectively. The observed changes in hydrodynamic diameters for nanoparticles were in correlation with their respective zeta potential values. The zeta potential and DLS analysis further corroborate the successful surface modification of TiNP at each step.

2.3.5.2 FE-SEM Analysis

Microscopic analyses of TiNPs have been reported numerously [193, 194]. the hydrodynamic stability of particles was measured by zeta potential and DLS analysis, however, SEM morphological analysis revealed the nanostructure of the particles in different modification stages after drying on the specimen mount (**Figure 10**). Although the stacking of the nanoparticles on each other during the drying process is evident in the SEM pictures, the homogenous dispersion and distinct spherical shape of the particles are depicted in each SEM picture. In accordance with the results obtained from zeta potential and DLS measurements, TiNPs exhibited a good distribution and mild aggregation before silane modification. Throughout the modification steps, aggregation behavior altered slightly by introducing different functional groups to the surface and notably increased on TiNP-SNAP particles with the highest zeta potential and DLS measurements. However, the polydispersity of the particles remained almost intact through the course of modifications according to previous measurements, and the results were reconfirmed with SEM analysis. The effect of APTES modification on aggregation behavior of TiNPs was reported previously by Wanag et al., and the obtained results of the current report closely correlate with previously reported ones [195].

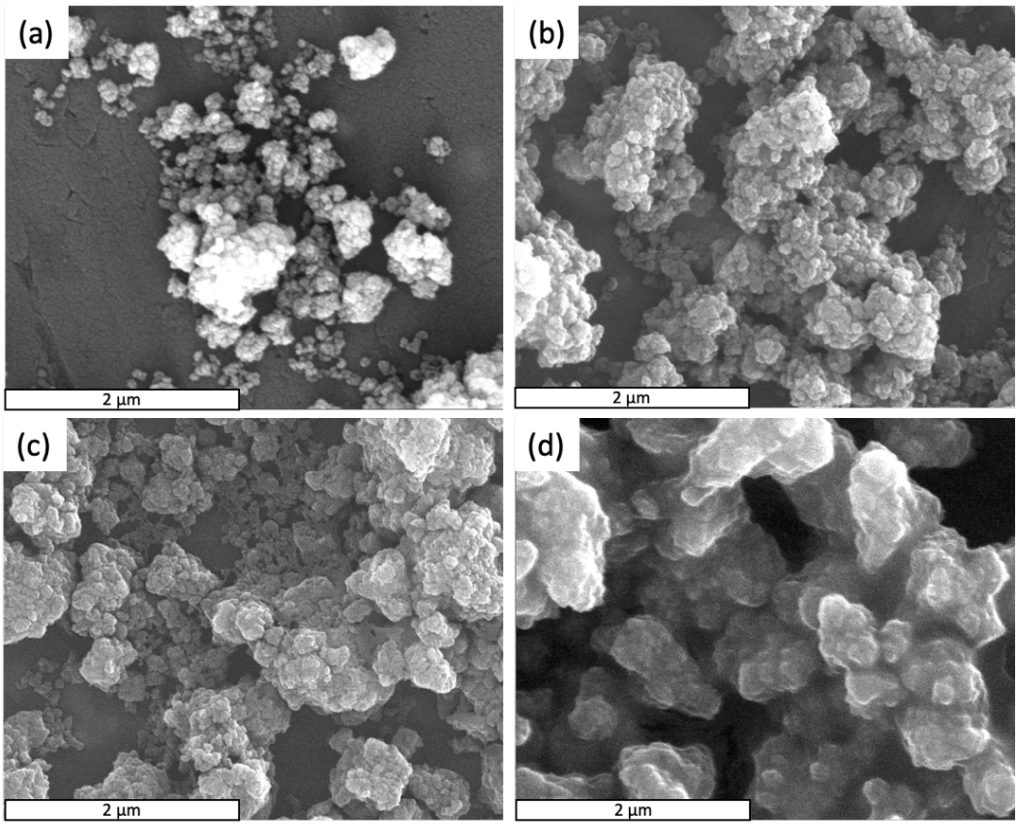

Figure 10. Representative SEM images of nanoparticles at 40K magnification and high voltage of 20 kV in different stages of modification illustrated the morphology of (a) TiNPs, (b) TiNP-APTES, (c) TiNP-NAP, and (d) TiNP-SNAP.

The morphological display and colloidal stability play a pivotal role in the reactivity of the nanoparticles in each modification step [142]. The unusual aggregation of the particles can shield the loaded therapeutic NO molecules from being released from the host particles [196]. In the meantime, exclusively solitary nanoparticles can lead to a burst and hindered prolonged-release behavior [196]. Finally, the homogenous dispersion of sulfur and carbon molecules on TiNP-SNAP was demonstrated by EDS analysis (**Figure 11**). Since the only sulfur-containing component on the structure is the NO-donor moiety (SNAP), EDS results illustrated successful SNAP conjugation to TiNPs.

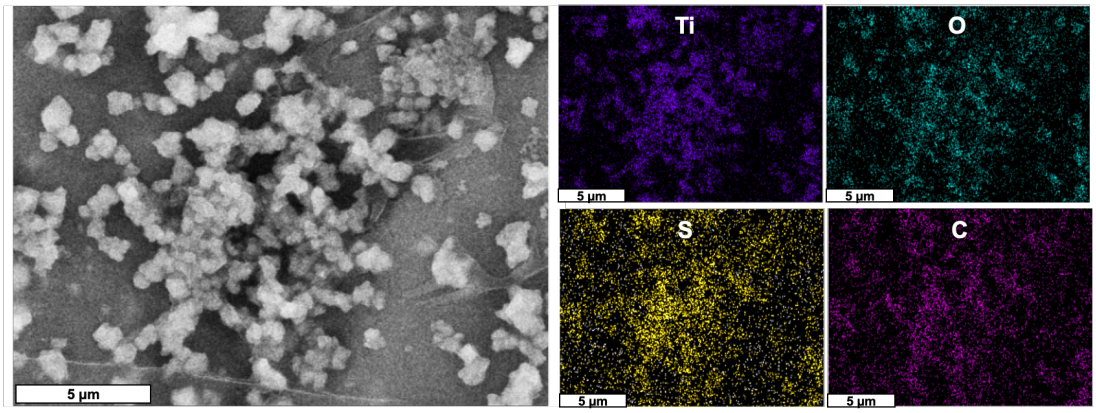

Figure 11. SEM image of TiNP-SNAP particle (black and white) with overlay EDS elemental maps of titanium (purple), oxygen (cyan), sulfur (yellow), carbon (pink). Each element is also labeled on its corresponding elemental map.

2.3.6 Total NO Loading

To evaluate the final reaction efficiency (i.e., the nitrosation of TiNP-NAP using *t*-butyl nitrite) chemiluminescence was utilized as the gold standard to evaluate the NO release [197, 198]. After dispersing the TiNP-SNAP in 1 mL of PBS, 1 mL of 0.25 M copper (II) chloride and 1 mL of 0.5 M ascorbic acid was injected into the NOA sample cell which led to the catalytic release of NO from the –SNO moiety on the surface of the TiNP-SNAP nanoparticles [183, 199].

The real-time NO release data collected from the NOA was used to evaluate the total amount of NO immobilized on the TiNP-SNAP nanoparticles. The results revealed that TiNP-SNAP was capable of storing NO up to 127.55 ± 4.68 nmol mg^{-1} (n = 3) which is higher than previously reported diatomaceous earth silica particles (31.2 nmol mg^{-1}) [141]. These differences can be attributed to the larger particle size of diatomaceous earth silica particles that provided a less overall surface area for reaction and SNAP conjugation. The conversion rate from TiNP-NAP to TiNP-SNAP was 63.77 ± 2% (n = 3), which revealed improvement of TiNPs in delivering NO comparing to previously reported

halloysite nanoparticles with approximately 50% conversion rate [142]. The higher conversion rate of TiNP-SNAP may relate to nanoparticles' spherical morphology and colloidal stability of NAP-attached particles, which provided higher surface area and subsequently increased the reaction success rate. The lack of complete conversion can be related to thermal decomposition of the –SNO moiety during the nitrosation reaction, plus, steric hindrance imposed by tertiary thiol functionality, and the existence of disulfides in the TiNP-NAP structure. Moreover, steric hindrance imposed by tertiary thiol functionality and finally, the existence of disulfides in the TiNP-NAP structure can be other impediments in nitrosation reaction [142, 191].

2.3.7 *In Vitro* NO Release Kinetics Under Physiological Conditions

The development of antibiotic-resistant bacteria strains has been a definitive challenge in medicine [143]. The development of nanoparticles with either innate or imparted antibacterial properties that can be delivered to the site of infections has become one of the most promising solutions to reduce the need for conventional antibiotics and the emergence of mutated resistant strains. In addition, utilizing endogenous substances to augment the bactericidal efficacy of nanoparticles while minimizing the bacterial resistance and required nanoparticle concentration has been a subject of interest recently. Although NO has been a target for such studies, the lack of efficient delivery from nanomaterials has limited its practical usage [144]. In this study for the first time, SNAP-TiNP is synthesized to deliver NO over the course of 20 h in an effective antibacterial range (**Figure 12**).

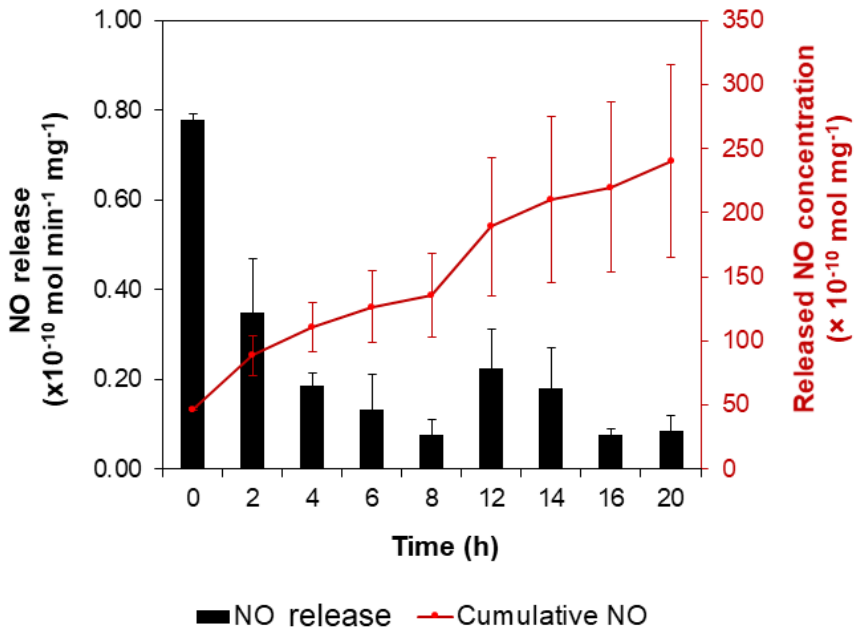

Figure 12. *In vitro* NO release kinetics of the TiNP-SNAP obtained from a 1 mg mL^{-1} colloidal suspension of the nanoparticles in PBS containing EDTA. Data represent as the mean ± SD (n = 3).

The TiNP-SNAP antibacterial efficacy relies on the NO delivery behavior of the particles under physiological conditions. The major mechanism of most NO donating materials that deliver NO is via thermal decomposition of the S–NO bond to disulfide species and a free NO molecule [7]. In this study, it is observed that within the first 2 h of particles' exposure to 37 °C and buffer environment, higher NO release values of around 0.8-0.4 × 10^{-10} mol min^{-1} mg^{-1} are observed. However, a more steady and gradual release behavior over 20 h with a cumulative NO concentration of 240.05 ± 74.94 × 10^{-10} mol mg^{-1} was observed. The release behavior of NO from TiNP-SNAP observed here indicates an improvement to the previously reported NO-releasing nanoparticles like SNAP conjugated diatomaceous earth silica with a burst release within the first 2 h of NOA studies or SNAP conjugated halloysite nanoparticles, which had a significantly higher concentration of NO

release (0.05 μmol mg^{-1}), but exhibited much shorter release time of 8 h [141, 142, 189-191, 200].

2.3.8 TiNP-SNAP 24 h Antibacterial Efficacy Evaluation

Two of the most common pathogens abundant in medical device infections are *S. aureus* and *E. coli*. Although several antibiotics are being used to combat infections, the growing threat of antibiotic-resistant strains and the emergence of mutated *S. aureus* and *E. coli* strains force the urge to develop better ways to deal with bacterial infections [201]. Through the past decades, nanoparticles have been investigated for various antimicrobial applications as they can be beneficial in different ways such as generating a broader spectrum of bactericidal mechanisms, enabling delivery of therapeutic agents in a targeted and controlled manner, expanding the versatility of new drugs, and facilitating the use of noninvasive mediators such as light [202]. However, the rise of bacterial resistance to new elements such as silver nanoparticles escaladed challenges in using metallic nanoparticles [203]. It has been proven that NO exhibits non-specific mechanisms of bactericidal activity. Production of reactive oxygen species (ROS), damaging the bacteria cell membrane, cleaving the DNA structure, disturbing the protein functionality of cell membrane are proposed as antibacterial mechanisms of NO [7]. TiNP, on the other hand, is known to have no antibacterial activity, unless excited in the presence of light irradiation although that can lead to systemic cell apoptosis or genotoxicity [150, 181].

Enhancing TiNPs with the NO donor moiety conjugation significantly reduced the viable CFUs from both *S. aureus* and *E. coli* bacterial cultures with no need for external stimulations like light irradiation (**Figure 13**). A concentration-dependent activity was observed in the bactericidal efficacy of SNAP-TiNPs (**Table**).

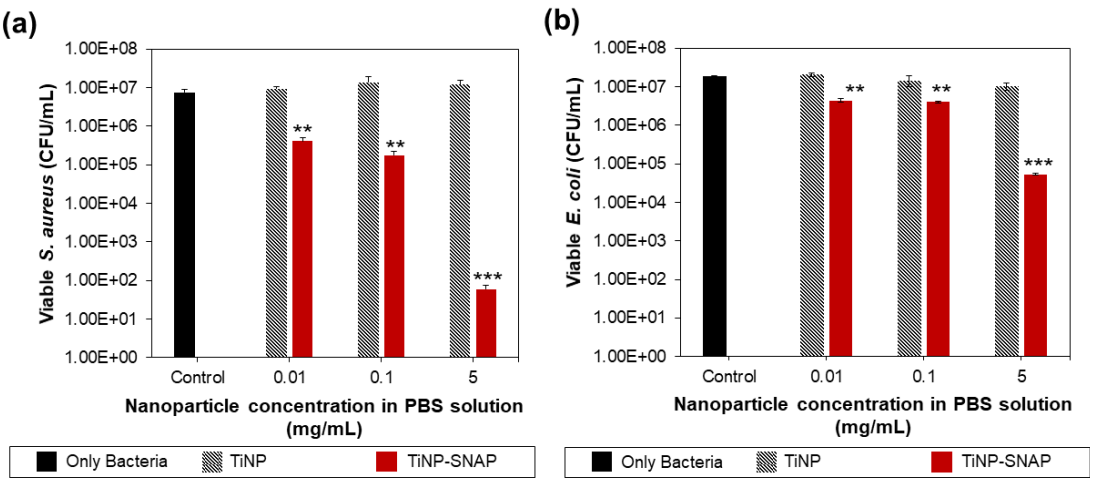

Figure 13. Bactericidal efficacy analysis of TiNP-SNAP against (a) Gram-positive *S. aureus*, and (b) Gram-negative *E. coli*. The concentration of bacteria (control) without exposure to nanoparticles is presented by solid black bars. Striped black and solid red bars are used to show the concentration of viable bacteria after 24 h exposure to TiNP and TiNP-SNAP, respectively. Data are presented as the mean values ± SD (n = 4) where ** = $p \leq 0.01$ and *** = $p \leq 0.001$ for TiNP vs. TiNP-SNAP.

Table 2. Viability reduction of bacterial cells (%) after 24 h exposure to TiNP-SNAP comparing to control bacteria wells containing no nanoparticles. Data are presented as the mean ± SD (n = 4).

Nanoparticles concentration (mg mL^{-1})	Bacteria cell viability reduction (%)	
	S. aureus	*E. coli*
0.01	94.52 ± 1.18	78.83 ± 2.46
0.1	97.66 ± 0.55	72.31 ± 1.67
5	99.99 ± 0.01	99.70 ± 0.01

More than 99.99 ± 0.01% reduction in viable *S. aureus* was achieved when it was exposed to a concentration of 5 mg mL^{-1} TiNP-SNAP. However, the antibacterial efficacy is slightly diminished against Gram-negative *E. coli* and 99.70 ± 0.01% reduction in viable CFUs was obtained by using the same concentration of 5 mg mL^{-1} TiNP-SNAP. Although the difference between the two bacteria strains is not significant, the slight reduction in antibacterial efficacy against Gram-negative bacteria can be related to a specific DNA

repair mechanism when exposed to NO that abates DNA damage induced by NO [204]. In addition, flavohemoglobins (Hmp) enzymes synthesized in Gram-negative bacteria strains can defend against nitrosative stress caused by NO [205]. These observations about NO dose-dependent antibacterial efficacy and less susceptibility of *E. coli* have been reported in prior studies [205]. It is also reported previously that a concentration of 21.5 mg mL^{-1} SNAP-conjugated diatomaceous earth silica and 10 mg mL^{-1} halloysite nanoparticles were capable of achieving 92.9 ± 2.6% and 99.6 ± 0.1% reduction in viable *S. aureus* CFUs, respectively [141, 142].

2.3.9 Cytotoxicity Analysis

In order to evaluate the cytocompatibility of TiNP and TiNP-SNAP particles, the particle leachates from different concentrations (0.01 – 5 mg/mL) were exposed to 3T3 mouse fibroblast cells for 24 h following a previously reported method [141]. Using the CCK-8 assay, the cell viability was determined compared to cells in DMEM media as control. The 3T3 cells exhibited no significant change in growth profile after the addition of leachates from TiNP-SNAP as well as TiNPs as compared to untreated control cells. Notably, all exposed cells and untreated control exhibited >90% cell viability over 24 h (**Figure 14**). In the past, studies involving NO-releasing nanoparticle/nanotubes for biomedical applications have reported similar results with no potential toxicity from the NO-donating functionalities, SNAP, or its degraded byproducts such as NAP and NAP dimer [141, 142]. Overall, the results obtained in this study corroborate with previously reported studies highlighting the biocompatibility of NO-releasing materials for clinical translation. Moreover, several studies have been done on the NO effect on the viability of mammalian cells.

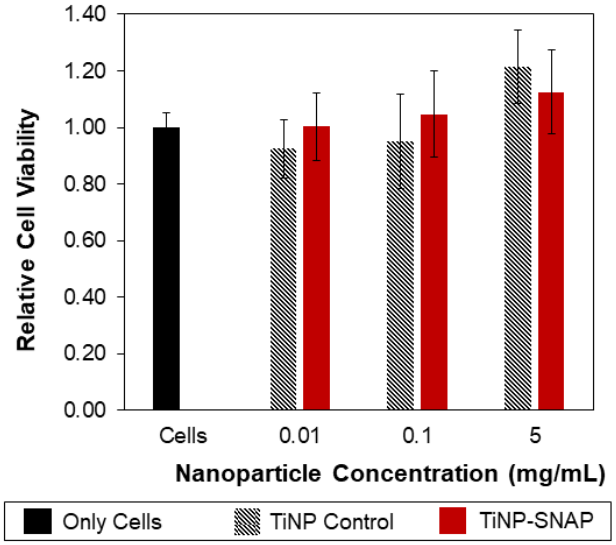

Figure 14. Cytocompatibility of TiNP and TiNP-SNAP leachates in media towards NIH 3T3 mouse fibroblast cells. The viability of cells was assessed using a CCK-8 cell viability kit. The cells exposed to the TiNP and TiNP-SNAP extracts depicted by striped black and solid red bars, respectively, exhibited cell viability similar to the untreated control cells in DMEM media that were not exposed to TiNPs, depicted in solid black bar, highlighting the non-toxic nature of the particle leachate. Data are presented as mean ± SD for n = 6, normalized to the untreated cell control.

It is well demonstrated that exposure to a low concentration of NO can impart a regulatory effect on several types of mammalian cells, and increase their growth and proliferation rates [137]. The toxicity profile and allergic reactivity of TiNP are also well-established in previous reports [147, 181]. Many cosmetic products are allowed to contain up to 25 wt.% TiNP in them under European regulations [206]. Although TiNPs are demonstrated to not exhibit cell cytotoxicity in their stable condition, it is reported that in a UV-excited state, oxidative stress-induced cell apoptosis can occur in a concentration-dependent manner [181], and the subject of potential risks in inhaling TiNPs has been studied previously. Lee et al. reported cystic keratinizing squamous cell carcinomas occurrence in a rat model, after long-term exposure to a high concentration of TiNPs (250 mg m^{-3} for 2 years, 5 days a week, and 6 h each day) [207]. Accordingly, in this study, the

SNAP immobilized TiNPs exhibit an excellent bactericidal activity without any light activation method, while the TiNP-SNAP leachates exhibit no cytotoxicity. These findings can expand TiNP-SNAP applications in cosmetic, drug delivery systems, and polymeric matrix nanofillers with a low risk of leaching of cytotoxic NO donor moiety, or loss of NO due to diffusion of the donors to the surrounding environment with the added benefit of antimicrobial activity and obviated need of UV excitation.

2.4 Conclusion

Antibiotic resistance is one of the most challenging burdens on medical systems. With the rapid expansion of resistant bacteria strains worldwide and a significant lag in creating new antibiotics, one of the most promising solutions to this problem is the development of nanoparticles to combat bacterial infections. One of the biocompatible nanoparticles that have been a matter of interest for a variety of applications is titanium dioxide nanoparticles (TiNPs). Titanium dioxide nanoparticles are being used in wide range of biomedical applications such as fillers, coatings, medicine, and pharmacology, and they are proven to be bioinert and exhibit antibacterial efficacy when exited under light irradiation. However, the lack of innate antibacterial property without an external source of irradiation hindered its application in the biomedical realm. In this study, for the first time, the NO-releasing SNAP functionality was covalently conjugated to the TiNPs surface through a sequence of chemical reactions. Successful conjugation was qualitatively confirmed via FTIR and NMR analysis. Primary amine group quantity on the surface of TiNP-APTES was measured to be 0.24 ± 0.01 μmol mg^{-1} according to ninhydrin assay results. More than 83% of primary amine groups were converted to sulfhydryl groups (~

0.20 ± 0.01 μmol mg^{-1}) as detected by Ellman's assay. The chemiluminescence NO analysis revealed 127.55 ± 4.68 nmol mg^{-1} NO loading on TiNP-SNAP, after nitrosation reaction with *t*-butyl nitrite with an efficiency rate of more than 63%. Zeta potential and DLS analysis results were in good correlation with chemical modifications and corroborated colloidal stability and nanostructural integrity of particles in each step of modification. The SEM and EDS morphological analysis confirmed the uniformity and polydispersity of nanoparticles, and a homogenous sulfur distribution on TiNP-SNAP. The TiNP-SNAP exhibited promising concentration-dependent antibacterial results against two of the most common healthcare-associated infections, *E. coli* and *S. aureus*. More than 99.99% and 99.70% reduction in viable CFUs of *S. aureus* and *E. coli* was observed, respectively, after 24 h of exposure to a 5 mg mL^{-1} TiNP-SNAP suspension. No cytotoxicity was observed from the leachate assay of TiNP-SNAP against mouse fibroblasts with respect to control. The results from this study illustrated the great potential of TiNPs as a suitable nanocarrier of NO donors. The resulting TiNP-SNAP can be used in many clinical and preclinical applications such as antimicrobial delivery, wound healing, polymer fillers, coatings, etc.

CHAPTER 3

S-Nitroso-*N*-acetyl-L-cysteine Ethyl Ester (SNACET) Incorporated Pluronic F-127 Hydrogel for Topical Applications

3.1 Introduction

It has been shown that if delivered to wounds in an appropriate concentration and duration of time, NO can accelerate the wound healing process while prevents bacterial infection as a potent antibacterial and antibiofilm agent [208-210]. To that end, topical NO delivery techniques have shown to be significantly successful in delivering the desired amount of NO to the wound site [211]. As mentioned before, owing to their biocompatibility, antibacterial, and antithrombotic properties, and most importantly their relative stability compared to other NO donor molecules a tremendous amount of attention has been given to RSNOs which are the adducts of R-SH and NO compounds [41]. One potential NO donor candidate for the wound healing application is a NO-releasing cysteine-derived small molecule, *S*-nitroso-*N*-acetyl-L-cysteine ethyl ester (SNACET), which has been previously studied for its pharmacologic properties and lock solution application [35, 212]. Because SNACET is a highly lipophilic, charge-free, and water-soluble NO donor molecule it is being considered as a suitable NO donor molecule for the development of a nonantibiotic hydrogel for topical bactericidal applications such as wound healing.

Fabricating materials that can stabilize NO donor molecules, and release them upon topical application can be a very promising approach in the usage of NO in wound healing

[123]. Hydrogels have attracted so much attention as appealing candidates for wound healing and topical drug delivery applications due to their workability, swelling capacity, flexibility, and high porosity in their structure [159, 160]. Pluronic F-127 (PF-127, Poloxamer 407) with a three-block structure of two hydrophilic PEO tails and a hydrophobic PPO unit in the middle can self-assemble to micelles in an aqueous environment [169]. Also due to the reverse thermal gelation behavior of F-127, the hydrogel forms a gel in elevated temperatures (ambient and body temperatures) as opposed to lower refrigerated temperatures (0-4 °C) in which it acquires a liquid form with makes it a [170]. The aforementioned properties of PF-127 have made it a suitable candidate to deliver NO in topical application [213].

In this study, for the first time, SNACET as a small NO-donor molecule has been incorporated into the thermogelling PF-127 hydrogel in three different weight percentages (i.e. 1, 2, and 5 wt%) and studied for its stability, NO release behavior, and bactericidal efficacy. After preparing an aqueous solution of 30% (w/v) PF-127 prepared in PBS (10 mM, pH 7.4) containing 100 μM EDTA by the cold method [214], the gel was stored at 4 °C for overnight to achieve complete dissolution. Calculated amounts of SNACET were dissolved in PF-127 hydrogel at 0 °C to formulate 1, 2, and 5 wt% of NO-releasing SNACET-Pluronic gel. The storage stability of the NO-releasing Pluronic gel was analyzed at –20 °C and 4 °C for up to 28 days. The NO release behavior of the formulated gels was monitored at the physiological conditions for up to 24 h. Further, the bactericidal efficacy of the SNACET-Pluronic gels was evaluated against *S. aureus* and *E. coli*.

3.2 Materials and Methods

3.2.1 Materials

N-Acetyl-*L*-cysteine (NAC), acetyl chloride, sodium nitrite ($NaNO_2$), ethanol, methanol, chloroform, hydrochloric acid (HCl), ethylenediaminetetraacetic acid (EDTA), sterile phosphate buffer saline (PBS) powder 0.01 M, pH 7.4, containing 138 mM NaCl, and 2.7 mM KCl, were purchased from Sigma-Aldrich (St. Louis, MO). Pluronic F-127 ([poly(ethylene oxide)]100-[poly(propylene oxide)]65-[poly(ethylene oxide)]100), (average molecular weight ~12,600 g/mol) was purchased from Sigma-Aldrich, USA. Platinum-cured silicone (PDMS) sheet 12 × 12 × 0.2" was obtained from (McMaster Carr, IL). All aqueous solutions were prepared using Milli-Q water for experimental usage. Luria Bertani (LB) broth media and agar were purchased from Sigma Aldrich. Bacterial strain *S. aureus*, (ATCC 6538) and *E. coli* (ATCC 25922) was obtained from American Type Culture Collection (ATCC).

3.2.2 *S*-Nitroso-*N*-Acetylcysteine Ethyl Ester (SNACET) Synthesis

In order to synthesize NACET, as the precursor of SNACET, the previously reported procedure was followed by slight modifications [35]. Briefly, *N*-Acetylcysteine (NAC) 10 g was dissolved in 500 mL absolute ethanol and slowly added the anhydrous hydrochloric acid while stirring at RT. After 4 h of stirring at 25 °C, the solvent was evaporated to give a crude residue. Analytically pure white NACET powder was obtained by purifying the crude residue by silica gel chromatography (40−60 nm) using $CHCl_3$ and MeOH (95:5 v/v) as the eluent. Furthermore, 5 g NACET was dissolved in 10 mL DI water, and 1 mL 2 M HCl subsequently was added to the mixture. Using an ice bath the reaction mixture was cooled to zero degrees for 30 min followed by the addition of 2 g

$NaNO_2$ while stirring at a low speed. After 10 min the SNACET was obtained as the solid pink precipitate. The obtained pink solid SNACET powder was washed with ice-cold water several times and dried in a desiccator overnight while protected from light. The powder was stored at –80 °C for further usage.

3.2.3 Preparation of SNACET- Pluronic Gel

Aqueous solutions of 30% (w/v) PF127 were prepared in PBS (10 mM, pH 7.4) containing 100 μM EDTA by the cold method [214]. Solid Pluronic F-127 flakes (3.0 g) were slowly added to 7.0 mL of PBS (10 mM, pH 7.4) containing 100 μM EDTA in a glass vial and stirred with a magnetic bar in an ice bath until the complete hydration of the polymer. Later, the vial was stored at 4 °C for overnight to achieve complete dissolution. A calculated amount of SNACET was dissolved in an aqueous solution of Pluronic gel to formulate 1, 2, and 5 wt% of NO-releasing SNACET-Pluronic gel.

3.2.4 SNACET-Pluronic Gel Storage Stability

The glass vials containing SNACET-Pluronic gel were stored at –20 °C and 4 °C in the dark. The storage stability of the SNACET-Pluronic gel was determined by measuring the weight percentage of SNACET remaining in the Pluronic gel samples at various time points over a month. The SNACET-Pluronic gel (10 mg) was freshly dissolved in one mL of PBS (10 mM, pH 7.4) containing 100 μM EDTA, and the UV-Vis spectra were recorded in the wavelength range of 250–650 nm using an Agilent Cary 60 UV-Vis Spectrometer at room temperature. Absorbance value measured at 334 nm corresponding to $n_O-\pi^*$ transition was taken into consideration for the stability analysis. The 30% (w/v) PF127 gel dissolved in PBS with a concentration of 10 mg/mL was used as the blank solution for all the measurements. The remaining percentage of SNACET in

the SNACET-Pluronic gel was calculated using the following equation, where A_0 = Absorbance at 334 nm at day 0 and A_t is the absorbance at 334 nm at the different timepoints:

$$\%SNACET\ remaining\ =\ 100 \times \frac{A_t}{A_0}\ (\boldsymbol{Eq.3})$$

3.2.5 SNACET-Pluronic Gel NO Release Measurements

3.2.5.1 Sample Preparation

Silicone rubber (PDMS) sheet (0.51 cm thick) was cut into 1 cm × 1 cm rectangles that were used as templates to hold the gel. In the middle of each template, a circular hole was made using a 6 mm puncher. The PDMS template was placed on a piece of Tegaderm™ transparent film (3M science, USA) and weighed. The prepared gel with known SNACET wt.% (1, 2, and 5 wt.%) kept in an ice bath (at zero degrees) was carefully poured into the cavity using a 3 mL plastic pipette to fill the hole in the middle of the PDMS template. The excess amount of gel was removed by sliding a flat and sharp razer over the PDMS template's surface to obtain a level surface of the gel inside the PDMS template. The Tegaderm™ gas-permeable film was then folded from one side to wrap the template completely from both sides only by one layer (**Figure 15**). The whole template with the gel inside was then weighed. The gel's weight inside the template was measured by the subtraction of the weights of the template wrapped in a Tegaderm film, before and after adding the gel.

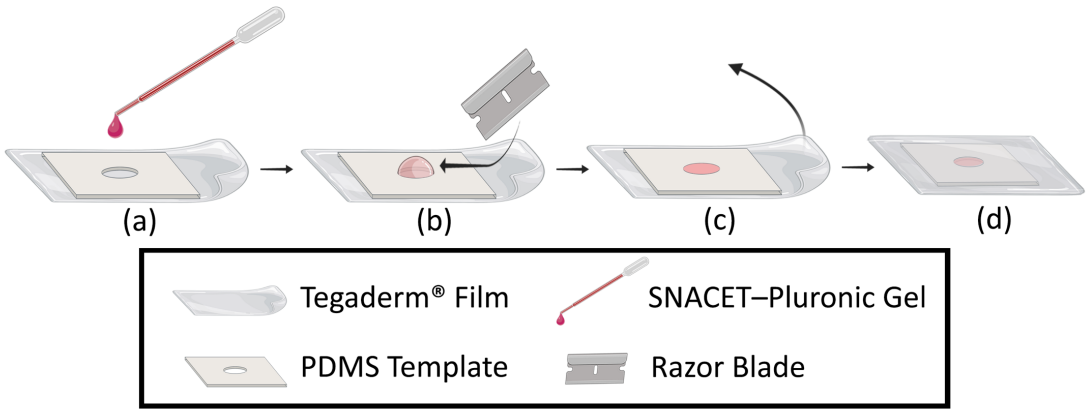

Figure 15. Schematic illustration depicting sample preparation steps for NO release measurements. After preparing the PDMS template, it placed on the adhesive side of a Tegaderm film. (a) SNACET-Pluronic gel with known concentration was poured in the cavity on the PDMS template, (b) the excess amount of gel was removed from the top of the template by sliding a sharp razor blade over the surface of the template. Furthermore, (c) the Tegaderm film was folded from one side to wrap the PDMS template completely, and (d) the final sample was immediately transferred to the NOAs for NO-release evaluations. The weight of SNACET-Pluronic gel content in each template was obtained by subtracting the weight of the template and Tegaderm before adding the gel at the first step (a), and after preparing the sample at the last step (d). Created with BioRender.com.

3.2.5.2 Real-Time NO Release Analysis

Sievers Chemiluminescence Nitric Oxide Analyzer 280i (NOA Zysense, Weddington, NC, USA) was utilized to analyze the real-time NO release behavior operating with ~6.6 psi O_2 supply and ~9.5 Torr cell pressure. The samples were suspended inside an amber NOA amber reaction vessel containing 1 mL 0.01 M PBS solution (pH 7.4) containing 100 µM EDTA to prevent the light and metallic ions from catalyzing the NO donor decomposition reaction at 37 °C. The reaction vessel was supplied with pure nitrogen gas (N_2) at a constant flow of 200 mL min^{-1}. The NO gas emitted from the SNACET-Pluronic gel was purged by supplied pure N_2 and continuously swept by vacuum to the chemiluminescence reaction chamber where NO reacted with ozone (O_3) to produce excited nitrogen dioxide (NO_2^*) [215]. Afterward, the excited NO_2^* is decayed, and photon emission from this decay is detected by the NOA, corresponding to the concentration of

NO molecule being measured in ppb to ppm values. Thereafter, considering the constant of the NOA instrument (1.63×10^{-13} mol ppb^{-1} s^{-1}) and weight of the gel incorporated into each template NO flux ($\times 10^{-10}$ mols mg^{-1} s^{-1}) was calculated.

3.2.6 Antibacterial Evaluation

3.2.6.1 Preparation of Bacterial Culture

A single isolated colony of *S. aureus* and *E. coli* was inoculated in LB media and incubated at 37 °C for 5 h at 120 rpm. Bacteria growth in media over time was monitored by measuring the optical density (OD) of the bacterial suspension at 600 nm wavelength using a UV-vis spectrophotometer (Cary 60, Agilent Technologies). A mid-log phase of bacteria was extracted from the suspension by centrifuging the culture at 3500 rpm for 7 min. Bacterial OD was adjusted to 0.1 corresponding to $\sim 10^7$ CFU mL^{-1} and was used for further analysis.

3.2.6.2 Zone of Inhibition Assay

A 100 µL of adjusted bacteria suspension was spread onto the agar plate and allowed to air dry for 10 min at room temperature. After all the liquid was absorbed into the agar, 50 µL of each sample (control Pluronic gel and 1, 2, and 5% SNACET-Pluronic gel) was added onto the bacteria spread plates (n=4). Gel-loaded plates were incubated at 37 °C overnight. The results from the study were calculated by measuring the diameter of zones where bacterial growth was inhibited on the plate surrounding the gel after overnight incubation. Pictures of the plates were captured using SphereFlash Colony Counter (IUL Instruments) and zone diameter was calculated using NIH ImageJ software.

3.2.7 Statistics

All the results are reported as the mean ± standard deviation (SD) values with at least three replicates unless noted otherwise. To evaluate significant statistical difference between treatment and control groups, a standard unpaired, two-tailed Student's t-test was used and *p* values are indicated by asterisks (i.e., * $p < 0.05$, ** $p < 0.001$, *** $p < 0.0001$).

3.3 Results and Discussion

3.3.1 Synthesis of NACET and SNACET

The small NO donor molecule SNACET is a lipophilic, charge-free, and water-soluble molecule (**Figure 16a**) that can degrade in the presence of metal ions (e.g., Cu^{+}), or due to light and heat exposure. The degradation product of SNACET is known to be NO and a corresponding disulfide (RSSR) product (**Figure 16b**).

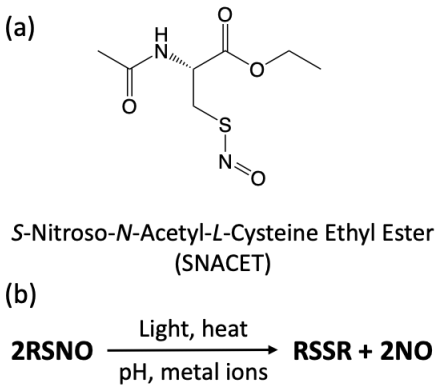

Figure 16. Illustration of (a) the chemical structure of *S*-Nitroso-*N*-Acetyl-L-Cysteine Ethyl Ester (SNACET) and (b) decomposition reaction of 2 mols RSNOs in the presence of one or more catalytic agents of light, heat, pH, or metal ions produces 1 mol of the corresponding disulfide and 2 mols of NO.

It is noteworthy that due to its high lipophilicity, SNACET is extractable into water-immiscible organic solvents such as chloroform and ethyl acetate [35, 212]. Synthesis of *S*-nitroso-*N*-acetyl-L-cysteine ethyl ester (SNACET) involved a convenient two-step

reaction. In the first step, the carboxylic (–COOH) group of *N*-acetyl-L-cysteine (NAC) was protected by using anhydrous HCl in presence of ethanol to obtain *N*-acetyl-L-cysteine ethyl ester (NACET). In the second step, sodium nitrite was used to nitrosate the ice-cold acidic water solution of NACET to synthesize SNACET. The synthesized NACET and SNACET were well characterized by various techniques such as ^{1}H and ^{13}C NMR, Mass spectrometry, and FT-IR. The purity of the product was evaluated and correspond with our prior report [35].

3.3.2 Storage Stability of SNACET-Pluronic Gel

The stability of the SNACET molecule in the solid-state was studied in our previous report [35]. The SNACET powder showed excellent stability at –80 °C however, exhibited poor stability even at –20 °C which limits its application in solid-state for long-term antimicrobial applications at physiological conditions. However, the stability of NO donors is generally improved when incorporated into a suitable polymer matrix probably because of non-covalent interactions with the polymer chain, and a sustained and long-term NO release behavior was observed [42, 216]. The stability of SNACET within the Pluronic gel matrix was studied at –20 °C and 4 °C (**Figure 17**). A calculated amount (10 mg) of 1, 2, and 5 wt.% SNACET Pluronic gel were dissolved into 1 mL of PBS (10 mM, pH 7.4) containing 100 μM EDTA, and their UV-Vis spectra were measured to determine the stability of the SNACET at 4 °C and –20 °C up to 4 weeks. Kumar et al. evaluated SNACET stability in an aqueous environment at –20 °C, and a poor stability behavior was reported, where ∼20 and ∼90% of SNACET content were degraded after 3 days and 3 weeks, respectively [35]. Nonetheless, SNACET showed better stability within the

Pluronic gel matrix at –20 °C, and only ~11, ~18, and ~26% of SNACET was degraded in Pluronic gels with a concentration of 1, 2, and 5 wt%.

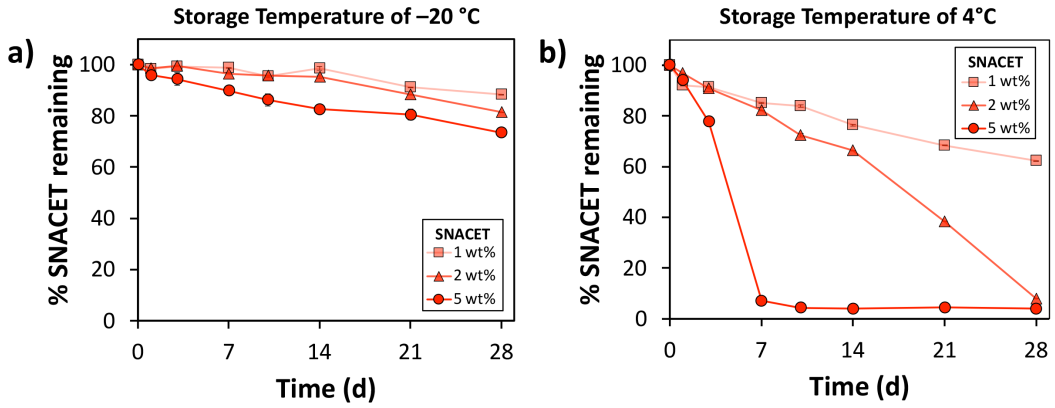

Figure 17. Storage stability of 1, 2, and 5 wt% SNACET Pluronic Gel at (a) 4 °C, and (b) -20 °C in dark. Data reported as mean ± SD of n ≥ 3 replicate measurements.

The Pluronic gel formulation containing 1 wt% SNACET showed better stability at 4 °C compared to 2 and 5 wt% concentrations. After 4 weeks of storage at 4 °C, 30% of SNACET was degraded in 1 wt% SNACET Pluronic gel, whereas over 90% degradation was observed for 2 and 5 wt% SNACET Pluronic gel formulations. The 5 wt% SNACET Pluronic gel showed the least stability at each timepoint and SNACET was almost degraded within one week of storage at 4 °C. These observations indicated the concentration-dependent decomposition of the SNACET within the Pluronic gel. The lower the concentration of SNACET within Pluronic gel, the better is its stability. As reported by Oae et al., RSNOs markedly decompose faster at higher concentrations in the solution state [217]. The SNACET was found to be more stable at –20 °C within the Pluronic gel comparing to the reported results of stability of SNACET in aqueous solution by Kumar et al. [35]. The hydrogel was able to retain more than 80% of the SNACET content in every concentration over the course of 3 weeks, while Kumar et al., reported the stability of 1

mM SNACET solution in PBS containing EDTA stored at –20 °C to be less than 10% in the same period [35]. However, the degradation behavior at –20 °C followed a similar concentration-dependent trend as observed at 4 °C. After 4 weeks of storage, ~12, 20, and 30% degradation was observed for 1, 2, and 5 wt% SNACET Pluronic gel formulations respectively.

3.3.3 Real-Time NO Release Analysis

The release behavior of the Pluronic gel containing different weight percentages of SNACET molecule was determined by utilizing NOA as the gold standard NO detection method [218]. As the gels were suspended in the NOA sample cell at the physiological temperature (37 °C), the homolytic scission of –S–N bond in the SNACET structure led to the release of NO from the gel (**Figure 18**). The initial NO release flux from all the samples types showed an increase proportional to the concentration of the NO donor within the hydrogel. While Pluronic gel containing 1 wt% SNACET initially exhibited an NO release with a flux of ~ 3×10^{-10} mol cm^{-2} min^{-1} at 0-1 h. Increasing the content of SNACET to 2 and 5 wt% magnified the flux values approximately 3.93 and 3.19 times more than that of 1 wt%. While the gradual decrease in NO release was observed for all the concentrations, during the first 8 h, the high NO flux rates obtained from 5 wt% SNACET-Pluronic gel fluctuated between 3.9 – 2.5 nmol cm^{-2} min^{-1} while the other two concentrations exhibited much less NO flux between 1.2 – 0.1 and 0.3 – 0.1 nmol cm^{-2} min^{-1} for 2 and 1 wt%, respectively. This observation during the first 8 h of NO release, is explained by the increase in the NO reservoir due to the increase in NO donor concentration and the elevated release within the initial timepoints is due to the presence of SNACET rich regions near

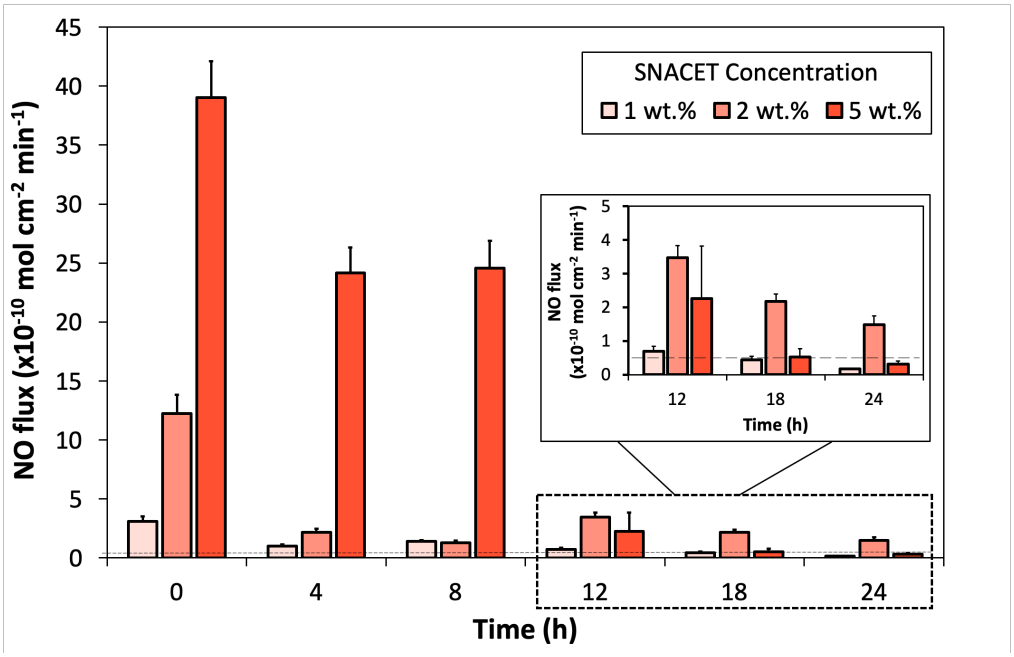

Figure 18. The NO release kinetics of Pluronic gels containing different wt% of SNACET (i.e. 1, 2, 5 wt%) over the course of 24 h.

the surface of the gel structure as well as in more porous regions [176]. After the initial release of the NO within the first 8 hours, a significant decrease in NO release is observed in every sample group which is due to depletion of NO reservoir over time while the gels were kept at saturated moisture at 37 °C. Schanuel et al. also observed the same release behavior from the GSNO-Pluronic F-127 hydrogel matrix with an initial increasing gradient in NO flux followed by a steady decrease in the NO release flux [219]. Champeau et al. fabricated PF127 micelles embedded in a poly(acrylic acid) (PAA) matrix, with GSNO molecules dissolved in the hydrophilic domain with different mass ratios between PAA:PF127 contents [176]. They also observed an NO flux of between 40 nmol g^{-1} h^{-1} to 1.5 µmol g^{-1} h^{-1} depending on the concentration of the NO donor molecule in the matrix which closely resembles the results obtained in this study. The facile way to tune the NO release from the SNACET-Pluronic gel matrix only by changing the NO donor molecule content makes this system a promising way for topical delivery of NO, especially for

wound healing applications where a controlled release of NO can significantly impact the wound healing process [219].

One of the observations in this study was the more consistent NO-release from the middle concentration sample groups (2 wt% SNACET) versus the more concentrated samples (5 wt% SNACET), especially after 12 h time point. It is hypothesized that when NO molecule separates from its parent donor after homolysis, the remaining thiyl radical is exposed to the opportunity of reacting with the molecules in the environment to create either disulfide, ROSs, or reactive nitrogen species (RNS) [180, 220]. The ROS and RNS production reactions can lead to further catalytic decomposition of SNACET molecule which leads to a shorter lifespan for the NO donor at the cost of an elevated initial burst release as was observed in this study and by Picheth et al. on *S*-nitrosothiol-terminated Pluronic F127 [180]. Moreover, the rate of decomposition of the terminal –S–NO group is expected to be dependent on environmental factors such as the mobility of the composition elements in addition to the temperature. In a more concentrated gel, it is expected that the terminal group of –S–NO is provided with less mobility comparing to a less concentrated environment; hence, the rate of radical combination must be elevated in higher concentrations as we observed in this study [180, 220, 221].

3.3.4 Antibacterial Efficacy

Successful antibacterial therapy should be able to reduce the burden of bacterial load and impede the spread of bacterial infection. Bacteria on open wounds (burns, cuts, foot ulcers, etc.) can infect and grow on the bare tissue, travel inside the body, and cause bloodstream infections [222-224]. Bacterial infections in the wound often cause delays in wound healing thereby negatively impacting the recovery process [225]. Delayed wound

healing becomes a significant cause of concern especially in chronic wounds like diabetic foot ulcers where infected wounds might take several months to years to heal, increasing the patient trauma and healthcare cost [226]. Current clinical guidelines recommend the topical use of antibiotics and antiseptics to treat and heal the infected acute and chronic wounds. However, a high dosage of antibiotics to treat bacteria can cause systemic toxicity in patients [227]. Moreover, the rise in antibiotic resistance has negatively influenced the use of antibiotics in medicine [105]. Therefore, there is an urgent need for alternative antibacterial regimens for the treatment of infected wounds.

It is reported that NO has been utilized in developing antibacterial wound therapies. NO's role in wound healing has been linked to several important regulatory functions like inflammation, homeostasis, and antibacterial action [119]. However, patients with a weakened immune system (e.g. cancer, diabetes) can have aberrant NO release levels in the body directly affecting the wound healing process [228]. To exogenously deliver NO, an antibacterial Pluronic gel for topical application has been synthesized in this study. Antibacterial activity of SNACET-Pluronic gel was evaluated using the zone of inhibition method [229]. All the control and SNACET-Pluronic gel samples were tested against *S. aureus* and *E. coli* bacteria on LB agar plates. SNACET loaded Pluronic gel showed visibly larger zones of inhibition. Quantitative analysis of the size of growth inhibition zones obtained from the bacteria study revealed direct proportionality to increasing SNACET concentration. For *S. aureus* bacteria, the mean zone diameters observed were *ca.* 3.92, 4.46, 5.47 cm with 1, 2 and 5% gels, respectively (**Figure 19a**). Similarly, for *E. coli* bacteria, 1,2 and 5% SNACET-gels resulted in mean zones with *ca.* 3.06, 3.73, and 4.86 cm diameters, respectively (**Figure 19b**). In both strains, the control group, Pluronic

gel without SNACET (0%) showed slight zones of inhibition of ~1.1 and ~1.3 cm for *E. coli* and *S. aureus*, respectively. This can be attributed to the presence of EDTA in the fabrication of the gels which is known to exhibit some antibacterial properties [230]. However, the zones were significantly enhanced with the addition of SNACET against both *S. aureus* and *E. coli* bacteria ($p < 0.001$) supporting the superior antibacterial effects of NO-releasing gel.

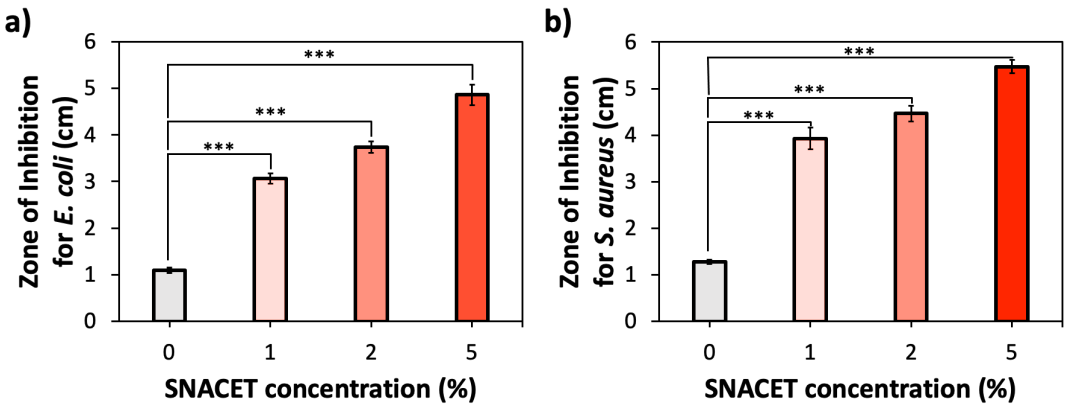

Figure 19. Antibacterial activity of SNACET Pluronic gel against (a) E. *coli* and (b) *S. aureus* bacteria tested in a zone of inhibition study. Data reported as mean diameter ± SEM of zones calculated for samples 0, 1, 2, 5% SNACET-Pluronic gels. *** represents $p < 0.001$.

Bacterial infection is considered one of the most prominent healthcare issues around the world [231]. There is an increasing number of studies on the bactericidal efficacy of RSNO structures that are trying to utilize these NO-donor molecules to address this issue while obviating or reducing the usage of antibiotics not only because of the potency of the RSNO molecules in suppressing bacterial infection but also to reduce the over usage of antibiotics that leads to the emergence of antibiotic-resistant bacterial isolates [100, 232]. In this study antibacterial efficacy of SNACET-Pluronic gel was evaluated against both Gram-negative and -positive bacterial strains, utilizing a zone of inhibition assay. The results obtained from this study are in agreement with the previously reported

bactericidal efficacy of NO-releasing chitosan-grafted-PAMAM/NONOate published by Li et at. recently [233]. The concentration-dependent zone of inhibition was observed for the NO-releasing chitosan matrix which is in correlation with the results obtained in this study. Li et al. also observed that with the increase in NO release capacity of the chitosan-PAMAM/NONOate matrix the zones of inhibition against *E. coli* and *S. aureus* strains reached 21 and 19 mm, respectively. Kabirian et al. also reported a zone of inhibition antibacterial study for a NO-releasing small vascular graft [234]. A Polyethylene glycol (PEG)- Polycaprolactone (PCL) coating was prepared to contain 10 wt% SNAP which released NO with a flux range of $0.5 – 4 \times 10^{-10}$ cm^{-2} min^{-1} over 14 d. It was observed that the grafts could create zones of inhibition against *E. coli* and *S. aureus* during 24 h exposure time approximately measured to be 13 mm for both strains. The increased zones of inhibition for SNACET-Pluronic gel can be explained by the increased NO flux values that lead to better bactericidal efficacy for the hydrogels designed in this study.

3.4 Conclusion

In this study, the SNACET molecule in three different weight percentages (i.e., 1, 2, and 5 wt%) was blended into a hydrogel comprised of Pluronic gel F-127. The concentration-dependent stability of the NO donor molecule within the hydrogel was demonstrated by storing the SNACET-Pluronic gels in two different temperatures (i.e. –20 and 4 °C) and it was shown that the SNACET is most stable at lower temperatures over the course of 4 weeks as more than 80% of the SNACET content remained stable in the hydrogels kept at –20 °C. In addition, it was noted that in each temperature, the gels containing the lower concentration of SNCAET exhibited higher storage stability which

was hypothesized to be related to free radical generations and catalytic decomposition of SNACET when its concentration is increased which leads to a shorter lifespan for the NO donor molecule but an elevated initial burst release as was observed in this study. The Pluronic gel F-127 containing 2 and 5 wt% SNACET molecule, exhibited an NO release flux higher than 0.5×10^{-10} mol cm^{-2} min^{-1} for more than 18 h. The bactericidal behavior as well proved to be concentration-dependent, with 5 wt% SNACET-Pluronic gel presenting the most impact and leaving the largest zones of inhibition (i.e., 5.47 and 4.86 cm against *S. aureus* and *E. coli*, respectively) in the antibacterial efficacy analysis of the gels. These results are in approval to the objective of this study which was to prove the potential application of SNACET-Pluronic gel for topical delivery of NO. This hydrogel structure showed proper workability, tunable and durable NO-release, and considerable bactericidal efficacy against both Gram-negative and -positive bacteria. Further examinations can illustrate the *in vitro*, *ex vivo*, and *in vivo* efficiency of the gels in wound healing and fibroblast cells proliferation and activation. Cytotoxicity studies can also reveal the safe concentration of SNACET molecules that can be incorporated into the hydrogels to obtain the optimum results from SNACET-Pluronic gel in a topical application.

CHAPTER 4

Summary and Recommendations

Through the course of this study, a NO-releasing TiNP was developed successfully which is capable of releasing NO for more than 20 h with a cumulative amount of approximately 25 nmol mg^{-1}. Zeta potential, DLS, and EDS analyses qualitatively indicated the success in the TiNP-SNAP structure development, and later the results were supported by quantitative measurements of amine and thiol functional groups on the surface of nanoparticles in each modification section and finally, by measuring the amount of SNAP loaded on the nanoparticles using NOA. The developed nanoparticle exhibited distinguished bactericidal efficacy against both Gram-negative and -positive *E. coli* and *S. aureus* bacteria, respectively, comparing to unmodified TiNPs. The modified TiNP-SNAP was capable of reducing bacteria viability by ca. 3- and 5-log for *E. coli* and *S. aureus*, respectively. Although the nitrosation rate in this study is in a good range comparing to previous studies which tried to immobilize an NO donor molecule to nanoparticles, it is believed that finding a solution to prevent aggregation of TiNPs will significantly improve the SNAP conjugation and indeed, will elevate the amount and duration of NO release from the nanoparticles.

Developing NO-releasing nanoparticles can expand their application as additive compounds in coatings and polymeric structures, cancer therapy, wound healing, biosensors, and many other biomedical engineering implementations [143]. This study can

expand the usage of TiO_2 nanoparticles by implying antibacterial properties to a nanoparticle that needed UV-irradiation to exhibit antibacterial behavior which in return can significantly increase its potential as a therapeutic agent in biomedical applications.

In addition, by introducing SNACET molecule in three different weight percentages (i.e., 1, 2, and 5 wt%) into a hydrogel structure comprised of Pluronic gel F-127, we demonstrated the concentration-dependent stability of the NO donor molecule within the hydrogel structure. The Pluronic gel F-127 containing 2 and 5 wt% SNACET molecule, exhibited an NO release flux higher than 0.5×10^{-10} mol cm^{-2} min^{-1} for more than 18 h and consequently, the bactericidal behavior proved to be concentration-dependent as well, with 5 wt% SNACET-Pluronic gel leaving largest zones of inhibition (i.e., 5.47 and 4.86 cm against *S. aureus* and *E. coli*, respectively). Moreover, it was illustrated that the stability of the SNACET molecule within the gel structure decreases by increasing its concentration which has been hypothesized to be related to the catalytic decomposition of the SNACET molecule which leads to a shorter lifespan for the NO donor but an elevated initial burst release as was observed in this study. Future work can include series of analyses including fibroblast cells cytocompatibility, proliferation, and migration studies [235], to evaluate the wound healing efficiency as well as extracellular secretion and collagen staining on the SNACET Pluronic gel. Moreover, *in vivo* studies of the NO-releasing hydrogels used in topical and wound healing applications have illustrated their potential in significantly improving the healing process. In addition, local NO release can imply vasodilation, thereby improve ischemic conditions in topical applications [176, 213, 236]. Therefore, further *in vivo* studies can illustrate the impact of SNACET-Pluronic gel on the healing process in infected, or chronic wounds. Finally, utilizing hydrogels for

wound healing applications dictates certain mechanical characteristics to the gel structure to obtain the best workability and application of the hydrogel in a topical application [180]. To that end, adding additional compounds like chitosan, or collagen can significantly impact the mechanical characteristics of the final hydrogel, and change its water absorbance and ultimately NO-release behavior [176]. Therefore, SNACET-Pluronic gel can be optimized to exhibit longer and more controllable NO release by investigating other possible combinations in producing the hydrogel structure.

Overall, in these two studies, the objective was to develop robust antimicrobial and NO-releasing nanoparticles and hydrogels to investigate their potential in combating bacterial infection and introducing their applications in biomedical engineering. Considering the relative properties of the developed TiO_2-SNAP nanoparticles and SNACET-Pluronic gel in delivering NO under physiological conditions throughout 24 h, these materials can be used in future studies to address problems such as bacterial infections in wounds or on medical device surfaces, delayed wound healing, cancer therapy, and many more applications.

References

[1] W.P. Arnold, C.K. Mittal, S. Katsuki, F. Murad, Nitric oxide activates guanylate cyclase and increases guanosine 3':5'-cyclic monophosphate levels in various tissue preparations, Proc Natl Acad Sci U S A 74(8) (1977) 3203-7.

[2] R.F. Furchgott, J.V. Zawadzki, The obligatory role of endothelial cells in the relaxation of arterial smooth muscle by acetylcholine, Nature 288(5789) (1980) 373-6.

[3] L.J. Ignarro, G.M. Buga, K.S. Wood, R.E. Byrns, G. Chaudhuri, Endothelium-derived relaxing factor produced and released from artery and vein is nitric oxide, Proc Natl Acad Sci U S A 84(24) (1987) 9265-9.

[4] S. Moncada, A. Higgs, R. Furchgott, XIV International Union of Pharmacology nomenclature in nitric oxide research, Pharmacol Rev 49(2) (1997) 137-142.

[5] M. Nicholls, Nitric oxide discovery Nobel Prize winners, Eur Heart J 40(22) (2019) 1747-1749.

[6] L.J. Ignarro, G.M. Buga, K.S. Wood, R.E. Byrns, G. Chaudhuri, Endothelium-derived relaxing factor produced and released from artery and vein is nitric oxide, Proc. Natl. Acad. Sci. U.S.A. 84(24) (1987) 9265-9269.

[7] Y. Wo, E.J. Brisbois, R.H. Bartlett, M.E. Meyerhoff, Recent advances in thromboresistant and antimicrobial polymers for biomedical applications: just say yes to nitric oxide (NO), Biomater Sci 4(8) (2016) 1161-1183.

[8] R.G. Knowles, S. Moncada, Nitric oxide synthases in mammals, Biochem J 298 (Pt 2)(2) (1994) 249-58.

[9] J.-P. Stasch, P. Pacher, O.V. Evgenov, Soluble guanylate cyclase as an emerging therapeutic target in cardiopulmonary disease, Circulation 123(20) (2011) 2263-2273.

[10] B.A. Maron, S.-S. Tang, J. Loscalzo, S-nitrosothiols and the S-nitrosoproteome of the cardiovascular system, Antioxidants & redox signaling 18(3) (2013) 270-287.

[11] P.-Y. Cheung, E. Salas, R. Schulz, M.W. Radomski, Nitric oxide and platelet function: Implications for neonatology, Seminars in Perinatology 21(5) (1997) 409-417.

[12] C. Farah, L.Y. Michel, J.-L. Balligand, Nitric oxide signalling in cardiovascular health and disease, Nature Reviews Cardiology 15(5) (2018) 292-316.

[13] G. Jin, Z. Gao, Y. Liu, J. Zhao, H. Ou, F. Xu, D. Ding, Polymeric Nitric Oxide Delivery Nanoplatforms for Treating Cancer, Cardiovascular Diseases, and Infection, Advanced Healthcare Materials 10(3) (2021) 2001550.

[14] Y. Xu, H. Ren, J. Liu, Y. Wang, Z. Meng, Z. He, W. Miao, G. Chen, X. Li, A switchable NO-releasing nanomedicine for enhanced cancer therapy and inhibition of metastasis, Nanoscale 11(12) (2019) 5474-5488.

[15] R. Kinoshita, Y. Ishima, M. Ikeda, U. Kragh-Hansen, J. Fang, H. Nakamura, V.T. Chuang, R. Tanaka, H. Maeda, A. Kodama, S-Nitrosated human serum albumin dimer as novel nano-EPR enhancer applied to macromolecular anti-tumor drugs such as micelles and liposomes, Journal of Controlled Release 217 (2015) 1-9.

[16] C. Riganti, E. Miraglia, D. Viarisio, C. Costamagna, G. Pescarmona, D. Ghigo, A. Bosia, Nitric oxide reverts the resistance to doxorubicin in human colon cancer cells by inhibiting the drug efflux, Cancer research 65(2) (2005) 516-525.

[17] Y. Wo, E.J. Brisbois, J. Wu, Z. Li, T.C. Major, A. Mohammed, X. Wang, A. Colletta, J.L. Bull, A.J. Matzger, C. Xi, R.H. Bartlett, M.E. Meyerhoff, Reduction of thrombosis and bacterial infection via controlled nitric oxide (NO) release from S-Nitroso-N-acetylpenicillamine (SNAP) impregnated CarboSil intravascular catheters, ACS Biomater Sci Eng 3(3) (2017) 349-359.

[18] E.J. Brisbois, T.C. Major, M.J. Goudie, R.H. Bartlett, M.E. Meyerhoff, H. Handa, Improved hemocompatibility of silicone rubber extracorporeal tubing via solvent swelling-impregnation of S-nitroso-N-acetylpenicillamine (SNAP) and evaluation in rabbit thrombogenicity model, Acta Biomater 37 (2016) 111-119.

[19] G. Walford, J. Loscalzo, Nitric oxide in vascular biology, J Thromb Haemost 1(10) (2003) 2112-8.

[20] D.O. Schairer, J.S. Chouake, J.D. Nosanchuk, A.J. Friedman, The potential of nitric oxide releasing therapies as antimicrobial agents, Virulence 3(3) (2012) 271-279.

[21] F. Rong, Y. Tang, T. Wang, T. Feng, J. Song, P. Li, W. Huang, Nitric Oxide-Releasing Polymeric Materials for Antimicrobial Applications: A Review, Antioxidants 8(11) (2019) 556.

[22] D.E. Williams, E.M. Boon, Towards Understanding the Molecular Basis of Nitric Oxide-Regulated Group Behaviors in Pathogenic Bacteria, Journal of Innate Immunity 11(3) (2019) 205-215.

[23] F. Allagnat, C. Dubuis, M. Lambelet, L. Le Gal, F. Alonso, J.-M. Corpataux, S. Déglise, J.-A. Haefliger, Connexin37 reduces smooth muscle cell proliferation and intimal hyperplasia in a mouse model of carotid artery ligation, Cardiovascular research 113(7) (2017) 805-816.

[24] A. Łuczak, M. Madej, A. Kasprzyk, A. Doroszko, Role of the eNOS Uncoupling and the Nitric Oxide Metabolic Pathway in the Pathogenesis of Autoimmune Rheumatic Diseases, Oxidative Medicine and Cellular Longevity 2020 (2020) 1417981.

[25] N. Naghavi, A. de Mel, O.S. Alavijeh, B.G. Cousins, A.M. Seifalian, Nitric oxide donors for cardiovascular implant applications, Small 9(1) (2013) 22-35.

[26] J.O. Lundberg, M.T. Gladwin, E. Weitzberg, Strategies to increase nitric oxide signalling in cardiovascular disease, Nat Rev Drug Discov 14(9) (2015) 623-41.

[27] M. Hauerslev, S.R. Mørk, K. Pryds, H. Contractor, J. Hansen, N.R. Jespersen, J. Johnsen, G. Heusch, P. Kleinbongard, R. Kharbanda, Influence of long-term treatment with glyceryl trinitrate on remote ischemic conditioning, American Journal of Physiology-Heart and Circulatory Physiology 315(1) (2018) H150-H158.

[28] M.R. Holme, T. Sharman, Sodium nitroprusside, (2020).

[29] J.M. Mir, R.C. Maurya, Nitric oxide as a therapeutic option for COVID-19 treatment: a concise perspective, New Journal of Chemistry 45(4) (2021) 1774-1784.

[30] H. Lv, B. Liu, Y. Qin, Isosorbide mononitrate promotes angiogenesis in embryonic development of zebrafish, Genetics and molecular biology 43(3) (2020) 20190233.

[31] P. Zhang, Y. Tian, H. Liu, J. Ren, H. Wang, R. Zeng, Y. Long, J. Chen, In vivo imaging of hepatocellular nitric oxide using a hepatocyte-targeting fluorescent sensor, Chemical Communications 54(52) (2018) 7231-7234.

[32] E. Kus, K. Jasiński, T. Skórka, I. Czyzynska-Cichon, S. Chlopicki, Short-term treatment with hepatoselective NO donor V-PYRRO/NO improves blood flow in hepatic microcirculation in liver steatosis in mice, Pharmacological Reports 70(3) (2018) 463-469.

[33] Y.-m. Cai, J.S. Webb, Optimization of nitric oxide donors for investigating biofilm dispersal response in Pseudomonas aeruginosa clinical isolates, Applied microbiology and biotechnology 104(20) (2020) 8859-8869.

[34] H. Qiu, P. Qi, J. Liu, Y. Yang, X. Tan, Y. Xiao, M.F. Maitz, N. Huang, Z. Yang, Biomimetic engineering endothelium-like coating on cardiovascular stent through heparin and nitric oxide-generating compound synergistic modification strategy, Biomaterials 207 (2019) 10-22.

[35] R. Kumar, H. Massoumi, M.K. Chug, E.J. Brisbois, S-Nitroso-N-acetyl-l-cysteine Ethyl Ester (SNACET) Catheter Lock Solution to Reduce Catheter-Associated Infections, ACS Applied Materials & Interfaces 13(22) (2021) 25813-25824.

[36] A. Mondal, R. Devine, L. Estes, J. Manuel, P. Singha, J. Mancha, M. Palmer, H. Handa, Highly hydrophobic polytetrafluoroethylene particle immobilization via polydopamine anchor layer on nitric oxide releasing polymer for biomedical applications, Journal of Colloid and Interface Science 585 (2021) 716-728.

[37] J.E. Saavedra, A.L. Fitzhugh, L.K. Keefer, Diazeniumdiolates (formerly NONOates) in cardiovascular research and potential clinical applications, Nitric oxide and the cardiovascular system, Springer2000, pp. 431-446.

[38] L.K. Keefer, J.E. Saavedra, Nitrogen-based diazeniumdiolates: versatile nitric oxide-releasing compounds for biomedical research and potential clinical applications, Journal of chemical education 79(12) (2002) 1427.

[39] N. Hasan, J. Lee, D. Kwak, H. Kim, A. Saparbayeva, H.-J. Ahn, I.-S. Yoon, M.-S. Kim, Y. Jung, J.-W. Yoo, Diethylenetriamine/NONOate-doped alginate hydrogel with sustained nitric oxide release and minimal toxicity to accelerate healing of MRSA-infected wounds, Carbohydrate Polymers 270 (2021) 118387.

[40] H. Liang, P. Nacharaju, A. Friedman, J.M. Friedman, Nitric oxide generating/releasing materials, Future science OA 1(1) (2015).

[41] P.G. Wang, M. Xian, X. Tang, X. Wu, Z. Wen, T. Cai, A.J. Janczuk, Nitric oxide donors: chemical activities and biological applications, Chem Rev 102(4) (2002) 1091-134.

[42] E.J. Brisbois, H. Handa, T.C. Major, R.H. Bartlett, M.E. Meyerhoff, Long-term nitric oxide release and elevated temperature stability with S-nitroso-N-acetylpenicillamine (SNAP)-doped Elast-eon E2As polymer, Biomaterials 34(28) (2013) 6957-6966.

[43] S. Hwang, W. Cha, M. Meyerhoff, Polymethacrylates with a Covalently Linked Cu II–Cyclen Complex for the In Situ Generation of Nitric Oxide from Nitrosothiols in Blood We thank the NIH (EB-000783 and EB-004527) for the financial support of this research, (2006).

[44] S. Hwang, M.E. Meyerhoff, Polyurethane with tethered copper(II)–cyclen complex: Preparation, characterization and catalytic generation of nitric oxide from S-nitrosothiols, Biomaterials 29(16) (2008) 2443-2452.

[45] L. Grossi, P.C. Montevecchi, A kinetic study of S-nitrosothiol decomposition, Chemistry 8(2) (2002) 380-7.

[46] R.A. Wapnir, Zinc Deficiency, Malnutrition and the Gastrointestinal Tract, The Journal of Nutrition 130(5) (2000) 1388S-1392S.

[47] N. Toda, H. Toda, Nitric oxide-mediated blood flow regulation as affected by smoking and nicotine, European Journal of Pharmacology 649(1) (2010) 1-13.

[48] E. Brscic, S. Bergerone, A. Gagnor, E. Colajanni, G. Matullo, L. Scaglione, M. Cassader, G. Gaschino, M. Di Leo, A. Brusca, G.F. Pagano, A. Piazza, G.P. Trevi, Acute myocardial infarction in young adults: Prognostic role of angiotensin-converting enzyme, angiotensin II type I receptor, apolipoprotein E, endothelial constitutive nitric oxide synthase, and glycoprotein IIIa genetic polymorphisms at medium-term follow-up, American Heart Journal 139(6) (2000) 979-984.

[49] G. Güncü, T. Tözüm, M. Güncü, N. YAMALIK, Relationships between implant stability, image-based measures and nitric oxide levels, Journal of oral rehabilitation 35(10) (2008) 745-753.

[50] K. Chen, R.N. Pittman, A.S. Popel, Nitric oxide in the vasculature: where does it come from and where does it go? A quantitative perspective, Antioxidants & redox signaling 10(7) (2008) 1185-1198.

[51] M.A. Elnaggar, S.H. Seo, S. Gobaa, K.S. Lim, I.H. Bae, M.H. Jeong, D.K. Han, Y.K. Joung, Nitric Oxide Releasing Coronary Stent: A New Approach Using Layer-by-Layer Coating and Liposomal Encapsulation, Small 12(43) (2016) 6012-6023.

[52] R.P. Tan, I. Ryder, N. Yang, Y.T. Lam, M. Santos, P.L. Michael, D.A. Robinson, M.K. Ng, S.G. Wise, Macrophage Polarization as a Novel Therapeutic Target for Endovascular Intervention in Peripheral Artery Disease, JACC: Basic to Translational Science 6(8) (2021) 693-704.

[53] F. Sharif, S.O. Hynes, K. McCullagh, S. Ganley, U. Greiser, P. McHugh, J. Crowley, F. Barry, T. O'brien, Gene-eluting stents: non-viral, liposome-based gene delivery of eNOS to the blood vessel wall in vivo results in enhanced endothelialization but does not reduce restenosis in a hypercholesterolemic model, Gene therapy 19(3) (2012) 321-328.

[54] V.B. Damodaran, J.M. Joslin, K.A. Wold, S.M. Lantvit, M.M. Reynolds, S-Nitrosated biodegradable polymers for biomedical applications: synthesis, characterization and impact of thiol structure on the physicochemical properties, Journal of Materials Chemistry 22(13) (2012) 5990-6001.

[55] R.S. Yamaguchi, D.T. Noritomi, N.V. Degaspare, G.O.C. Muñoz, A.P.M. Porto, S.F. Costa, O.T. Ranzani, Peripherally inserted central catheters are associated with lower risk of bloodstream infection compared with central venous catheters in paediatric intensive care patients: a propensity-adjusted analysis, Intensive Care Medicine 43(8) (2017) 1097-1104.

[56] J.D. Edwards, C.T. Herzig, H. Liu, M. Pogorzelska-Maziarz, P. Zachariah, A.W. Dick, L. Saiman, P.W. Stone, E.Y. Furuya, Central line–associated blood stream infections in pediatric intensive care units: Longitudinal trends and compliance with bundle strategies, American journal of infection control 43(5) (2015) 489-493.

[57] A.G. Randolph, Pragmatic trials in critically ill children are CATCHing on, Lancet (London, England) 387(10029) (2016) 1697-1698.

[58] M.E. Douglass, M.J. Goudie, J. Pant, P. Singha, S. Hopkins, R. Devine, C.W. Schmiedt, H. Handa, Catalyzed Nitric Oxide Release Via Cu Nanoparticles Leads to an Increase in Antimicrobial Effects and Hemocompatibility for Short Term Extracorporeal Circulation, ACS Appl Bio Mater 2(6) (2019) 2539-2548.

[59] S.P. Hopkins, J. Pant, M.J. Goudie, C. Schmiedt, H. Handa, Achieving long-term biocompatible silicone via covalently immobilized S-nitroso-N-acetylpenicillamine

(SNAP) that exhibits 4 months of sustained nitric oxide release, ACS applied materials & interfaces 10(32) (2018) 27316-27325.

[60] Y. Wo, Z. Li, A. Colletta, J. Wu, C. Xi, A.J. Matzger, E.J. Brisbois, R.H. Bartlett, M.E. Meyerhoff, Study of crystal formation and nitric oxide (no) release mechanism from s-nitroso-n-acetylpenicillamine (snap)-doped carbosil polymer composites for potential antimicrobial applications, Compos B Eng 121 (2017) 23-33.

[61] M. Gominet, F. Compain, C. Beloin, D. Lebeaux, Central venous catheters and biofilms: where do we stand in 2017?, Apmis 125(4) (2017) 365-375.

[62] E.J. Brisbois, M. Kim, X. Wang, A. Mohammed, T.C. Major, J. Wu, J. Brownstein, C. Xi, H. Handa, R.H. Bartlett, M.E. Meyerhoff, Improved Hemocompatibility of Multilumen Catheters via Nitric Oxide (NO) Release from S-Nitroso-N-acetylpenicillamine (SNAP) Composite Filled Lumen, ACS Appl Mater Interfaces 8(43) (2016) 29270-29279.

[63] M. Barnes, C. Feit, T.-A. Grant, E.J. Brisbois, Antimicrobial polymer modifications to reduce microbial bioburden on endotracheal tubes and ventilator associated pneumonia, Acta biomaterialia 91 (2019) 220-234.

[64] E.J. Brisbois, R.P. Davis, A.M. Jones, T.C. Major, R.H. Bartlett, M.E. Meyerhoff, H. Handa, Reduction in thrombosis and bacterial adhesion with 7 day implantation of S-nitroso-N-acetylpenicillamine (SNAP)-doped Elast-eon E2As catheters in sheep, Journal of Materials Chemistry B 3(8) (2015) 1639-1645.

[65] Y. Wo, Z. Li, E.J. Brisbois, A. Colletta, J. Wu, T.C. Major, C. Xi, R.H. Bartlett, A.J. Matzger, M.E. Meyerhoff, Origin of long-term storage stability and nitric oxide release behavior of carbosil polymer doped with s-nitroso-n-acetyl-d-penicillamine, ACS Appl Mater Interfaces 7(40) (2015) 22218-27.

[66] A. Colletta, J. Wu, Y. Wo, M. Kappler, H. Chen, C. Xi, M.E. Meyerhoff, S-Nitroso-N-acetylpenicillamine (SNAP) Impregnated Silicone Foley Catheters: A Potential Biomaterial/Device To Prevent Catheter-Associated Urinary Tract Infections, ACS Biomaterials Science & Engineering 1(6) (2015) 416-424.

[67] R. Devine, M.J. Goudie, P. Singha, C. Schmiedt, M. Douglass, E.J. Brisbois, H. Handa, Mimicking the Endothelium: Dual Action Heparinized Nitric Oxide Releasing Surface, ACS Applied Materials & Interfaces 12(18) (2020) 20158-20171.

[68] H. Ren, M.A. Coughlin, T.C. Major, S. Aiello, A. Rojas Pena, R.H. Bartlett, M.E. Meyerhoff, Improved in Vivo Performance of Amperometric Oxygen (PO2) Sensing Catheters via Electrochemical Nitric Oxide Generation/Release, Analytical Chemistry 87(16) (2015) 8067-8072.

[69] Y. Wu, M.E. Meyerhoff, Nitric oxide-releasing/generating polymers for the development of implantable chemical sensors with enhanced biocompatibility, Talanta 75(3) (2008) 642-650.

[70] M.C. Frost, S.M. Rudich, H. Zhang, M.A. Maraschio, M.E. Meyerhoff, In Vivo Biocompatibility and Analytical Performance of Intravascular Amperometric Oxygen Sensors Prepared with Improved Nitric Oxide-Releasing Silicone Rubber Coating, Analytical Chemistry 74(23) (2002) 5942-5947.

[71] Q. Zhang, G.P. Murray, J.E. Hill, S.L. Harvey, A. Rojas-Pena, J. Choi, Y. Zhou, R.H. Bartlett, M.E. Meyerhoff, Enhanced Hemocompatibility and In Vivo Analytical Accuracy of Intravascular Potentiometric Carbon Dioxide Sensors via Nitric Oxide Release, Analytical Chemistry 92(20) (2020) 13641-13646.

[72] B.Y. Lee, A.E. Wiringa, R.R. Bailey, V. Goyal, B. Tsui, G.J. Lewis, R.R. Muder, L.M. Harrison, The economic effect of screening orthopedic surgery patients preoperatively for methicillin-resistant Staphylococcus aureus, Infection Control & Hospital Epidemiology 31(11) (2010) 1130-1138.

[73] R. Finkelstein, G. Rabino, T. Mashiah, Y. Bar-El, Z. Adler, V. Kertzman, O. Cohen, S. Milo, Vancomycin versus cefazolin prophylaxis for cardiac surgery in the setting of a high prevalence of methicillin-resistant staphylococcal infections, The Journal of thoracic and cardiovascular surgery 123(2) (2002) 326-332.

[74] P.A. De Cock, H. Mulla, S. Desmet, F. De Somer, B.C. McWhinney, J.P. Ungerer, A. Moerman, S. Commeyne, J. Vande Walle, K. Francois, Population pharmacokinetics of cefazolin before, during and after cardiopulmonary bypass to optimize dosing regimens for children undergoing cardiac surgery, Journal of Antimicrobial Chemotherapy 72(3) (2017) 791-800.

[75] J.-G. Ma, J.-X. An, Deep sternal wound infection after cardiac surgery: a comparison of three different wound infection types and an analysis of antibiotic resistance, Journal of thoracic disease 10(1) (2018) 377.

[76] A.W. Carpenter, M.H. Schoenfisch, Nitric oxide release: Part II. Therapeutic applications, Chemical Society Reviews 41(10) (2012) 3742-3752.

[77] A.R. Coates, G. Halls, Y. Hu, Novel classes of antibiotics or more of the same?, British journal of pharmacology 163(1) (2011) 184-194.

[78] P.S. Stewart, J.W. Costerton, Antibiotic resistance of bacteria in biofilms, The lancet 358(9276) (2001) 135-138.

[79] J.R. Hall, K.R. Rouillard, D.J. Suchyta, M.D. Brown, M.J.R. Ahonen, M.H. Schoenfisch, Mode of Nitric Oxide Delivery Affects Antibacterial Action, ACS Biomaterials Science & Engineering 6(1) (2020) 433-441.

[80] M.R. Garren, M. Ashcraft, Y. Qian, M. Douglass, E.J. Brisbois, H. Handa, Nitric oxide and viral infection: Recent developments in antiviral therapies and platforms, Applied Materials Today 22 (2021) 100887.

[81] D. Cánovas, J.F. Marcos, A.T. Marcos, J. Strauss, Nitric oxide in fungi: is there NO light at the end of the tunnel?, Current genetics 62(3) (2016) 513-518.

[82] B.J. Privett, A.D. Broadnax, S.J. Bauman, D.A. Riccio, M.H. Schoenfisch, Examination of bacterial resistance to exogenous nitric oxide, Nitric Oxide 26(3) (2012) 169-173.

[83] S.T. Gregg, Q. Yuan, R.E. Morris, B. Xiao, Functionalised solids delivering bioactive nitric oxide gas for therapeutic applications, Materials Today Communications 12 (2017) 95-105.

[84] M.E. Rupp, R. Karnatak, Intravascular catheter–related bloodstream infections, Infectious Disease Clinics 32(4) (2018) 765-787.

[85] J. Chandra, L. Long, N. Isham, P.K. Mukherjee, G. DiSciullo, K. Appelt, M.A. Ghannoum, In vitro and in vivo activity of a novel catheter lock solution against bacterial and fungal biofilms, Antimicrobial agents and chemotherapy 62(8) (2018) e00722-18.

[86] H. Derakhshandeh, F. Aghabaglou, A. McCarthy, A. Mostafavi, C. Wiseman, Z. Bonick, I. Ghanavati, S. Harris, C. Kreikemeier-Bower, S.M. Moosavi Basri, J. Rosenbohm, R. Yang, P. Mostafalu, D. Orgill, A. Tamayol, A Wirelessly Controlled Smart Bandage with 3D-Printed Miniaturized Needle Arrays, Advanced Functional Materials 30(13) (2020).

[87] M.J. Goudie, P. Singha, S.P. Hopkins, E.J. Brisbois, H. Handa, Active Release of an Antimicrobial and Antiplatelet Agent from a Nonfouling Surface Modification, ACS Appl Mater Interfaces 11(4) (2019) 4523-4530.

[88] L. Höfler, D. Koley, J. Wu, C. Xi, M.E. Meyerhoff, Electromodulated release of nitric oxide through polymer material from reservoir of inorganic nitrite salt, RSC Advances 2(17) (2012) 6765-6767.

[89] H. Ren, A. Colletta, D. Koley, J. Wu, C. Xi, T.C. Major, R.H. Bartlett, M.E. Meyerhoff, Thromboresistant/anti-biofilm catheters via electrochemically modulated nitric oxide release, Bioelectrochemistry 104 (2015) 10-16.

[90] E.M. Hetrick, J.H. Shin, H.S. Paul, M.H. Schoenfisch, Anti-biofilm efficacy of nitric oxide-releasing silica nanoparticles, Biomaterials 30(14) (2009) 2782-2789.

[91] R.G. Frykberg, J. Banks, Challenges in the Treatment of Chronic Wounds, Adv Wound Care (New Rochelle) 4(9) (2015) 560-582.

[92] A.C.D. Gonzalez, T.F. Costa, Z.D. Andrade, A.R.A.P. Medrado, Wound healing - A literature review, Anais Brasileiros De Dermatologia 91(5) (2016) 614-620.

[93] S. Dhivya, V.V. Padma, E. Santhini, Wound dressings - a review, Biomedicine (Taipei) 5(4) (2015) 22.

[94] T. Maver, U. Maver, K. Stana Kleinschek, D.M. Smrke, S. Kreft, A review of herbal medicines in wound healing, Int J Dermatol 54(7) (2015) 740-51.

[95] L.C. Tapsell, I. Hemphill, L. Cobiac, C.S. Patch, D.R. Sullivan, M. Fenech, S. Roodenrys, J.B. Keogh, P.M. Clifton, P.G. Williams, V.A. Fazio, K.E. Inge, Health benefits of herbs and spices: the past, the present, the future, Med J Aust 185(S4) (2006) S1-S24.

[96] V. Vachhrajani, P. Khakhkhar, Science of Wound Healing and Dressing Materials, Springer2020.

[97] M. Mercandetti, A. Cohen, Wound healing and repair, E Medicine (cited 2002 Oct 7). Available from URL: http://www. eMedicine. com. Inc (2017).

[98] S. Guo, L.A. Dipietro, Factors affecting wound healing, J Dent Res 89(3) (2010) 219-29.

[99] G. Han, R. Ceilley, Chronic Wound Healing: A Review of Current Management and Treatments, Adv Ther 34(3) (2017) 599-610.

[100] Y. Wo, E.J. Brisbois, R.H. Bartlett, M.E. Meyerhoff, Recent advances in thromboresistant and antimicrobial polymers for biomedical applications: just say yes to nitric oxide (NO), Biomater Sci 4(8) (2016) 1161-83.

[101] M.B. Witte, A. Barbul, GENERAL PRINCIPLES OF WOUND HEALING, Surgical Clinics of North America 77(3) (1997) 509-528.

[102] C. Thomas Hess, Checklist for factors affecting wound healing, Adv Skin Wound Care 24(4) (2011) 192.

[103] W.G. Payne, D.K. Naidu, C.K. Wheeler, D. Barkoe, M. Mentis, R.E. Salas, D.J. Smith, Jr., M.C. Robson, Wound healing in patients with cancer, Eplasty 8 (2008) e9.

[104] H. Bonifant, S. Holloway, A review of the effects of ageing on skin integrity and wound healing, Br J Community Nurs 24(Sup3) (2019) S28-S33.

[105] M.D. Caldwell, Bacteria and Antibiotics in Wound Healing, Surg Clin North Am 100(4) (2020) 757-776.

[106] J.Y. Lin, K.Y. Lo, Y.S. Sun, A microfluidics-based wound-healing assay for studying the effects of shear stresses, wound widths, and chemicals on the wound-healing process, Sci Rep 9(1) (2019) 20016.

[107] M.J. Westby, J.C. Dumville, N. Stubbs, G. Norman, J.K.F. Wong, N. Cullum, R.D. Riley, Protease activity as a prognostic factor for wound healing in venous leg ulcers, Cochrane Database of Systematic Reviews 9(9) (2018) CD012841.

[108] C. Hu, L. Zhao, D. Wu, L. Li, Modulating autophagy in mesenchymal stem cells effectively protects against hypoxia- or ischemia-induced injury, Stem Cell Res Ther 10(1) (2019) 120.

[109] V.W. Wong, G.C. Gurtner, M.T. Longaker, Wound healing: a paradigm for regeneration, Mayo Clin Proc 88(9) (2013) 1022-31.

[110] M.R. Schäffer, U. Tantry, S.S. Gross, H.L. Wasserkrug, A. Barbul, Nitric Oxide Regulates Wound Healing, Journal of Surgical Research 63(1) (1996) 237-240.

[111] M.B. Witte, F.J. Thornton, D.T. Efron, A. Barbul, Enhancement of Fibroblast Collagen Synthesis by Nitric Oxide, Nitric Oxide 4(6) (2000) 572-582.

[112] A.B. Shekhter, R.K. Kabisov, A.V. Pekshev, N.P. Kozlov, Y.L. Perov, Experimental and clinical validation of plasmadynamic therapy of wounds with nitric oxide, Bulletin of Experimental Biology and Medicine 126(2) (1998) 829-834.

[113] J.-d. Luo, A.F. Chen, Nitric oxide: a newly discovered function on wound healing, Acta Pharmacologica Sinica 26(3) (2005) 259-264.

[114] M. Rizk, M.B. Witte, A. Barbul, Nitric Oxide and Wound Healing, World Journal of Surgery 28(3) (2004) 301-306.

[115] S. Taleb, P. Moghaddas, M. Rahimi Balaei, S. Taleb, S. Rahimpour, A. Abbasi, S. Ejtemaei-Mehr, A.R. Dehpour, Metformin improves skin flap survival through nitric oxide system, Journal of Surgical Research 192(2) (2014) 686-691.

[116] S. Donnini, M. Ziche, Constitutive and inducible nitric oxide synthase: role in angiogenesis, Antioxidants and Redox Signaling 4(5) (2002) 817-823.

[117] C.F. Nathan, J.B. Hibbs Jr, Role of nitric oxide synthesis in macrophage antimicrobial activity, Current opinion in immunology 3(1) (1991) 65-70.

[118] D.T. Efron, D. Most, A. Barbul, Role of nitric oxide in wound healing, Current Opinion in Clinical Nutrition & Metabolic Care 3(3) (2000) 197-204.

[119] M.J. Malone-Povolny, S.E. Maloney, M.H. Schoenfisch, Nitric oxide therapy for diabetic wound healing, Advanced healthcare materials 8(12) (2019) 1801210.

[120] J. Loscalzo, J. Freedman, A. Inbal, J. Keaney Jr, A. Michelson, J. Vita, Nitric oxide insufficiency and arterial thrombosis, Transactions of the American Clinical and Climatological Association 111 (2000) 158.

[121] K.S.B. Masters, S.J. Leibovich, P. Belem, J.L. West, L.A. Poole-Warren, Effects of nitric oxide releasing poly (vinyl alcohol) hydrogel dressings on dermal wound healing in diabetic mice, Wound Repair and regeneration 10(5) (2002) 286-294.

[122] T.P. Amadeu, A.B. Seabra, M.G. De Oliveira, A.M. Costa, S-nitrosoglutathione-containing hydrogel accelerates rat cutaneous wound repair, Journal of the European Academy of Dermatology and Venereology 21(5) (2007) 629-637.

[123] V.C. Póvoa, G.J. Dos Santos, G.F. Picheth, C.P. Jara, L.C. da Silva, E.P. de Araujo, M.G. de Oliveira, Wound healing action of nitric oxide-releasing self-expandable collagen sponge, Journal of tissue engineering and regenerative medicine 14(6) (2020) 807-818.

[124] J. Kim, G. Saravanakumar, H.W. Choi, D. Park, W.J. Kim, A platform for nitric oxide delivery, Journal of Materials Chemistry B 2(4) (2014) 341-356.

[125] W. Wu, C. Gaucher, I. Fries, X.-M. Hu, P. Maincent, A. Sapin-Minet, Polymer nanocomposite particles of S-nitrosoglutathione: A suitable formulation for protection and sustained oral delivery, International journal of pharmaceutics 495(1) (2015) 354-361.

[126] S.U. Shah, N. Martinho, M. Socha, C. Pinto Reis, S. Gibaud, Synthesis and characterization of S-nitrosoglutathione-oligosaccharide-chitosan as a nitric oxide donor, Expert opinion on drug delivery 12(8) (2015) 1209-1223.

[127] S.U. Shah, M. Socha, I. Fries, S. Gibaud, Synthesis of S-nitrosoglutathione-alginate for prolonged delivery of nitric oxide in intestines, Drug delivery 23(8) (2016) 2927-2935.

[128] G. Lautner, B. Stringer, E.J. Brisbois, M.E. Meyerhoff, S.P. Schwendeman, Controlled light-induced gas phase nitric oxide release from S-nitrosothiol-doped silicone rubber films, Nitric Oxide 86 (2019) 31-37.

[129] M.K. Chug, C. Feit, E.J. Brisbois, Increasing the lifetime of insulin cannula with antifouling and nitric oxide releasing properties, ACS Appl. Bio Mater. 2(12) (2019) 5965-5975.

[130] C.G. Feit, M.K. Chug, E.J. Brisbois, Development of S-Nitroso-N-Acetylpenicillamine Impregnated Medical Grade Polyvinyl Chloride for Antimicrobial Medical Device Interfaces, ACS Applied Bio Materials 2(10) (2019) 4335-4345.

[131] L.-C. Xu, M.E. Meyerhoff, C.A. Siedlecki, Blood coagulation response and bacterial adhesion to biomimetic polyurethane biomaterials prepared with surface texturing and nitric oxide release, Acta Biomaterialia 84 (2019) 77-87.

[132] M.J. Malone-Povolny, M.H. Schoenfisch, Extended nitric oxide-releasing polyurethanes via S-nitrosothiol-modified mesoporous silica nanoparticles, ACS applied materials & interfaces 11(13) (2019) 12216-12223.

[133] P. Singha, J. Pant, M.J. Goudie, C.D. Workman, H. Handa, Enhanced antibacterial efficacy of nitric oxide releasing thermoplastic polyurethanes with antifouling hydrophilic topcoats, Biomaterials science 5(7) (2017) 1246-1255.

[134] M.K. Chug, E. Bachtiar, N. Narwold, K. Gall, E.J. Brisbois, Tailoring nitric oxide release with additive manufacturing to create antimicrobial surfaces, Biomater. Sci 9(8) (2021) 3100-3111.

[135] A. Mondal, M. Douglass, S.P. Hopkins, P. Singha, M. Tran, H. Handa, E.J. Brisbois, Multifunctional S-Nitroso-N-acetylpenicillamine-incorporated medical-grade polymer with selenium interface for biomedical applications, ACS Appl Mater Interfaces 11(38) (2019) 34652-34662.

[136] S. Ghalei, J. Li, M. Douglass, M. Garren, H. Handa, Synergistic approach to develop antibacterial electrospun scaffolds using honey and S-nitroso-N-acetyl penicillamine, ACS Biomater Sci Eng 7(2) (2021) 517-526.

[137] S. Ghalei, A. Mondal, S. Hopkins, P. Singha, R. Devine, H. Handa, Silk nanoparticles: a natural polymeric platform for nitric oxide delivery in biomedical applications, ACS Appl Mater Interfaces 12(48) (2020) 53615-53623.

[138] Y. Wo, Z. Li, E.J. Brisbois, A. Colletta, J. Wu, T.C. Major, C. Xi, R.H. Bartlett, A.J. Matzger, M.E. Meyerhoff, Origin of long-term storage stability and nitric oxide release behavior of carbosil polymer doped with s-nitroso-n-acetyl-d-penicillamine, ACS Appl Mater Interfaces 7(40) (2015) 22218-22227.

[139] S.P. Hopkins, M.C. Frost, Synthesis and characterization of controlled nitric oxide release from S-nitroso-N-acetyl-d-penicillamine covalently linked to polyvinyl chloride (SNAP-PVC), Bioengineering (Basel) 5(3) (2018) 72.

[140] M.C. Frost, M.E. Meyerhoff, Controlled photoinitiated release of nitric oxide from polymer films containing S-nitroso-N-acetyl-DL-penicillamine derivatized fumed silica filler, J Am Chem Soc 126(5) (2004) 1348-9.

[141] B.M. Grommersch, J. Pant, S.P. Hopkins, M.J. Goudie, H. Handa, Biotemplated synthesis and characterization of mesoporous nitric oxide-releasing diatomaceous earth silica particles, ACS Appl. Mater. Interfaces 10(3) (2018) 2291-2301.

[142] S. Ghalei, S. Hopkins, M. Douglass, M. Garren, A. Mondal, H. Handa, Nitric oxide releasing halloysite nanotubes for biomedical applications, J Colloid Interface Sci 590 (2021) 277-289.

[143] A.B. Seabra, M.T. Pelegrino, L. Ferraz, T. Rodrigue, W.J. Fávaro, N. Durán, Nitric oxide-releasing engineered nanoparticles: tools for overcoming drug resistance in chemotherapy, in: L. Morbidelli, B. Bonavida (Eds.), Therapeutic Application of Nitric Oxide in Cancer and Inflammatory Disorders, Academic Press2019, pp. 3-28.

[144] J. Rosen, A. Landriscina, J.D. Nosanchuk, Nitric oxide–releasing nanoparticles as an antimicrobial therapeutic, in: M.R. Hamblin, P. Avci, T.W. Prow (Eds.), Nanoscience in Dermatology, Academic Press, Boston, 2016, pp. 127-134.

[145] Z. Youssef, R. Vanderesse, L. Colombeau, F. Baros, T. Roques-Carmes, C. Frochot, H. Wahab, J. Toufaily, T. Hamieh, S. Acherar, A.M. Gazzali, The application of titanium dioxide, zinc oxide, fullerene, and graphene nanoparticles in photodynamic therapy, Cancer Nanotechnol 8(1) (2017) 6.

[146] Q. Feng, Y. Li, X. Yang, W. Zhang, Y. Hao, H. Zhang, L. Hou, Z. Zhang, Hypoxia-specific therapeutic agents delivery nanotheranostics: A sequential strategy for ultrasound mediated on-demand tritherapies and imaging of cancer, J Control Release 275 (2018) 192-200.

[147] D. Ziental, B. Czarczynska-Goslinska, D.T. Mlynarczyk, A. Glowacka-Sobotta, B. Stanisz, T. Goslinski, L. Sobotta, Titanium dioxide nanoparticles: Prospects and applications in medicine, Nanomaterials (Basel) 10(2) (2020) 387.

[148] S.M. Santhosh, K. Natarajan, Antibiofilm activity of Epoxy/Ag-TiO2 polymer nanocomposite coatings against Staphylococcus Aureus and Escherichia Coli, Coatings 5(2) (2015) 95-114.

[149] T. Verdier, M. Coutand, A. Bertron, C. Roques, Antibacterial activity of TiO2 photocatalyst alone or in coatings on E. coli: the influence of methodological aspects, Coatings 4(3) (2014) 670-686.

[150] P. Rokicka-Konieczna, A. Wanag, A. Sienkiewicz, E. Kusiak-Nejman, A.W. Morawski, Antibacterial effect of TiO2 nanoparticles modified with APTES, Catal Commun 134 (2020) 105862.

[151] B. Gokdere, A. Uzer, S. Durmazel, E. Ercag, R. Apak, Titanium dioxide nanoparticles-based colorimetric sensors for determination of hydrogen peroxide and triacetone triperoxide (TATP), Talanta 202 (2019) 402-410.

[152] L. Di Giampaolo, G. Zaccariello, A. Benedetti, G. Vecchiotti, F. Caposano, E. Sabbioni, F. Groppi, S. Manenti, Q. Niu, A.M.G. Poma, M. Di Gioacchino, C. Petrarca, Genotoxicity and immunotoxicity of titanium dioxide-embedded mesoporous silica nanoparticles (TiO2@MSN) in primary peripheral human blood mononuclear cells (PBMC), Nanomaterials (Basel) 11(2) (2021) 270.

[153] S. Zhou, Y. Zhang, L. Ni, Y. Pei, H. Zhang, H. Zhang, Applied organic-inorganic nanocomposite of PLA-TiO2 for preparing polysulfone membrane: structure, performance and UV-assisted cleaning strategy, Water Sci Technol 83(1) (2021) 198-211.

[154] T.H.A. Ngo, C.T.M. Nguyen, K.D. Do, Q.X. Duong, N.H. Tran, H.T.V. Nguyen, D.T. Tran, Improvement of hydrophilicity for polyamide composite membrane by incorporation of graphene oxide-titanium dioxide nanoparticles, J Anal Methods Chem 2020 (2020) 6641225.

[155] N.G. Ireni, M. Karuppaiah, R. Narayan, K.V.S.N. Raju, P. Basak, TiO2/Poly(thiourethane-urethane)-urea nanocomposites: Anticorrosion materials with NIR-reflectivity and high refractive index, Polymer 119 (2017) 142-151.

[156] L. López-Zamora, H.N. Martínez-Martínez, J.A. González-Calderón, Improvement of the colloidal stability of titanium dioxide particles in water through silicon based coupling agent, Mater. Chem. Phys. 217 (2018) 285-290.

[157] Mineral commodity summaries 2021, Mineral Commodity Summaries, Reston, VA, 2021, p. 200.

[158] N. Salahuddin, M. Gaber, S. Elneanaey, M.R. Snowdon, M.A. Abdelwahab, Co-delivery of norfloxacin and tenoxicam in Ag-TiO2/poly(lactic acid) nanohybrid, Int J Biol Macromol 180 (2021) 771-781.

[159] V. Kant, A. Gopal, D. Kumar, A. Gopalkrishnan, N.N. Pathak, N.P. Kurade, S.K. Tandan, D. Kumar, Topical pluronic F-127 gel application enhances cutaneous wound healing in rats, Acta Histochemica 116(1) (2014) 5-13.

[160] A.A. Zahid, R. Ahmed, S.R. ur Rehman, R. Augustine, M. Tariq, A. Hasan, Nitric oxide releasing chitosan-poly (vinyl alcohol) hydrogel promotes angiogenesis in chick embryo model, International journal of biological macromolecules 136 (2019) 901-910.

[161] M.P. Ribeiro, A. Espiga, D. Silva, P. Baptista, J. Henriques, C. Ferreira, J.C. Silva, J.P. Borges, E. Pires, P. Chaves, Development of a new chitosan hydrogel for wound dressing, Wound repair and regeneration 17(6) (2009) 817-824.

[162] K. Hori, C. Sotozono, J. Hamuro, K. Yamasaki, Y. Kimura, M. Ozeki, Y. Tabata, S. Kinoshita, Controlled-release of epidermal growth factor from cationized gelatin hydrogel enhances corneal epithelial wound healing, Journal of Controlled Release 118(2) (2007) 169-176.

[163] M. Zhang, X. Zhao, Alginate hydrogel dressings for advanced wound management, International Journal of Biological Macromolecules 162 (2020) 1414-1428.

[164] Q. Xu, S. A, Y. Gao, L. Guo, J. Creagh-Flynn, D. Zhou, U. Greiser, Y. Dong, F. Wang, H. Tai, W. Liu, W. Wang, W. Wang, A hybrid injectable hydrogel from hyperbranched PEG macromer as a stem cell delivery and retention platform for diabetic wound healing, Acta Biomaterialia 75 (2018) 63-74.

[165] H. Bi, T. Feng, B. Li, Y. Han, In Vitro and In Vivo Comparison Study of Electrospun PLA and PLA/PVA/SA Fiber Membranes for Wound Healing, Polymers 12(4) (2020) 839.

[166] Y.-H. Lee, J.-J. Chang, M.-C. Yang, C.-T. Chien, W.-F. Lai, Acceleration of wound healing in diabetic rats by layered hydrogel dressing, Carbohydrate Polymers 88(3) (2012) 809-819.

[167] J.C. Gilbert, J. Hadgraft, A. Bye, L.G. Brookes, Drug release from Pluronic F-127 gels, International journal of pharmaceutics 32(2-3) (1986) 223-228.

[168] M.T. Pelegrino, D.R. de Araújo, A.B. Seabra, S-nitrosoglutathione-containing chitosan nanoparticles dispersed in Pluronic F-127 hydrogel: Potential uses in topical applications, Journal of Drug Delivery Science and Technology 43 (2018) 211-220.

[169] M.S.H. Akash, K. Rehman, Recent progress in biomedical applications of Pluronic (PF127): Pharmaceutical perspectives, Journal of Controlled Release 209 (2015) 120-138.

[170] Y. Qiu, S.K. Hamilton, J. Temenoff, 4 - Improving mechanical properties of injectable polymers and composites, in: B. Vernon (Ed.), Injectable Biomaterials, Woodhead Publishing2011, pp. 61-91.

[171] K. Harding, H. Morris, G. Patel, Healing chronic wounds, Bmj 324(7330) (2002) 160-163.

[172] N.L. McCartney-Francis, S.M. Wahl, TGF-β and macrophages in the rise and fall of inflammation, TGF-β and Related Cytokines in Inflammation, Springer2001, pp. 65-90.

[173] S. Werner, R. Grose, Regulation of wound healing by growth factors and cytokines, Physiological reviews 83(3) (2003) 835-870.

[174] E.V. Batrakova, A.V. Kabanov, Pluronic block copolymers: evolution of drug delivery concept from inert nanocarriers to biological response modifiers, Journal of controlled release 130(2) (2008) 98-106.

[175] A.V. Kabanov, E.V. Batrakova, D.W. Miller, Pluronic® block copolymers as modulators of drug efflux transporter activity in the blood–brain barrier, Advanced drug delivery reviews 55(1) (2003) 151-164.

[176] M. Champeau, V. Póvoa, L. Militão, F.M. Cabrini, G.F. Picheth, F. Meneau, C.P. Jara, E.P. de Araujo, M.G. de Oliveira, Supramolecular poly(acrylic acid)/F127 hydrogel with hydration-controlled nitric oxide release for enhancing wound healing, Acta Biomaterialia 74 (2018) 312-325.

[177] S.l.M. Shishido, A.B. Seabra, W. Loh, M. Ganzarolli de Oliveira, Thermal and photochemical nitric oxide release from S-nitrosothiols incorporated in Pluronic F127 gel: potential uses for local and controlled nitric oxide release, Biomaterials 24(20) (2003) 3543-3553.

[178] F.S. Schanuel, K.S.R. Santos, A. Monte-Alto-Costa, M.G. de Oliveira, Combined nitric oxide-releasing poly (vinyl alcohol) film/F127 hydrogel for accelerating wound healing, Colloids and Surfaces B: Biointerfaces 130 (2015) 182-191.

[179] M. Champeau, V. Póvoa, L. Militão, F.M. Cabrini, G.F. Picheth, F. Meneau, C.P. Jara, E.P. de Araujo, M.G. de Oliveira, Supramolecular poly (acrylic acid)/F127 hydrogel with hydration-controlled nitric oxide release for enhancing wound healing, Acta biomaterialia 74 (2018) 312-325.

[180] G.F. Picheth, L.C. Da Silva, L.P. Giglio, T.S. Plivelic, M.G. de Oliveira, S-nitrosothiol-terminated Pluronic F127: Influence of microstructure on nitric oxide release, Journal of colloid and interface science 576 (2020) 457-467.

[181] L. Di Giampaolo, G. Zaccariello, A. Benedetti, G. Vecchiotti, F. Caposano, E. Sabbioni, F. Groppi, S. Manenti, Q. Niu, A.M.G. Poma, M. Di Gioacchino, C. Petrarca, Genotoxicity and immunotoxicity of titanium dioxide-embedded mesoporous silica nanoparticles (TiO2@MSN) in primary peripheral human blood mononuclear cells (PBMC), Nanomaterials 11(2) (2021) 270.

[182] H.A. Moynihan, S.M. Roberts, Preparation of some novel S-nitroso compounds as potential slow-release agents of nitric oxide in vivo, J. Chem. Soc., Perkin Trans. 1 (7) (1994) 797-805.

[183] M.C. Frost, M.E. Meyerhoff, Synthesis, characterization, and controlled nitric oxide release from S-nitrosothiol-derivatized fumed silica polymer filler particles, J Biomed Mater Res A 72(4) (2005) 409-19.

[184] D.R. Hristov, L. Rocks, P.M. Kelly, S.S. Thomas, A.S. Pitek, P. Verderio, E. Mahon, K.A. Dawson, Tuning of nanoparticle biological functionality through controlled surface chemistry and characterisation at the bioconjugated nanoparticle surface, Sci Rep 5(1) (2015) 17040.

[185] Y. Sun, F. Kunc, V. Balhara, B. Coleman, O. Kodra, M. Raza, M.H. Chen, A. Brinkmann, G.P. Lopinski, L.J. Johnston, Quantification of amine functional groups on silica nanoparticles: a multi-method approach, Nanoscale Adv 1(4) (2019) 1598-1607.

[186] C.K. Riener, G. Kada, H.J. Gruber, Quick measurement of protein sulfhydryls with Ellman's reagent and with 4,4'-dithiodipyridine, Anal Bioanal Chem 373(4-5) (2002) 266-76.

[187] C.W. McCarthy, J. Goldman, M.C. Frost, Synthesis and characterization of the novel nitric oxide (NO) donating compound, S-nitroso-N-acetyl-D-penicillamine derivatized cyclam (SNAP-cyclam), ACS Appl Mater Interfaces 8(9) (2016) 5898-905.

[188] S. Hopkins, M. Frost, Synthesis and characterization of controlled nitric oxide release from S-nitroso-N-acetyl-d-penicillamine covalently linked to polyvinyl chloride (SNAP-PVC), Bioengineering 5(3) (2018) 72.

[189] J.H. Shin, S.K. Metzger, M.H. Schoenfisch, Synthesis of nitric oxide-releasing silica nanoparticles, J Am Chem Soc 129(15) (2007) 4612-9.

[190] P. Cabrales, G. Han, C. Roche, P. Nacharaju, A.J. Friedman, J.M. Friedman, Sustained release nitric oxide from long-lived circulating nanoparticles, Free Radic Biol Med 49(4) (2010) 530-8.

[191] D.A. Riccio, J.L. Nugent, M.H. Schoenfisch, Stober synthesis of nitric oxide-releasing S-nitrosothiol-modified silica particles, Chem Mater 23(7) (2011) 1727-1735.

[192] F. Thielbeer, K. Donaldson, M. Bradley, Zeta Potential Mediated Reaction Monitoring on Nano and Microparticles, Bioconjugate Chemistry 22(2) (2011) 144-150.

[193] S. Filice, G. Compagnini, R. Fiorenza, S. Scire, L. D'Urso, M.E. Fragala, P. Russo, E. Fazio, S. Scalese, Laser processing of TiO2 colloids for an enhanced photocatalytic water splitting activity, J Colloid Interface Sci 489 (2017) 131-137.

[194] K.A. Guzman, M.P. Finnegan, J.F. Banfield, Influence of surface potential on aggregation and transport of titania nanoparticles, Environ Sci Technol 40(24) (2006) 7688-93.

[195] A. Wanag, A. Sienkiewicz, P. Rokicka-Konieczna, E. Kusiak-Nejman, A.W. Morawski, Influence of modification of titanium dioxide by silane coupling agents on the photocatalytic activity and stability, J Environ Chem Eng 8(4) (2020) 103917.

[196] W. Stöber, A. Fink, E. Bohn, Controlled growth of monodisperse silica spheres in the micron size range, J Colloid Interface Sci 26(1) (1968) 62-69.

[197] A. Gill, J. Zajda, M.E. Meyerhoff, Comparison of electrochemical nitric oxide detection methods with chemiluminescence for measuring nitrite concentration in food samples, Anal Chim Acta 1077 (2019) 167-173.

[198] V. Hampl, C. Walters, S. Archer, Determination of nitric oxide by the chemiluminescence reaction with ozone. , in: M. Feelisch, J. Stamler (Eds.), Methods in Nitric Oxide Research, John Wiley & Sons1996, pp. 309-318.

[199] H. Ren, J. Wu, C. Xi, N. Lehnert, T. Major, R.H. Bartlett, M.E. Meyerhoff, Electrochemically modulated nitric oxide (NO) releasing biomedical devices via Copper(II)-Tri(2-pyridylmethyl)amine mediated reduction of nitrite, ACS Appl. Mater. Interfaces 6(6) (2014) 3779-3783.

[200] A.J. Friedman, G. Han, M.S. Navati, M. Chacko, L. Gunther, A. Alfieri, J.M. Friedman, Sustained release nitric oxide releasing nanoparticles: characterization of a novel delivery platform based on nitrite containing hydrogel/glass composites, Nitric Oxide 19(1) (2008) 12-20.

[201] J.L. Martinez, General principles of antibiotic resistance in bacteria, Drug Discov Today Technol 11 (2014) 33-9.

[202] L. Wang, C. Hu, L. Shao, The antimicrobial activity of nanoparticles: present situation and prospects for the future, Int J Nanomedicine 12 (2017) 1227-1249.

[203] C. Kaweeteerawat, P. Na Ubol, S. Sangmuang, S. Aueviriyavit, R. Maniratanachote, Mechanisms of antibiotic resistance in bacteria mediated by silver nanoparticles, J Toxicol Environ Health A 80(23-24) (2017) 1276-1289.

[204] L.R. Jarboe, D.R. Hyduke, L.M. Tran, K.J. Chou, J.C. Liao, Determination of the Escherichia coli S-nitrosoglutathione response network using integrated biochemical and systems analysis, J Biol Chem 283(8) (2008) 5148-57.

[205] A. Friedman, K. Blecher, D. Sanchez, C. Tuckman-Vernon, P. Gialanella, J.M. Friedman, L.R. Martinez, J.D. Nosanchuk, Susceptibility of Gram-positive and -negative bacteria to novel nitric oxide-releasing nanoparticle technology, Virulence 2(3) (2011) 217-21.

[206] M. Trivedi, J. Murase, Titanium Dioxide in Sunscreen, in: M. Janus (Ed.), Application of Titanium Dioxide, InTech2017, pp. 61-71.

[207] K. Lee, H. Trochimowicz, C. Reinhardt, Pulmonary response of rats exposed to titanium dioxide (TiO2) by inhalation for two years, Toxicol. Appl. Pharmacol. 79(2) (1985) 179-192.

[208] Y.T. Duan, Y. Wang, X.H. Li, G.Z. Zhang, G.Y. Zhang, J.M. Hu, Light-triggered nitric oxide (NO) release from photoresponsive polymersomes for corneal wound healing, Chemical Science 11(1) (2020) 186-194.

[209] H.W. Choi, J. Kim, J. Kim, Y. Kim, H.B. Song, J.H. Kim, K. Kim, W.J. Kim, Light-Induced Acid Generation on a Gatekeeper for Smart Nitric Oxide Delivery, ACS Nano 10(4) (2016) 4199-208.

[210] J.O. Kim, J.-K. Noh, R.K. Thapa, N. Hasan, M. Choi, J.H. Kim, J.-H. Lee, S.K. Ku, J.-W. Yoo, Nitric oxide-releasing chitosan film for enhanced antibacterial and in vivo wound-healing efficacy, International Journal of Biological Macromolecules 79 (2015) 217-225.

[211] X. Zhou, H. Wang, J. Zhang, X. Li, Y. Wu, Y. Wei, S. Ji, D. Kong, Q. Zhao, Functional poly(epsilon-caprolactone)/chitosan dressings with nitric oxide-releasing property improve wound healing, Acta Biomater 54 (2017) 128-137.

[212] D. Tsikas, S. Dehnert, K. Urban, A. Surdacki, H.H. Meyer, GC–MS analysis of S-nitrosothiols after conversion to S-nitroso-N-acetyl cysteine ethyl ester and in-injector nitrosation of ethyl acetate, Journal of Chromatography B 877(28) (2009) 3442-3455.

[213] M.I. Santos, L.C. Da Silva, M.P. Bomediano, D.M. Catori, M. do Carmo Gonçalves, M.G. de Oliveira, 3D printed nitric oxide-releasing poly (acrylic acid)/F127/cellulose nanocrystal hydrogels, Soft Matter (2021).

[214] J.C. Gilbert, J.L. Richardson, M.C. Davies, K.J. Palin, J. Hadgraft, The effect of solutes and polymers on the gelation properties of pluronic F-127 solutions for controlled drug delivery, Journal of Controlled Release 5(2) (1987) 113-118.

[215] R.S. Drago, F.E. Paulik, The Reaction of Nitrogen(II) Oxide with Diethylamine, Journal of the American Chemical Society 82(1) (1960) 96-98.

[216] Y. Wo, Z. Li, E.J. Brisbois, A. Colletta, J. Wu, T.C. Major, C. Xi, R.H. Bartlett, A.J. Matzger, M.E. Meyerhoff, Origin of long-term storage stability and nitric oxide release behavior of carbosil polymer doped with S-nitroso-N-acetyl-D-penicillamine, ACS applied materials & interfaces 7(40) (2015) 22218-22227.

[217] S. Oae, D. Fukushima, Y.H. Kim, Novel method of activating thiols by their conversion into thionitrites with dinitrogen tetroxide, Journal of the Chemical Society, Chemical Communications (12) (1977) 407-408.

[218] L.M. Estes, P. Singha, S. Singh, T.S. Sakthivel, M. Garren, R. Devine, E.J. Brisbois, S. Seal, H. Handa, Characterization of a nitric oxide (NO) donor molecule and cerium oxide nanoparticle (CNP) interactions and their synergistic antimicrobial potential for biomedical applications, Journal of Colloid and Interface Science 586 (2021) 163-177.

[219] F.S. Schanuel, K.S. Raggio Santos, A. Monte-Alto-Costa, M.G. de Oliveira, Combined nitric oxide-releasing poly(vinyl alcohol) film/F127 hydrogel for accelerating wound healing, Colloids and Surfaces B: Biointerfaces 130 (2015) 182-191.

[220] T.-M. Hu, T.-C. Chou, The kinetics of thiol-mediated decomposition of S-nitrosothiols, The AAPS journal 8(3) (2006) E485-E492.

[221] D.L.H. Williams, The chemistry of S-nitrosothiols, Accounts of chemical research 32(10) (1999) 869-876.

[222] J. Leake, S. Dowd, R. Wolcott, A. Zischkau, Y. Sun, Identification of yeast in chronic wounds using new pathogen-detection technologies, Journal of wound care 18(3) (2009) 103-108.

[223] C. Le Brun, M. Gombert, S. Robert, E. Mercier, P. Lanotte, Association of necrotizing wounds colonized by maggots with Ignatzschineria–associated septicemia, Emerging Infectious Diseases 21(10) (2015) 1881.

[224] B. Sharma, D. Harish, V.P. Singh, S. Bangar, Septicemia as a cause of death in burns: an autopsy study, Burns 32(5) (2006) 545-549.

[225] X. Ji, R. Li, W.Y. Jia, G.M. Liu, Y.G. Luo, Z.Q. Cheng, Co-Axial Fibers with Janus-Structured Sheaths by Electrospinning Release Corn Peptides for Wound Healing, Acs Applied Bio Materials 3(9) (2020) 6430-6438.

[226] G. Reiber, B. Lipsky, G. Gibbons, The burden of diabetic foot ulcers, The American journal of surgery 176(2) (1998) 5S-10S.

[227] R. Everts, How to Treat Wound Infection, Prevention and Treatment (2016).

[228] P. Tessari, D. Cecchet, A. Cosma, M. Vettore, A. Coracina, R. Millioni, E. Iori, L. Puricelli, A. Avogaro, M. Vedovato, Nitric oxide synthesis is reduced in subjects with type 2 diabetes and nephropathy, Diabetes 59(9) (2010) 2152-2159.

[229] B.H. Ericsson, G. Tunevall, K. Wickman, The paper disc method for determination of bacterial sensitivity to antibiotics: Relationship between the diameter of the zone of inhibition and the minimum inhibitory concentration, Scandinavian journal of clinical and laboratory investigation 12(4) (1960) 414-422.

[230] S. Finnegan, S.L. Percival, EDTA: an antimicrobial and antibiofilm agent for use in wound care, Advances in wound care 4(7) (2015) 415-421.

[231] R. Gonzales, J.G. Bartlett, R.E. Besser, J.M. Hickner, J.R. Hoffman, M.A. Sande, Principles of appropriate antibiotic use for treatment of nonspecific upper respiratory tract infections in adults: background, Annals of internal medicine 134(6) (2001) 490-494.

[232] A. Morris, J.D. Kellner, D.E. Low, The superbugs: evolution, dissemination and fitness, Curr Opin Microbiol 1(5) (1998) 524-529.

[233] G. Li, S. Yu, W. Xue, D. Ma, W. Zhang, Chitosan-graft-PAMAM loading nitric oxide for efficient antibacterial application, Chemical Engineering Journal 347 (2018) 923-931.

[234] F. Kabirian, P. Brouki Milan, A. Zamanian, R. Heying, M. Mozafari, Nitric oxide-releasing vascular grafts: A therapeutic strategy to promote angiogenic activity and endothelium regeneration, Acta Biomaterialia 92 (2019) 82-91.

[235] H. Massoumi, J. Nourmohammadi, M.S. Marvi, F. Mortarzadeh, Comparative study of the properties of sericin-gelatin nanofibrous wound dressing containing halloysite nanotubes loaded with zinc and copper ions, Int J Polym Mater Po 68(18) (2019) 1142-1153.

[236] V. Baldim, M.G. de Oliveira, Poly-ε-caprolactone/polysulfhydrylated polyester blend: A platform for topical and degradable nitric oxide-releasing materials, European Polymer Journal 109 (2018) 143-152.